MUSCLE INSULIN RESISTANCE:

NOVEL MECHANISMS AND NEW TREATMENT TARGETS

By

Jeffrey S. Bonner

Dissertation

Submitted to the Faculty of the

Graduate School of Vanderbilt University

in partial fulfillment of the requirements

for the degree of

DOCTOR OF PHILOSOPHY

In

Molecular Physiology and Biophysics

August, 2013

Nashville, Tennessee

Approved:

Owen McGuinness

Kate Ellacott

Dale Edgerton

Colleen Brophy

Ambra Pozzi

ACKNOWLEDGEMENTS

This work would not have been possible without the generous contributions of numerous people. I am so grateful for the Wasserman Laboratory. All the former and current lab members truly enriched my experience and facilitated my personal and profession growth. I would like to thank Dr. Wasserman for his efforts as a mentor and coach. His support and patience was invaluable to my professional development and I can't thank Dave enough for his entertainment and friendship. The friendships and assistance from lab members were critical to my success including: Clint Hasenour, Ashley Williams, Li Kang, Louise Lantier, Deanna Bracy, Freyja James, Rob Lee-Young, Mickael Goelzer, Wes Mayes, and Emerson Ridley. Dr. Li Kang, Deanna Bracy, and Freyja James deserve special thanks for generously teaching me laboratory techniques and assisting with surgeries, clamps, and overall support.

My Dissertation Committee has been instrumental. Drs. Owen McGuinness (Chair), Ambra Pozzi, Dale Edgerton, Kate Ellacott, and Colleen Brophy have all provided critical guidance and support to reach my goals. I am truly appreciative of all their time and efforts. Our collaboration with the Brophy Laboratory and the assistance of Kyle Hocking was valuable to my research. The technical support from the Vanderbilt University Mouse Metabolic Phenotyping Core, Translational Pathology Shared Resource Core, and Cell Imaging Shared Resource Core were essential to address my research questions. In particular, I am grateful for the efforts of Jay Jerome, Sam Wells, Janice Williams, Mary Dawes, ZhiZhang Wang, and Melissa B. Downing.

Without the support and encouragement from my incredible family and friends I would not have completed this project. The love and guidance my parents and brother have always shown provided indispensable motivation. The continued support of Mitch, Bonnie, Lauren, and the Dobbins family has made this experience possible. Finally, I can’t thank my wonderful wife Kate enough for her enduring confidence and inspiration.

TABLE OF CONTENTS

Page

LIST OF FIGURES

Figure **Page**

LIST OF TABLES

Table **Page**

Chapter I

INTRODUCTION

Metabolic Homeostasis: Skeletal Muscle as a Key Metabolic Organ

The incidence of metabolic syndrome in the U.S. is on the rise with approximately 34% of the adult population meeting the criteria (1). Metabolic syndrome is a grouping of risk factors for the development of cardiovascular disease including three or more of the following: abdominal obesity, low HDL cholesterol, high triglycerides, raised blood pressure, and insulin resistance. The rise in metabolic syndrome is, in part, due to the increased diagnosis of type 2 diabetes and insulin resistance. Nearly 26 million people in the U.S. have diabetes and an alarming 79 million adults currently live with prediabetes (insulin resistance) (2). Insulin resistance and metabolic syndrome are multifactorial health issues that involve the potential interaction between lifestyle characteristics such as diet and physical activity level, obesity, genetic predisposition, chronic inflammation, elevated free fatty acids, mitochondrial dysfunction, and impairments in insulin signaling (3). Diabetes is the seventh leading cause of death due to increased risk for heart disease and stroke (2).

Skeletal muscle is the primary site of action for insulin-stimulated glucose disposal. β-cells respond to postprandial hyperglycemia to secrete insulin into the circulation, which acts on peripheral tissues. The liver is responsible for approximately 30% of postprandial glucose clearance while the periphery responds to the circulating insulin to stimulate skeletal muscle glucose uptake (MGU), thus promoting a return to

euglycemia (4-7). Furthermore, DeFronzo et al. demonstrated that skeletal muscle is the primary site of glucose disposal during hyperinsulinemic-euglycemic clamps corresponding to 80% of whole body glucose uptake and this response is blunted in diabetic subjects (8). Prediabetic and type 2 diabetic patients have an impaired response to insulin to stimulate MGU causing extended or unresolved hyperglycemia after a meal. Skeletal muscle insulin resistance is present prior to an overtly elevated fasting plasma glucose and a diagnosis of type 2 diabetes (5). There is an association between factors of metabolic syndrome and insulin resistance. Patients with essential hypertension and ischemic heart disease have a 35-50% decrease in insulin-stimulated glucose disposal (9, 10). The majority of hypertensive patients are either insulin resistant or diagnosed type 2 diabetics suggesting a clear link between vascular and metabolic function in obese populations (11). The action of insulin to promote vasodilation and enhance skeletal muscle perfusion is a potential link between insulin resistance and vascular disease. However, the exact mechanisms for the pathogenesis of skeletal muscle insulin resistance are not fully elucidated and further studies are required to corroborate the potential interplay between vascular and metabolic dysfunction that could result in novel treatment targets for metabolic syndrome.

Skeletal Muscle Perfusion: A Critical Component of *In Vivo* Insulin-Stimulated Muscle Glucose Uptake

The ability of insulin to stimulate glucose disposal is principally regulated by skeletal muscle glucose influx (12). The control of MGU is distributed between 3-steps, as depicted in Figure 1 (13, 14). To elucidate the resistances to glucose flux through the

three steps an *in vivo* model must be employed due to the complex regulation of fluxes via multiple organ systems.

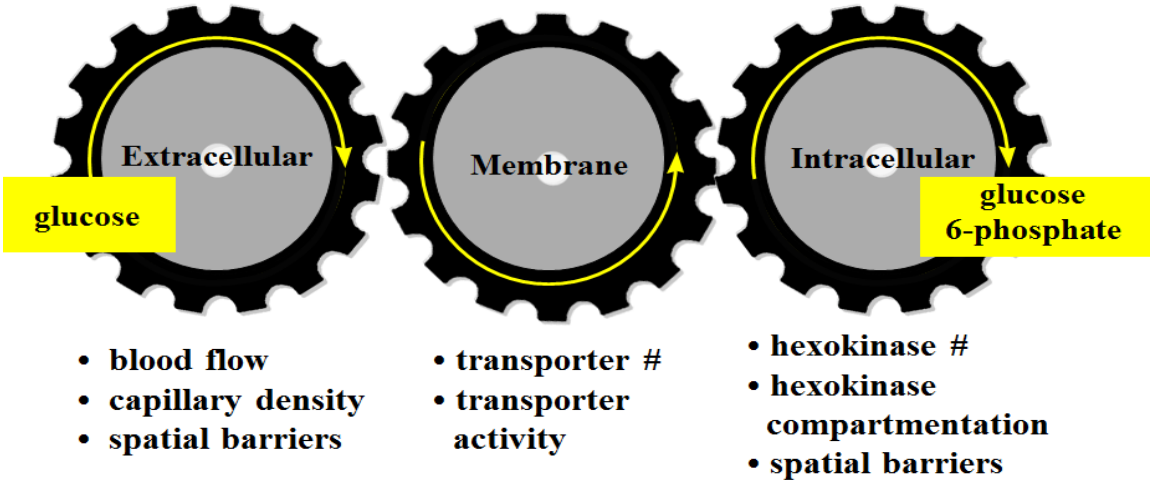

Figure 1.1 - Distributed Control of Muscle Glucose Uptake – Representation of the three step process of muscle glucose uptake and the contributing factors of each component

Furthermore, *in vivo* glucoregulatory analysis is best studied under well-controlled conditions where the subject is conscious, unstressed, and arterial glucose levels are clamped. The clamping of glucose concentration prevents activation of compensatory hormone or autoregulatory systems. For example, clamping glucose at euglycemic levels averts hypoglycemia during an insulin infusion, which prevents the body from responding by increasing glucagon, corticosterone (in rodents), catecholamines, and other glucose counterregulatory factors. Also, *in vivo* glucose flux analysis is optimally performed in conscious animals because anesthesia decreases metabolism and hormone sensitivity. By utilizing the Vanderbilt Hyperinsulinemic-Euglycemic Clamp Method (insulin clamp) we are able to determine muscle glucose influx without the concerns delineated above or inducing a stress response from handling of mice (15, 16). *In vivo*

metabolic studies facilitate the comprehensive understanding of how an experimental factor (e.g. increase in fat mass) affects MGU. Cell culture and *ex vivo* models remove the delivery component of MGU and require supraphysiological levels of insulin to stimulate glucose uptake. As a result, these experimental models isolate the glucose transport and phosphorylation components of insulin-stimulated MGU, but exclude the extramyocellular factors that contribute to insulin action.

To understand the integrated regulation of MGU that occurs in a physiological state the three steps must be present in the experimental model. Glucose delivery is regulated by arterial concentration and perfusion of the muscle bed. Muscle blood flow is controlled by capillary recruitment and total blood flow in response to insulin stimulation (step 1). At the muscle interstitium glucose is transported across the sarcolemma membrane by GLUT4 after translocation to the membrane in response to myocellular insulin signaling events (step 2). Intramyocellular glucose is phosphorylated to glucose-6-phosphate, which is regulated by hexokinase activity and compartmentation (step 3). Glucose phosphorylation is the terminal step of MGU as muscle lacks glucose-6-phosphatase activity trapping phosphorylated glucose in muscle. In the fasted state, control of MGU is at the transport step due to the low number of GLUT4 at the sarcolemma membrane rendering the muscle impermeable to glucose (17). Utilizing the principles of glucose countertransport, Halseth et al. showed that the transport barrier is minimal during insulin stimulation due to the muscle being highly permeable to glucose after GLUT4 insertion into the membrane. The control of insulin-mediated MGU is distributed between glucose delivery and phosphorylation (18-20).

Fueger et al. further defined the barriers to MGU utilizing genetic mouse models to functionally remove the transport barrier by overexpression of GLUT4, the phosphorylation barrier with hexokinase II overexpression, or the combination of both proteins (17). Data collected from insulin clamp studies in these mouse models support the conclusions of the countertransport studies of Halseth et al. (18). Fueger et al. applied control theory to determine the functional barriers to MGU (21): $C_{Tg} = \Delta\ln(R_g)/\Delta\ln(P_{Tg})$ where C_{Tg} is the control coefficient, R_g is the index for MGU, and P_{Tg} is the level of hexokinase II or GLUT4 relative to controls. The assumptions in this model are twofold; MGU is a defined pathway in which the sum of the control coefficients for each MGU equals 1 and the increase in protein expression directly correlates to its activity. As shown in Table 1.1, the primary barriers to MGU during insulin stimulation are delivery and phosphorylation.

Control Step	Delivery	Transport	Phosphorylation
Rest	0.1	0.9	0.0
Insulin Clamp; 4 mU·kg^{-1}·min^{-1}	0.5	0.1	0.4

Table 1.1 - Control Coefficients for Muscle Glucose Uptake – Control coefficients for each component of muscle glucose uptake at rest and during insulin stimulation in lean mice

The countertransport and genetic models emphasize the importance of glucose delivery during insulin-stimulated MGU. Glucose delivery is dependent on arterial concentration, which is regulated by nutrient absorption by the gut, liver glucose output in addition to the action of insulin to enhance muscle perfusion. Glucose delivery augments the

myocyte exposure of glucose by mass action down the glucose concentration gradient from the plasma to muscle interstitium.

Any factor that causes changes in MGU, whether it is a characteristic of health or disease, works through one of these three steps. For example, skeletal muscle accumulation of glucose-6-phosphate reduces MGU by regulating glucose phosphorylation through negative feedback inhibition of hexokinase activity. Furthermore, the delivery component of MGU does not rest only on glucose movement from the vascular to muscle compartment. The delivery of arterial insulin to the interstitium of skeletal muscle is the rate-limiting step for the onset of insulin-stimulated MGU, suggesting the importance of insulin delivery to MGU (22).

The metabolic action of insulin at skeletal muscle is limited by its transport from the plasma compartment to the interstitial compartment (23). Investigation by the laboratory of Olefsky extensively demonstrated the delayed onset of insulin action and insulin receptor kinase activation in skeletal muscle (24-26). During insulin clamps in healthy human subjects the half-maximal plasma insulin levels occurs between 4.9-7.2 min with corresponding half-maximal glucose disposal rate and insulin receptor kinase activation between 40-60 min (24). Furthermore, obese subjects have a much slower onset of peripheral glucose disposal compared to healthy controls. Notably, there was no difference in the time to reach half-maximal suppression of hepatic glucose production (~20 min) in obese subjects, which is likely due to differences in microvascular structure (e.g. the liver has discontinuous capillaries and muscle has tight capillaries) and the high liver perfusion causing a more rapid appearance of insulin (26). The blood flow to the liver is homogenous and 33-fold higher at rest than skeletal muscle, which in congruence

to the leaky capillary structure permits much higher insulin extraction (27). Nolan et al. further demonstrated that the diabetic patients had a marked delay in the activation of glucose disposal and leg glucose uptake when comparing obese patients to diagnosed type 2 diabetics (25). Bergman and colleagues showed that the concentration of interstitial and lymph insulin correlates more closely to the onset of glucose disposal than the rise in plasma (28-30). The importance of insulin appearance at the muscle interstitium was confirmed by studies that directly injected skeletal muscle of dogs with insulin and showed an immediate stimulation of MGU (31).

The architecture of the capillary wall within skeletal muscle determines the transport and delivery capacity of large molecules such as insulin. Skeletal muscle capillaries are characterized by tight junctions and an enrichment of caveolae number (27). King and Johnson were the first to propose that insulin moves across the endothelial layer in a receptor-mediated mechanism (32). This finding was supported by *in vivo* evidence. Wang et al. obtained serial muscle biopsies while performing an insulin clamp with FITC-labeled insulin and demonstrated that the labeled insulin was bound to the endothelium but was yet to be transported to the muscle interstitium 10 min after the outset of the clamp (33). Wang and Barrett further showed the co-localization of the labeled insulin with the insulin receptor and caveolin-1 on the luminal membrane of endothelial cells (33). The transport potential of the endothelium is dependent on the activation and downstream signaling of the endothelial insulin receptor. The transport of insulin is impaired with exposure to inflammatory cytokines such as TNFα and with knockdown of the caveolin-1 protein, which is critical to the formation of caveolae (34). However, the *in vivo* effects of diet-induced insulin resistance on skeletal muscle

capillary transport capacity of insulin and whether structural changes occur that could alter the transport potential is unknown.

Obesity is a major risk factor for cardiovascular morbidity and mortality that associates with the development of insulin resistance at tissues such as skeletal muscle, liver, and adipose tissue. A deficit at any of the three steps to MGU can cause insulin resistance. In animal models of obesity impairments in the action of insulin to augment muscle blood volume (35-38), glucose sarcolemma transport (39-41), and glucose phosphorylation can be present (42, 43). However, in high fat-fed rats the primary deficit in insulin-stimulated MGU is in the delivery component (18). The hemodynamic action of insulin to increase muscle blood volume is blunted in obesity supporting the paradigm that the delivery step of MGU is critical to the etiology of skeletal muscle insulin resistance (35, 36, 44).

Loss of Vascular Function

The initiation of skeletal muscle insulin action is dependent on the appearance of interstitial insulin. The transcapillary delivery of insulin to muscle is rate-limiting in healthy subjects and is delayed in insulin resistant patients (23). Insulin acts on the vascular tree to enhance its own delivery by relaxing resistance arteries and arterioles to augment total limb blood flow, relaxing precapillary arterioles to recruit unperfused capillaries thus increasing the surface area for substrate exchange, and enhancing capillary vasomotion to enhance blood flow distribution (23, 45, 46). The hemodynamic actions of insulin precede insulin-stimulated MGU. Bergman et al. demonstrated that *in vivo* insulin injection directly into skeletal muscle immediately induces MGU, supporting

the hypothesis that insulin delivery is a significant barrier to the onset of insulin-stimulated MGU (31).

The increase in capillary blood volume occurs within minutes of insulin administration with a delayed increase in total limb blood flow (45). Ellmerer et al. showed that insulin augments macronutrient delivery to skeletal muscle during an insulin clamp and appearance of macromolecules in skeletal muscle lymph, a surrogate for the interstitium, is diminished in obese dogs (47). Moreover, the presence of the endothelial insulin signaling machinery is essential for the vascular actions. The significance of insulin and glucose delivery to tissue glucose uptake is specific to muscle. The structure of the endothelium in muscle is continuous, which contrasts with the discontinuous endothelial barrier of liver and the blood flow to the liver is naturally high in the basal state (27, 48). Insulin resistance occurs at the level of large arteries and the microcirculation that prevents the rise in skeletal muscle perfusion during insulin stimulation (49, 50). Structural and functional capillary rarefaction contribute to the blunted muscle blood volume during insulin stimulation. Structural capillary rarefaction is the attenuation in capillary to myocyte ratio and functional capillary rarefaction is the impairment in endothelial function preventing arterial relaxation at sites of resistance. Structural and functional capillary rarefaction develops in insulin resistant patients and experimental models of type 2 diabetes (36-38, 44, 49, 51-57).

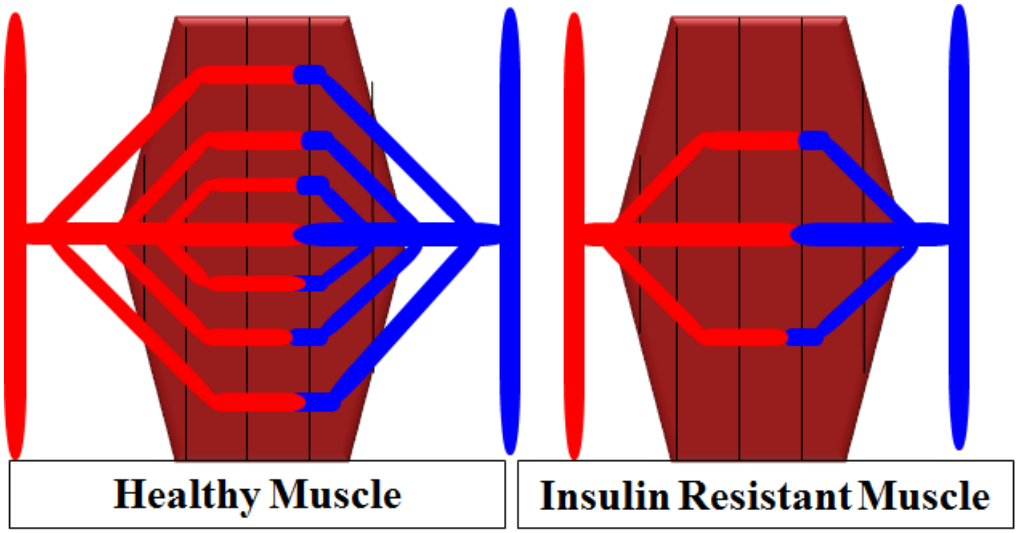

Figure 1.2 - Capillary Density in Healthy and Insulin Resistant Muscle – Insulin resistant subjects have decreases in the number of capillaries perfusing skeletal muscle compared to healthy controls

The abnormal vascular responses to insulin diminish the surface area available for insulin and glucose exchange exacerbating the insulin resistant phenotype. Benedict et al. performed a complex analysis of the capillary network connectivity and structure in Zucker diabetic fatty rats before and after the onset of type 2 diabetes. After the development of insulin resistance, there was a 37% decrease in capillary branching and a 44% decrease in capillary flow per muscle compared to non-diabetic controls (49). This large deficit in functional capillary reserve limits the action of insulin to augment microvascular blood volume. Moreover, a graded occlusion of skeletal muscle capillaries with 15μm diameter microspheres, in a healthy perfused hindlimb, is sufficient to impair muscle insulin action supporting the importance of the skeletal muscle capillary reserve (58). However, it is currently unknown whether structural capillary rarefaction is critical to the pathogenesis of muscle insulin resistance.

Functional capillary rarefaction contributes to the deficit in insulin-stimulated muscle perfusion. Inhibiting the action of insulin to recruit unperfused capillaries impairs insulin-stimulated glucose disposal (59). Multiple experimental techniques, such as 1-methylxanthine metabolism and contrast enhanced ultrasound, permit the characterization of the effect of insulin to rapidly recruit unperfused capillaries, thus increasing skeletal muscle blood volume (23, 45, 60). Endothelial dysfunction in large arteries parallels the deficit in capillary recruitment contributing to the overall decrease in skeletal muscle perfusion (61). A large systemic review and meta-analysis showed that markers of vascular dysfunction strongly associate with type 2 diabetes. Specifically, this comprehensive review determined that plasma soluble adhesion molecules, vascular reactivity, arteriole to venule ratio, and microalbuminuria (all markers of vascular dysfunction) correlate to the presence of type 2 diabetes in patients (62). Vincent et al. determined that inhibiting insulin-induced activation of nitric oxide synthase (NOS) attenuates glucose disposal by 30-40% (59). Extending this concept, subjects with the greatest muscle blood volume have the greatest glucose disposal during an insulin clamp even in healthy, normotensive, and non-obese subjects (63). Vascular dysfunction is an important risk factor for cardiovascular mortality, which is the leading cause of death in diabetic patients (64). Vascular dysfunction may be a common characteristic linking the co-prevalence of cardiovascular and metabolic diseases.

The binding of insulin to the endothelial insulin receptor initiates a PI3-kinase-dependent pathway similar to other insulin responsive tissues. Activation of endothelial insulin signaling causes Akt-mediated phosphorylation of endothelial NOS (eNOS) that stimulates nitric oxide synthesis and vasodilation (46). Insulin concurrently activates the

mitogen-activated protein kinase pathway, which increases the expression of the vasoconstrictor endothelin-1 (ET-1); however, in healthy subjects the eNOS pathway dominates (46, 65). The endothelium is characterized by pathway selective insulin resistance in obesity blunting PI3-kinase activation and promoting ET-1 production resulting in further endothelial dysfunctional (66).

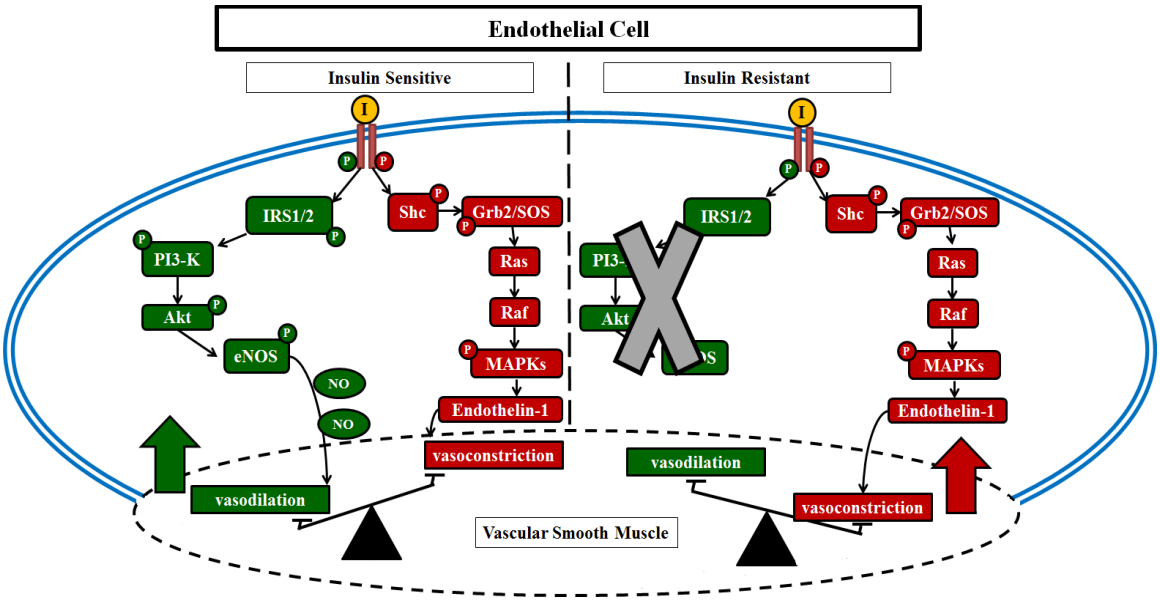

Figure 1.3 - Endothelial Insulin Signaling in Health and Disease – The vasodilatory and capillary recruitment actions of insulin occur via the canonical insulin receptor pathway in endothelial cells, which is defective in insulin resistant states

Pharmacologically or genetically eliminating eNOS activation in the presence of insulin diminishes glucose disposal and skeletal muscle perfusion (67, 68). Kubota et al. characterized the essential role of endothelial insulin signaling to MGU. The enhancement in skeletal muscle perfusion during an insulin clamp is abolished in obese and IRS-2 deficient mice, the primary endothelial isoform (48). Both mouse models have decreased insulin-mediated eNOS activation, insulin delivery to skeletal muscle

interstitium, and MGU. In diet-induced insulin resistant animal models, the deficit in vascular insulin signaling precedes the onset of peripheral insulin resistance, suggesting that the endothelium is more susceptible to dietary fat ingestion (50). Moreover, activity restriction in lean non-human primates impairs microvascular function and induces insulin resistance providing a potential link between obesity and physical inactivity to the pathogenesis of insulin resistance (69). This vascular detriment is an early and likely a causative factor for the development of skeletal muscle insulin resistance.

VEGF-Dependent Angiogenesis

Vascular endothelial growth factor-A (VEGF) is essential for the coordinated development of the vascular system during embryonic maturation and angiogenesis in adult animals. Notably, global deletion of a single VEGF allele is sufficient to cause embryonic death (70-72). Eukaryotic organisms have a family of VEGF proteins, listed in Table 1.2, that regulate vasculogenesis, angiogenesis, and lymphanogenesis. VEGF binds primarily to two receptors, VEGFR1 and R2. The angiogenic action of VEGF is mediated through VEGFR2. The role of VEGFR1 is less characterized and considered to be anti-angiogenic, in particular soluble VEGFR1. VEGFR1 has a high affinity for VEGF sequestering it from VEGF2 interaction and the induction of angiogenesis. VEGF action is essential for the adaptive response to changes in substrate demand. For example, increases in oxygen and energy demands during exercise stimulates the growth and branching of tissue capillaries to increase the surface area for substrate and waste exchange in metabolically active tissues. VEGF induces chemotaxis and differentiation

of endothelial precursor cells, endothelial cell proliferation, the assembly of endothelial cells into the vascular network, and remodeling (73)

VEGF isoform	Receptor	Physiological Action
VEGF-A	VEGFR1 and 2	Angiogenesis, migration, permeability, survival, and proliferation
VEGF-B	VEGFR1	Permeability, monocyte migration, fatty acid transport, regulation of endothelial pool during development, and neuroprotection
VEGF-C	VEGFR3	Lymphangiogenesis
VEGF-D	VEGFR3	Lymphangiogenesis

Table 1.2 - VEGF Isoforms, Receptors, and Physiological Actions – VEGF-A is the critical isoform that regulates angiogenesis and microvascular density

There is an augmentation of skeletal muscle VEGF expression during exercise in response to the increase in energy demand (74). Skeletal muscle adapts to the greater oxygen and substrate requirements to increase capillary density, and thus, muscle perfusion. Tang et al. demonstrated that skeletal muscle VEGF deletion causes capillary rarefaction characterizing the critical role of VEGF in the maintenance of muscle capillary density (75, 76). In accordance with the results in skeletal muscle, Giordano et al. discovered that the deletion of VEGF in cardiac muscle induces fewer capillaries perfusing the heart (77). These studies describe the importance of paracrine VEGF signaling from the muscle to the endothelium to sustain tissue capillary requirements. This contrasts with endothelial specific VEGF expression that is necessary for endothelial cell integrity and survival via an autocrine signaling mechanism (78).

There is impairment in VEGF action in diabetic patients that causes capillary rarefaction and a blunted adaptive response to increases in metabolic demand (79-83). Animal models of diabetes develop cardiomyopathy due to a progressive loss of myocardial VEGF expression (81). In peripheral and cardiac ischemia, diabetic animals and patients are unable to induce collateral vessel growth to ameliorate the hypoxic event (79, 82). The detriment in angiogenesis worsens outcomes in diabetic patients leading to increase mortality after an ischemic event compared to non-diabetics.

Gain of Vascular Function

Modulation of skeletal muscle perfusion impacts MGU as described in equation 1 for the calculation for MGU:

$$MGU = \Delta AV glucose \times LBF$$

Femoral $\Delta AV glucose$ is the arterial-venous difference across the muscle of interest and LBF is the total blood flow to that muscle. Baron et al. showed that limb blood flow independently modulates femoral glucose uptake (84). Baron and colleagues performed insulin clamps on lean subjects and determined glucose uptake during steady-state period (equation 1). The investigators next increased blood flow with metacholine, a NO dependent vasodilator. The study determined that elevating blood flow during steady-state hyperinsulinemia augments femoral glucose uptake (84). This seminal result showed the significance of modulating blood flow to enhance insulin-mediated MGU and highlighted the importance to consider muscle perfusion in the treatment of insulin resistance.

Baron and colleagues furthered defined the influence of muscle blood flow in type 2 diabetic patients. In this study, the authors performed a constant insulin infusion at $120mU/m^2 \cdot min^{-1}$ in diabetic and healthy subjects with glucose concentrations clamped at incremental levels. At all steady-state glucose concentrations there was no change in femoral ΔAVglucose; however; limb blood flow was significantly lower at each glucose step in the diabetic patients and plateaued at a lower glucose concentration resulting in the lower limb glucose uptake (36). These results indicate that reduced glucose and insulin delivery to skeletal muscle is critical to the pathogenesis of diabetes. Moreover, large artery dysfunction correlates to the state of metabolic impairment evident in obese, type 2 diabetics (27). The permeability surface area for glucose during insulin stimulation, a measurement of the capacity for glucose to reach the interstitial fluid, in forearm muscle is impaired in obese insulin resistant subjects compared to obese insulin sensitive controls. This deficit that can be overcome by co-infusion of a vasodilator (85).

The diseased vasculature associated with insulin resistance and type 2 diabetes provides an important pharmacological target to comprehensively treat the metabolic syndrome. Murdolo et al. demonstrated that an acute infusion with the vasodilator metacholine, during hyperinsulinemia, improves the delayed onset of insulin action at skeletal muscle present in insulin resistant subjects (85). It is important to note that this study was performed in an acute setting and without focus on intervention to treat muscle insulin resistance. Our laboratory investigated the effects of inhibiting cGMP breakdown using the phosphodiesterase-5 inhibitor sildenafil at the onset and duration of diet-induced insulin resistance (86). Nitric oxide rapidly diffuses from the endothelium to smooth muscle stimulating cGMP synthesis by soluble guanylate cyclase, the secondary

messenger necessary for NO-mediated vasodilation. Ayala et al. demonstrated the protective effect of pharmacologically targeting the vasculature at the outset of a high fat (HF) diet to prevent the development of skeletal muscle insulin resistance (86). While this study provided evidence consistent with improved vascular function in the prevention of diet-induced insulin resistance, it was not designed to address the more clinically relevant issue of reversing insulin resistance. Kang et al. expanded on these studies to show that capillary density was greater in mice treated with sildenafil for the duration of an obesogenic diet, suggesting that the actions of sildenafil to maintain capillary density and muscle perfusion are important (87). Additionally, a study in fructose-fed rats showed that an intervention with an angiotensin II receptor inhibitor reverses skeletal muscle insulin resistance attributed to a normalization of capillary density compared to chow-fed controls (53). These studies support the concept that the vascular system provides novel and viable therapeutic targets to concomitantly treat metabolic and cardiovascular diseases that associate with the growing obesity epidemic.

Relaxin: A Novel Therapeutic Agent with Possibilities to the Treatment of Diabetes

The hormone relaxin was first discovered by Frederick Hisaw in 1926 and described as a hormone of pregnancy (88). Relaxin is now characterized as a critical hormone for the cardiovascular and renal adaptations during pregnancy. The pleiotropic actions of relaxin include systemic vasodilation to increase fetal nutrient delivery and enhanced renal function to accommodate higher demand for waste excretion (89). Recent clinical and animal data have expanded the cardiovascular actions of relaxin to males. Relaxin was originally described to belong to the insulin hormone superfamily due to the

6 kDa size of both peptides and disulfide bonds that are crucial for structural integrity. However, current data now suggests that relaxin diverged from the insulin family of proteins early in vertebrate evolution forming a specific relaxin peptide family (90). There are three unique relaxin genes in humans (*RLN1, RLN2,* and *RLN3*) that encode for H1, H2, and H3 relaxin respectively (90). In non-human primates there are only two relaxin genes (*RLN1* and *RLN3*), in which the *RLN1* gene corresponds to H2 relaxin. The physiological actions described herein refer to H2 relaxin as relaxin. Relaxin is expressed in reproductive and non-reproductive tissues including uterus, prostate gland, brain, pancreas, kidney, and heart (91, 92). Relaxin acts through two G-protein coupled receptors RXFP1 and RXFP2, which contain leucine-rich repeats (93). Relaxin has a much higher affinity for RXFP1. RXFP1 is widely expressed and abundantly present in the reproductive, nervous, and cardiovascular systems in both male and female animals (93).

The vascular effects of relaxin, inducing vasodilation and a decrease in systemic vascular resistance, are mediated by the endothelin system. The close proximity of the relaxin and the ET-1 signalosomes support this mechanism. ET-1 is synthesized by endothelial cells and processed to ET_{1-32}, which specifically induces the vasodilatory actions of relaxin. ET-1 binds to the ET_A and ET_B receptors on vascular smooth muscle to cause vasoconstriction; however, the ET_B receptor is present on endothelial cells and induces NO dependent relaxation (94). Relaxin increases matrix metalloproteinase (MMP) activity that regulates the processing of ET-1 and MMPs are required for the acute vasodilatory effects of relaxin (94). The *in vivo* actions of relaxin to alter vascular compliance are not fully understood. Specific mechanisms depend on the exposure time

such that the fast acting (minutes) response is dependent on components of RXFP1 signaling directly, the intermediate response (hours) is primarily dependent on MMP-9 activation, and the long-term (days) action of relaxin is dependent on both ET-1 and VEGF signaling mechanisms (95). Convergence on eNOS activation and NO synthesis is common between all three pathways.

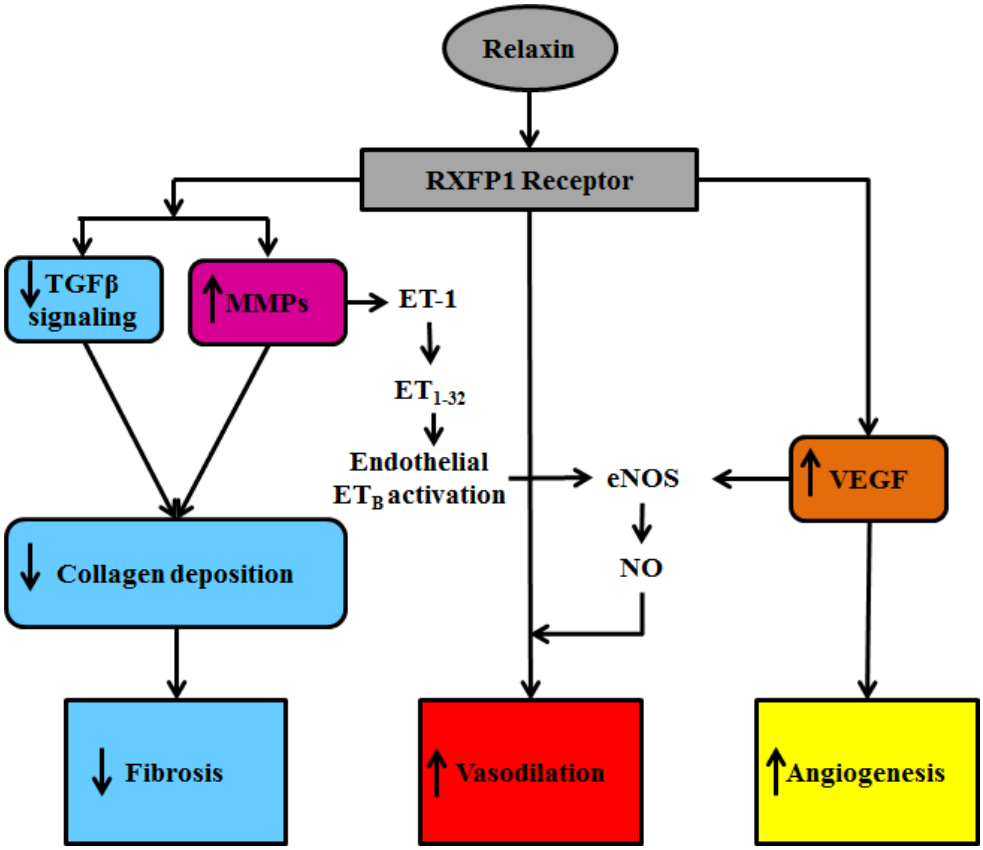

Figure 1.4 - Mechanisms of Relaxin Action – Physiology of relaxin that result in the anti-fibrotic, vasodilatory, and angiogenic actions and proposed to be important to intervene on the development of insulin resistance

The physiological actions of relaxin are not limited to the cardiovascular effects. Relaxin decreases collagen biosynthesis and promotes collagen degradation. The regulation of connective tissue homeostasis promotes an anti-fibrotic environment. Relaxin inhibits transforming growth factor-β (TGFβ) signaling to prevent collagen

biosynthesis (96-99). Relaxin augments MMP expression and/or decreases expression of tissue inhibitor of metalloproteinase to enhance the activity of MMPs (100-103). Importantly, the anti-fibrotic action of relaxin occurs only in the presence of aberrant fibrosis and does not alter extracellular matrix proteins in healthy tissue. Genetically engineered mice with *RLN1* deletion corroborate the extracellular matrix remodeling characteristics of the hormone. Relaxin-deficient mice exhibit an age-induced increase in cardiac fibrosis compared to wild-type controls, and this phenotype was normalized after a 2 week relaxin intervention (103).

The stimulation of VEGF expression is critical to the vasodilatory and angiogenic mechanisms of relaxin physiology (104, 105). Hisaw and colleagues first discovered the angiogenic role of relaxin showing the importance of relaxin for the increase in capillary density in the endometrium during pregnancy (106). Additionally, relaxin causes angiogenesis in a rat model for chronic myocardial infarction (107). This conclusion was further confirmed in a swine model of heart failure. In the swine model, Formigli et al. transfected myoblasts with the relaxin gene and grafted the cells into the post-infarcted heart. The transplanted relaxin expressing cardiomyoblasts increases VEGF expression in the endogenous myocardial cells to expand capillary density (108). The angiogeneic mechanism of relaxin is, in part, by acting on bone marrow derived endothelial cells (BMDEC) to mobilize and enhance homing to sites of angiogenesis (104). Relaxin acts via the RXFP1 receptor on BMDECs to increase NO synthesis, which is critical for function (104). This is an important discovery because many secreted factors that mobilize BMDEC to integrate into sites of angiogenesis are concurrently described as

inflammatory agents (e.g. granulocyte-colony stimulating factor), which differs from the actions of relaxin.

The cardiovascular, angiogenic, and anti-fibrotic properties of relaxin make the hormone a promising candidate for intervention. The diverse actions of relaxin have provided enthusiasm and promise in several clinical disease states. There are ongoing clinical trials for the therapeutic application of relaxin. The first clinical trial to test the efficacy of relaxin was in scleroderma patients. In phase III trials relaxin decreased fibrosis of the skin, improved renal function, and decreased diastolic blood pressure, but the results were not considered clinically significant enough for market approval (109). The focuses of two current trials are pre-eclampsia and congestive heart failure. Pre-eclampsia is a disorder in pregnant woman manifested by systemic vascular constriction resulting in the development of hypertension and impaired organ function, particularly of the kidney. The pathogenesis of pre-eclampsia is, in part, due to the endogenous inhibition of VEGF signaling. The goal of relaxin intervention is to alleviate hypertension, improve renal function, and maintain endometrial vascular capacity to accommodate the requirements for placental perfusion (109). The RELAX-AHF phase III clinical trial for congestive heart failure has shown encouraging results. Congestive heart failure is the most common reason for hospitalization of patients older than 65 years. These patients have a very poor prognosis attributable to end-organ dysfunction in heart, liver, and kidney. The vascular and anti-fibrotic actions of relaxin have potential to ameliorate these early clinical symptoms and extend long-term survival by promoting cardiac oxygen delivery and abating fibrosis. The RELAX-AHF clinical trial has shown

positive outcomes that indicate reduced cardiac, renal, and hepatic damage after the initial hospitalization and increased 180-day survival rate (110).

The advantage of relaxin intervention is the unique property of the hormone to reverse disease pathology by invoking multiple systems and not affecting healthy tissue. Cardiovascular disease is the major risk factor for mortality in obese, diabetic patients. Furthermore, macro- and microvascular dysfunction in addition to collagen deposition associate with the development of insulin resistance and type 2 diabetes (62, 87, 111). To decrease the risk of cardiovascular disease in the obese population, it is critical to consider endothelial health in drug development. Endothelial health is important to organ metabolism and function. The endothelial cell layer was originally considered a simple physical barrier between the blood and perfused tissue; however, the endothelium is a functioning cell type important for tissue integrity. The functional properties of the endothelium are primarily regulated by eNOS activity and synthesis of NO. Our goal is to investigate the potential for relaxin to reverse the extramyocellular adaptations associated with a high fat (HF) diet to treat insulin resistance and cardiovascular dysfunction.

Hypotheses

The hypothesis investigated in the dissertation is that skeletal muscle vascular integrity is critical for skeletal muscle insulin action. More specifically, I propose that capillary rarefaction directly impairs insulin-stimulated MGU by creating a resistance to the delivery component of MGU, the vascular impairments induced by a HF diet are viable intervention targets to reverse muscle insulin resistance by removing the

resistance, and HF-fed mice have a decrease in caveolae density in skeletal muscle capillaries.

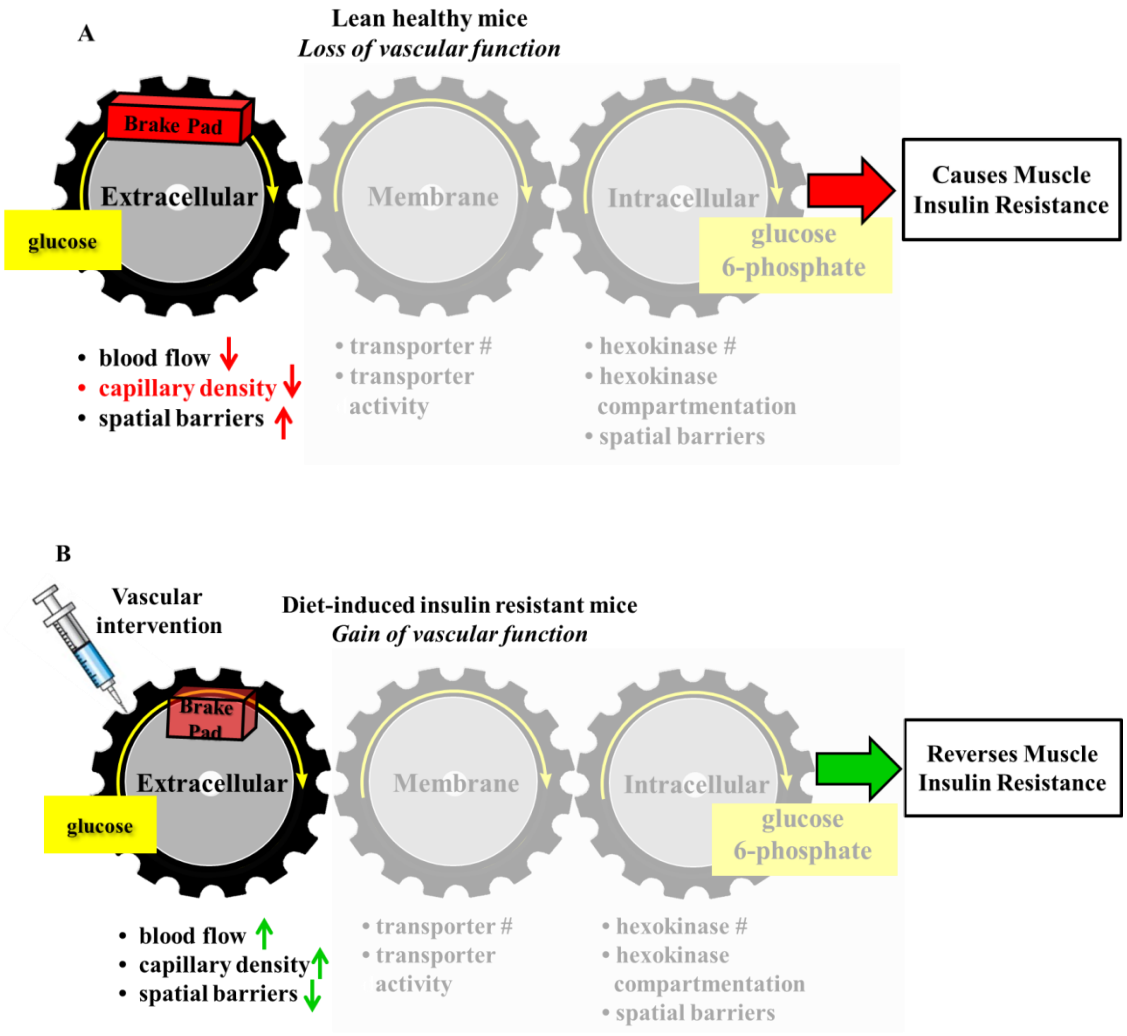

Figure 1.5 - Hypotheses - Loss of Vascular Function (A) and Gain of Vascular Function (B) – Hypothesis A is designed to test whether a decrease in capillary density is sufficient, absent of any other insulin resistance-inducing factors, to cause muscle insulin resistance. Hypothesis B is designed to test whether targeting the extramyocellular adaptations to a HF diet - vascular dysfunction and capillary rarefaction - with the hormone relaxin reverses diet-induced skeletal muscle insulin resistance

The goal of Aim 1 (Chapter III) is to determine whether capillary rarefaction is a cause or a consequence of muscle insulin resistance. To address Aim 1, mice with

muscle-specific genetic deletion of vascular endothelial growth factor-A were utilized to induce muscle capillary rarefaction in a lean mouse model. This model permits the investigation into the specific consequence of reducing capillary number to insulin-stimulated MGU. I hypothesize that a genetic decrease in skeletal muscle capillary density by VEGF ablation will induce skeletal muscle insulin resistance in otherwise healthy mice.

The goal of Aim 2 (Chapter IV) is to determine whether pharmacologically targeting the vasculature with the hormone relaxin rescues HF diet-induced muscle insulin resistance. To address Aim 2, lean C57BL/6J mice were first studied to determine the hemodynamic and metabolic effects of relaxin during a hyperinsulinemic-euglycemic clamp. To investigate the therapeutic potential of relaxin C57BL/6J mice were fed a HF diet for 13 weeks with the final 3 weeks of the diet mice received a continuous infusion of relaxin or vehicle via osmotic minipumps. I hypothesize that a chronic intervention of relaxin will reverse the extramyocellular adaptations to a HF diet thus ameliorating diet-induced skeletal muscle insulin resistance.

The goal of Aim 3 (Chapter V) is to determine whether microstructural changes to endothelial caveolae occur after 16 weeks of HF-feeding. Caveolae have been hypothesized to play a critical role in transendothelial insulin transport specifically in skeletal muscle microvasculature. To address Aim 3 C57BL/6J mice were fed a HF diet for 16 weeks or a low fat chow diet. Mice underwent perfused fixation to preserve *in vivo* microstructures of skeletal muscle capillaries for visualization by transmission electron microscopy. I hypothesize that a decrease in caveolae number within skeletal muscle

capillaries contributes to the etiology of skeletal muscle insulin resistance by increasing the delivery barrier for insulin.

Chapter II

RESEARCH MATERIALS AND METHODS

Mouse Models

The Vanderbilt University Animal Care and Use Committee approved all animal protocols. Mice were housed with a 12:12 h light-dark cycle in a temperature and humidity controlled environment. Mice with muscle-specific genetic deletion of VEGF were studied in Chapter III. Mice with LoxP sites flanking exon 3 of the VEGF gene (generously provided by Dr. Alvin Powers Laboratory) on a congenic background (112) and mice expressing Cre recombinase under the muscle creatine kinase (MCK) promoter (purchased from Jackson Laboratory) were crossed to generate the MCK-cre/VEGF$^{lox/lox}$ (*mVEGF*$^{-/-}$) mice and wild-type littermates VEGF$^{lox/lox}$ (*mVEGF*$^{+/+}$). Mice were backcrossed on to a C57BL/6 background for at least 10 generations. The MCK promoter is expressed in skeletal and cardiac muscle. *mVEGF*$^{-/-}$ mice lack all VEGF-A isoforms. Female *mVEGF*$^{+/+}$ mice were mated with male *mVEGF*$^{-/-}$ to prevent cardiac complications during gestation. Mice were weaned at 3 weeks of age and separated by sex. Mice were briefly anesthetized using isofluorane to obtain a sample of tail tissue for genotyping and to ear punch for identification. The genotype of each mouse was determined by polymerase chain reaction (PCR) with DNA isolated using the DNeasy Tissue Kit (Quiagen) with primers displayed in table 2.1. Mice were fed a chow diet (5.5% fat by weight; 5001 Purina Laboratory Rodent Diet) *ad libitum* for 9 weeks beginning at 3 weeks of age and all studies were performed at 12 weeks of age.

Primer	Sequence
Cre	GTGAAACAGCATTGCTGTCACTT
MCK forward	TAAGTCTGAACCCGGTCTGC
+ Control Forward	CAAATGTTGCTTGTCTGGTG
+ Control Reverse	GTCAGTCGAGTGCACAGTTT
VEGF LOX Forward	CCTGGCCCTCAAGTACACCTT
VEGF LOX Reverse	TCCGTACGACGCATTTCTAG

Table 2.1 – PCR primer sequences 5' to 3' to genotype *mVEGF*$^{+/+}$ and *mVEGF*$^{-/-}$ mice

Commercially available C57BL/6J mice male mice were ordered from Jackson Laboratory at 6 weeks of age and were either fed *ad libitum* a chow (5001 Laboratory Rodent Diet) or high fat (F3282 Bioserv) diet containing 5.5% or 60% calories as fat to metabolically stress the mice in Chapter IV and V. The cohorts of mice in Chapter IV were all studied at 19 weeks of age and were individual housed to protect mice from injury due to fighting. Mice in Chapter V were studied at 22 weeks of age. In all studies mice were weighed and handled weekly to observe any health issues and to acclimate mice to prevent stress from handling during the studies.

Surgical Procedures

Prior to the onset of any surgical procedure mice were anesthetized with 40-85 mg/kg pentobarbital or with isoflurane. Surgical setup and processes were performed in an aseptic environment to prevent infection. Once anesthetized, mice were prepped by

removing hair around the surgical site. The shaved area was disinfected with alcohol followed by betadine scrub.

An incision was first made 5 mm cephalic to the sternum and the left sternomastoid muscle was exposed. The sternomastoid muscle was reflected to reveal the left carotid artery. Once the artery has been located the connective tissue and vagus nerve were separated from the vessel. A silk suture was tied at the cephalic end and another loosely knotted on the caudal end of the carotid. The artery was clamped with a micro-serrefine and cut just below the ligated end and the catheter was inserted until the tip reached the aortic arch. The ligatures were secured and catheter sampling confirmed.

An incision was made 5 mm to the right of the midline and 2 mm caudal to the incision for the carotid catheter. The jugular vein was isolated and ligated at the cephalic end with a loose knot at the caudal end similar to the carotid catheter. The catheter for the jugular vein was inserted after a small incision and flushed to assure infusion. For the glucose tolerance tests the catheter was inserted directly into the stomach cavity in lieu of the jugular vein.

A third incision was made between the shoulder blades of each mouse and a 14-gauge needle was tunneled under the skin. The catheters (carotid and jugular or gastric) were threaded through the needle to tunnel out of the back of the mouse. The ventral incisions were closed with a nylon suture. The arterial catheter was clamped with micro-serrefine at the incision site between the shoulder blades. The catheter was cut 1 cm above the clamp and connected to the MASA™ with a silk suture and repeated for the either the venous or gastric catheter. The dorsal incision was closed with nylon sutures.

Special attention was given to post-operative care to assure each mouse fully recovered within a 5-7 day timeline before performing each study by observing body weight, grooming behavior, and other signs of stress daily. This care was important to perform quality studies. Mice were immediately placed into clean cages, which sit on a heating pad. Animals were observed daily for any abnormal behavior cues and weighed daily.

Surgical procedures are outlined in the Vanderbilt Mouse Metabolic Phenotyping website for their annual clamping course (www.mc.vanderbilt.edu/mmpc) (113).

In Vivo Experiments

Hyperinsulinemic-Euglycemic Clamp (insulin clamp)

Mice were allowed to recover for five-seven days after surgical implantation of carotid artery and jugular vein catheters. Mice that did not weigh within 10% of the presurgical weight were excluded from any clamp studies. Mice were fasted for 5 h prior to the start of clamps to assure all mice were in the post-absorptive phase. The mice were placed in a 1 L plastic tub at the start of the fast (7:00am) and after an hour acclimation period mice were attached to a swivel from their catheter lines to allow free movement. The method employed by our laboratory differs from those performed by most other laboratories (114, 115) in that mice were not handled and were unstressed (15). Red blood cells were replaced to prevent a fall in hematocrit that would inevitably occur. Samples for basal arterial glucose specific activity were taken at t = -15 and -5 min and arterial insulin at t= -5 min. The clamp was initiated at t=0 min with a continuous insulin infusion ($4 mU \cdot kg^{-1} \cdot min^{-1}$) that persisted for 155 min. Arterial glucose concentrations

were determined at 10 min intervals to provide feedback to adjust the rate of exogenous glucose (glucose infusion rate; GIR) as needed to clamp mice between 150-160 mg/dL. Steady state [3-^{3}H]glucose kinetics were determined at 10 min intervals between *t*= 80-120 min. The [3-^{3}H]glucose infusion began at *t*= -90 min to allow for a priming dose (2 µCi/min for 1.2 min, then 0.04 µCi/min) to reach a steady-state level and continued at 0.12 µCi/min during the clamp period. Plasma insulin concentrations during the clamp were determined at *t*= 100 and 120 min. A 13 µCi injection of 2[^{14}C]deoxyglucose (2[^{14}C]2DG) was administered as an intravenous bolus at *t*=120 min. 2[^{14}C]2DG was used to determine the glucose metabolic index (R_g), an indication of tissue specific glucose uptake. Blood samples were then collected at *t*= 2, 15, 25 and 35 min after the bolus to measure the disappearance of 2[^{14}C]DG from the plasma. After the last sample of the insulin clamp, 50 µL yellow DYE-TRAK® 15µm microspheres were injected into the carotid artery to determine microsphere content in skeletal muscle and the left and right kidney. Clamp setups are depicted in Figures 2.1-2.3.

Saline Clamp

Saline infusion protocols were performed using the same design as the insulin clamp. However, saline was infused in lieu of insulin and glucose during the 155 min clamp period. This setup permitted the measurement of fasting muscle glucose uptake and served as a time control for the insulin clamp.

Glucose Tolerance Tests

One week prior to glucose tolerance tests (GTT), mice had indwelling carotid artery and gastric catheters surgically implanted for sampling and glucose administration. Mice were studied in the postabsorptive state after a 5 h fast. Baseline arterial glucose and insulin measurements were obtained via the arterial catheter to avoid handling of mice. Mice were then administered 2g/kg body weight of glucose through the gastric catheter. The gastric catheter permitted the mice to absorb the glucose via physiological mechanisms and to avoid a stress response from intraperitoneal injection or gavage. Arterial glucose was measured at 5, 10, 15, 20, 30 45, 60, 90, and 120 min after glucose administration. Arterial insulin levels during the GTT were assessed at 10, 20, 30, 60, and 120 min.

Body Composition and Cardiac Function

Body composition was determined with a mq10 nuclear magnetic resonance analyzer (Bruker Optics) in 5 h fasted mice. Echocardiogram (Sonos 5500 system; Agilent) was used to assess cardiac function, and blood pressure was measured with a blood pressure transducer via a carotid arterial catheter with the assistance of the Cardiovascular Pathophysiology and Complications Core of the Vanderbilt Mouse Metabolic Phenotyping Center.

Ex Vivo Experiments

Isolated Muscle Glucose Uptake

Isolated soleus (mainly slow-twitch fibers) and extensor digitorum longus (mainly fast-twitch fibers) muscles were obtained from 5 h fasted, anesthetized mice to measure glucose uptake. After a 15 min basal incubation period, muscles were transferred to fresh media and incubated for 30 min in the absence or presence of insulin (10mU/mL). Following stimulation, 2-deoxy-D-glucose uptake was measured for 10 min in fresh media in the absence or presence of insulin, by adding cold 2-deoxy-D-glucose (1mM), 2-[1,2-^{3}H]deoxy-D-glucose (0.25μCi/mL), and D-[1-^{14}C]mannitol (0.16Ci/mL). Muscles were then lysed and radioactivity in the supernatant was measured using liquid scintillation counting (116).

Aortic Ring Reactivity

Mouse aortas were excised after the clamp and placed directly in HEPES buffer (140 mM NaCl, 4.7 mM KCl, 1.0 mM $MgSO_4$, 1.0 mM NaH_2PO_4, 1.5 mM $CaCl_2$, 10 mM glucose, and 10 mM HEPES, pH 7.4). The aortas were equilibrated with 95% oxygen and 5% carbon dioxide at 37°C. The excised aortas were suspended in a muscle bath apparatus. Subcutaneous fat and adventitial tissues were removed after which the aorta was sectioned to create rings. The rings were progressively stretched to an optimal resting tension that produced a maximal response to contractile agents. Force measurements were obtained with a Radnoti Glass Technology force transducer interfaced with a Powerlab data acquisition and Chart Software (ADInstruments).

Contraction was first generated with 110 mM KCl to determine functional viability and the rings that did not contract were discarded. Functioning aortic rings were equilibrated in bicarbonate buffer for 30 min and then contraction was induced by phenylephrine (10^{-6} M). Percent endothelial relaxation was measured from precontracted rings that were treated with carbachol (5×10^{-7} M). Quality of the intact endothelial layer was determined by whether carbachol induced vasoconstriction in lieu of dilation. Carbachol causes smooth muscle dependent constriction in the absence of functional endothelium. Sodium nitroprusside (10^{-7} M) was applied to determine smooth muscle specific relaxation. The percent relaxation was calculated by the change in stress compared with the maximal tension induced by phenylephrine (117, 118). Stress was determined by converting force measurements with the following equation:

$$10^5 \text{ N/m}^2 = \text{force (g)} \times 0.0987/\text{area}$$

where the area was equal to the wet weight in milligrams divided by the length divided by 1.055.

P**rocessing Plasma Samples**

Plasma Radioactivity

Radioisotopes of glucose were infused during the insulin clamp protocol to measure steady-state plasma [3-^{3}H]glucose and the disappearance of plasma 2[^{14}C]DG after the venous injection. Plasma samples were treated with diluted 0.3 N barium hydroxide and 0.3 N zinc sulfate for deproteinization. Radioactivity of plasma [3-^{3}H]glucose and of 2[^{14}C]DG were assessed by liquid (Ultima Gold; Packard) scintillation

counting (Packard TRI-CARB 2900TR). Samples for the measurement of plasma [3-^{3}H]glucose underwent a drying procedure to remove all $^{3}H_2O$ from the plasma as a result of glycolysis of the radioactive glucose tracer.

Plasma Enzyme-Linked Immunosorbent Assay of Insulin

Plasma insulin was collected during all the insulin and saline clamps performed at indicated times from each protocol. Ten µL of plasma, standard, and control were transferred into a 96-well plate as instructed by the manufacturer (80-INSMS-E01; Alpco). The supplied plate has mouse monoclonal antibodies specific for insulin immobilized to each well. A conjugate was added that includes horseradish peroxidase enzyme labeled monoclonal antibody resulting in the insulin from the plasma samples to be sandwiched between the immobilized and conjugate antibodies. Unbound conjugate was washed and TMB substrate added for incubation. The final step was the addition of a stop solution and the optical density was measured at 450 nm with a reference at 620 nm. The intensity of the optical density read at 450 nm was proportional to the amount of insulin from the plasma sample.

Plasma Non-Esterified Fatty Acid

Non-esterified free fatty acids (NEFA) were assessed spectrometrically by an enzymatic calorimetric assay (NEFA C Kit; Wako Chemicals). Basal FFAs were an average of samples taken at t= -15 and -5 min and the FFA levels during the insulin clamp were the average at t= 80 and 120 min. Whole blood was collected in EDTA tubes

and the plasma transferred to dried THL. The NEFA assay is based on the following chemical reactions:

$$\text{NEFA} + \text{ATP} + \text{CoA-SH} \xrightarrow{\text{ACS}} \text{Acyl-CoA} + \text{AMP} + \text{PPi}$$

$$\text{Acyl-CoA} + O_2 \xrightarrow{\text{ACOD}} \text{2,3-trans-Enoyl-CoA} + H_2O_2$$

$$2\ H_2O_2 + \text{4-Aminophenazone} + \text{MEHA} \xrightarrow{\text{POD}} \text{Quinoneimine-color} + 4H_2O$$

The intensity of the red pigment was proportional to the NEFA concentration of the plasma sample. The ascorbic acid was removed by ascorbate oxidase and the absorbance of the 96-well plate read at 550 nm.

Processing Tissue Samples

Tissue Radioactivity

Tissue samples were weighed to approximately 30 mg and the appropriate amount and style of Bullet Blender™ beads were added for tissue homogenization. The combined tissue and beads were homogenized using the Bullet Blender™ in 750 µL 0.5% perchloric acid according to the manufacturer's instructions. Samples were then centrifuged at 13,000 rpm for 10 min. To measure the radioactivity of 2[^{14}C]DG-6-phosphate and 2[^{14}C]DG, 125 µL of the supernatants were transferred directly into a scintillation vial for counting. Another 125 µL aliquot from each sample was deproteinized with 0.3 N barium hydroxide and 0.3 N zinc sulfate. The supernatant, 250 µL, from this mixture was transferred to scintillation vials for the counting of 2[^{14}C]DG.

To determine the quantity of tissue 2[^{14}C]DG-6-phosphate, the amount of 2[^{14}C]DG was subtracted from the total quantity of the tracer within the tissue.

Hepatic Glycogen Content

Liver glycogen content was determined after the insulin clamp and a time control experiment during which saline was infused as previously reported by Chan and Exton (119). The latter experiment was useful in obtaining a measure of fasting liver glycogen for comparison to insulin clamp glycogen concentrations. Livers were homogenized in 10% (w/v) in 0.03 N HCl. The liver suspensions were boiled for 10 min and 200 µL of each sample was transferred to the corresponding chromatography paper and briefly dried. As a standard and control, 200 µL oyster glycogen (5 mg/mL) and 0.03 N HCl were transferred to paper strips. The paper strips were washed 3x for 40 min per wash in a 70% ethanol solution using a stir plate. After the last wash, the ethanol was poured off and the strips were briefly rinsed with acetone. The paper strips were dried overnight in a ventilation hood. The dried strips were transferred into a 5 mL solution of aminoglucosidase containing 20 mg aminoglucosidase, 100 mL 0.2 M NaOAc buffer, and 400 mL distilled water. The tubes were placed in a shaking water bath at 37°C for 3 h. Glucose concentration was then measured enzymatically in a 96 well plate at 340 nm. The following reaction was used:

$$\text{Glucose + ATP} \xrightarrow{\text{Hexokinase}} \text{Glucose-6-phosphate + ADP}$$

$$\text{Glucose-6-phosphate + ADP} \xrightarrow{\text{G6PDH}} \text{6-phospho-D-gluconolactone + NADPH}$$

Standard glucose concentrations were used to measure known equivalent NADPH, which was used to generate a standard curve for the measurement of the absorbance for the glucose concentrations of each sample.

Glycogen Synthase Activity

Liver tissues were homogenized in buffer containing 50 mM Tris buffer, 100 mM sodium fluoride, 10 mM EDTA, 0.5% glycogen, and 5 mM dithiothreitol at pH 6.8. Twenty-five µL of homogenates were added to 50 µL of a solution that contains 50 mM Tris buffer pH 7.5, 5 mM EDTA, 1% glycogen; 1.5 mM UDPG and UDPG labeled with ^{14}C in glucose. The medium for the *synthase* a activity contains 15 mM in Na_2SO_4 and the medium for *total synthase (a + b)* had the sulfate replaced with 3 mM glucose-6-phosphate. The samples were the incubated at 37°C for 0, 15, and 30 min and glycogen was analyzed as described in the previous section. Synthase activity in the presence of glucose-6-phosphate reflects the maximal enzyme activity, while activity in the absence of glucose-6-phosphate reflects the active form of glycogen synthase as previously described (120).

Microsphere Tissue Content

Gastrocnemius and both kidneys were collected in 15 mL polypropylene tubes and digested overnight in 6 mL of 1 M KOH in a temperature controlled oven set to 60°C. After the overnight incubation, the tubes were vortexed to completely homogenize each sample and incubated again at 60°C for 1 h. Each sample was filled to 14 mL total volume with 50°C distilled water. Tubes were centrifuged for 15 min at 1,500 g and the

supernatant aspirated. The pellets were resuspended in 12 mL 10% Triton X-100 and sonicated prior to repeating the centrifugation step for 5 min. The pellets were resuspended in 12 mL acidified ethanol and centrifuged. The pellets were resuspended in 12 mL ethanol. After the centrifugation step the samples were left to dry overnight in a ventilation hood. The fluorescent dye in the microspheres was eluted with 150 µL of *N*,*N*-dimethylformide and absorbance measured from 100 µL of each sample. Absorbance was measured at 450 nm (yellow) and 670 nm (blue) in 96-well polypropylene plates. Blue microspheres were added after the overnight digestion to monitor assay recovery to permit correction of microspheres lost during processing. The number of microspheres per muscle was normalized to weight of each tissue processed and the number of microspheres was based on a known standard curve from the manufacturer.

Immunoprecipitation and Immunoblotting

Cardiac, liver, and gastrocnemius samples were homogenized in buffer containing 50 mM Tris-HCl, pH 7.5, 1 mM EDTA, 1 mM EGTA, 10% glycerol, 1% Triton X-100, 1 mM DTT, 1 mM PMSF, 5 µg/mL protease inhibitor, 50 mM NaF, and 5 mM sodium pyrophosphate. Samples were then centrifuged at 13,000 rpm for 20 min at 4°C and supernatants collected. All samples were diluted 1:20 to determine protein concentrations using the Bradford protein assay. Protein was assessed using 96-well plates at a wavelength of 595 nm and albumin protein standards were used to generate a standard curve to calculate protein concentrations. 30 µg of the supernatant was loaded onto 4-12% SDS-PAGE gel and then transferred to a PVDF membrane. All membranes were

blocked in commercially available Odyssey Blocking Buffer or 5% milk for 1 h at room temperature. Membranes were incubated overnight at 4°C with primary antibodies for phosphorylated Akt (Ser 473), total Akt (Cell Signal), glyceraldehyde-3-phosphate dehydrogenase (GAPDH; Abcam), phosphorylated SMAD2 (Ser 465/467; Cell Signal) and total SMAD2 (cell signal). Membranes were washed then incubated with secondary antibodies for α-mouse or α-rabbit IRDye™ 700/800 to be visualized using the Odyssey system (Li-Cor). Enhanced chemiluminescence was performed with horseradish peroxidase conjugated α-rabbit secondary antibody for phospho-SMAD2 visualization. GAPDH was used as the loading control for each blot.

Immunoprecipitation was performed using 500 µg of the gastrocnemius protein supernatant and incubated with 3 µg of IRS-1 antibody (Santa Cruz Biotechnology) overnight at 4° C. Then, 20 µl of protein A/G PLUS-Agarose (Santa Cruz Biotechnology) was added and incubated overnight at 4° C. The mixture was centrifuged at 1,000 g and the supernatant removed. The beads were washed 4 times with cold PBS and centrifugation step repeated. Beads were resuspended in 30 µl NuPAGE LDS loading buffer and heated at 80° C for 5 min. Immunoblots were incubated with primary antibodies for phospho-IRS-1 (Tyr612; Invitrogen) and the p85 subunit of phosphoinositide (PI) 3-kinase (Millipore). For all blots, secondary antibodies were incubated at room temperature for 1 h and visualization and quantifications were performed using the Odyssey imaging system and ImageJ software.

Tissue and Plasma VEGF Protein

The gastrocnemius and cardiac muscles were homogenized in a lysis buffer containing 50 mM Tris-HCl (pH 7.4), 150 mM Na Cl, 0.5% Triton X-100, and protease inhibitors (Halt™ Protease Inhibitor Cocktail; Fisher Scientific) as previously described (76). Tissue homogenates were centrifuged at 4°C, 7200 g, for 10 min and protein content measured. The plasma and tissue VEGF concentrations were assayed by the manufacturer's specifications (VEGF ELISA Kit, Mouse No. QIA52; Calbiochem), which detects $VEGF_{120}$ and $VEGF_{164}$ isoforms.

Immunohistochemistry Analysis of Capillary Density and Extracellular Matrix Composition

CD31, collagen III, and collagen IV proteins were assessed by immunohistochemistry in paraffin-embedded cardiac, skeletal, and liver sections. Five µm sections were incubated for 60 min with anti-CD31 (BD Biosciences), collagen III (CosmoBio), and collagen IV (Abcam) primary antibodies. Slides were counterstainted with Mayer hematoxylin. The EnVision+HRP/DAB System (DakoCytomation) was used to produce localized, visible staining with assistance from the Vanderbilt University Immunohistochemistry Core. Images were obtained using a Q-Imaging Micropublisher camera mounted on an Olympus microscope. Muscle capillary density was determined by counting CD31 positive structures. Collagen protein content was quantified by measuring integrated intensity of staining. Quantification was carried out by ImageJ software.

Transmission Electron Microscopy of Skeletal Muscle Capillaries

Mice were anesthetized and chest cavity opened for insertion of a catheter into the left ventricle. With gentle pressure, cacodylate buffer (0.1 M) was perfused through the mouse vascular system to rinse erythrocytes from the circulation (~50 mL). Once flow was confirmed by observing rigidity in organs such as the kidney, the liver was nicked to relieve pressure to prevent rupture of blood vessels. Blood and buffer leaked from the liver until the solution was a pale pink, which indicates the mouse had been sufficiently rinsed with the buffer. At this time point the buffer was replaced with 2.5% glutaraldehyde in cacodylate buffer (~75 mL) to allow for muscle fixation. Contractino of the arms and legs indicated that the muscle had been appropriately fixed. The left red gastrocnemius was excised from the mouse and cut into pieces (less than 1 mm on two sides) and placed in a vial of fresh fixative. The tissues were allowed to rest for 1 h and then placed into a 4°C refrigerator until further processing.

Once samples were fixed the Vanderbilt University Cell Imaging Shared Resource Core further processed the samples for transmission electron microscopy. The tissues were dehydrated through a series of diluted ethanol up to 100% and embedded in Spur resin. Thick sections (0.5 µm) were cut and stained with toluidine blue for light microscopic examination to select regions of interest. An area of 500 µm x 500 µm was selected from each sample with equivalent cross sections to permit equivalent imaging across all samples. Thin sections were cut (80 nm) from the regions of interest and examined using a Philips/FEI T-12 transmission electron microscope operated at 80 kilo-electron volts. Capillary structures were identified with a random and unbiased technique that allows the location of a structure at low magnification to be marked by observing the

section grid without detecting ultrastructures. Images were acquired at 67,000 magnification for quantification of caveolae area per endothelial cell area.

ImageJ software was used to quantify the caveolae area per single endothelial cell capillary within skeletal muscle. ImageJ generates a random grid box that overlays the micrograph and by counting the number of points within the caveolae / number of points within the endothelial cell permits calculation of area of caveolae per each endothelial cell. Two ImageJ plugins were downloaded for this analysis: Grid and Multipurpose Grid (121-123).

Reverse Transcription (RT) Polymerase Chain Reaction (PCR)

Total RNA was isolated from liver tissue using the RNeasy Mini Kit (Qiagen). Total RNA (1 mg) was reverse transcribed using the iScript cDNA Synthesis Kit (Bio-Rad). RNA concentration and quality were measured at absorbance wavelength 260 and 280 nm. Real-time PCR was then performed using TaqMan® Universal PCR Master Mix (Applied Biosystems) on the CFX Real Time PCR Instrument (Bio-Rad). Expression of phosphoenolpyruvate carboxykinase (PEPCK) and glucose-6-phosphatase (G6Pase) were measured. Data were normalized with either control gene, ribosomal protein 18S.

Primer	Assay ID
PEPCK	Mm01247058_m1
G6Pase	Mm00839363_m1
18S	Mm03928990_g1

Table 2.2 – RT- PCR assay ID numbers purchased from Life Technologies

Gelatin Zymography

The activation of MMP-2 and -9 were determined using the gelatin zymograph technique. Gastrocnemius muscles were homogenized in buffer containing 0.5% Triton X-100, 100 mM EDTA, and 10 µL/mL protease inhibitor (pH 7.5). Homogenates were centrifuged at 13,000 rpm for 20 min. Supernatants were incubated at 4°C for 2 h with 40 µL of gelatin-Sepharose (Pharmacia) to concentrate the protein and washed 3x with equilibration buffer containing 200 mM NaCl. The gelatin-Sepharose beads were resuspended in 20 µL of 4x nonreducing SDS-sample buffer and loaded on 10% zymogram gels (Invitrogen). The gel was incubated at 37°C in a buffer containing 50 mM Tris-HCl, 0.2 M NaCl, 20 mM $CaCl_2$, pH 7.4 for 12 h. Gels were stained with Coomassie brilliant blue R-250 0.5% (w/v) in 45% methanol (v/v), 10% ascetic acid (v/v), and destained in the solution without Coomassie. Gels were developed according to manufacturer's instructions and quantified using ImageJ software.

Calculations

Glucose Flux Analyses

Glucose production (Ra) and disappearance (Rd) were calculated using Steele non-steady state equations (124). The endogenous Ra was determined by subtracting the GIR rate during the clamp from the total Ra. When the tracer infusion was in steady-state, which should correspond to minutes 80-120 of the clamp, the equation for Ra simplifies:

$$Ra = \frac{I}{SA}$$

where I is the tracer infusion rate and SA is the specific activity of the tracee (dpm/mg). To measure the index for tissue glucose uptake (Rg), the following equation was applied (86):

$$Rg = \frac{2[^{14}\mathrm{C}]\mathrm{DGP}_{\mathrm{tissue}}}{AUC2[^{14}\mathrm{C}]DG_{\mathrm{plasma}}} \times [arterial\ glucose]$$

where $2[^{14}\mathrm{C}]\mathrm{DGP}_{\mathrm{tissue}}$ is the $2[^{14}\mathrm{C}]$DGP in the muscle (dpm/g), $AUC2[^{14}\mathrm{C}]DG_{\mathrm{plasma}}$ is the area under the curve for the disappearance of plasma $2[^{14}\mathrm{C}]DG$ (dpm·min·mL^{-1}), and $[arterial\ glucose]$ is the average blood glucose (mmol/L) from t= 122-155 min of the clamp.

Western Blot and RT-PCR Quantification

Western blot protein intensities were determined by ImageJ or Odyssey software analysis image intensity and all proteins were normalized to GAPDH. Real-time RT-PCR gene expression levels were analyzed using the $2^{-\Delta\Delta Ct}$ method (125) and presented as relative expression. GAPDH or 18S were used to standardize for gene loading of each sample.

Statistical Analysis

Student *t*-test or two-way ANOVA, followed by Tukey's post hoc tests when appropriate, were used to determine statistical significance. Data are expressed as mean ± SE. The significance level was $P \leq 0.05$.

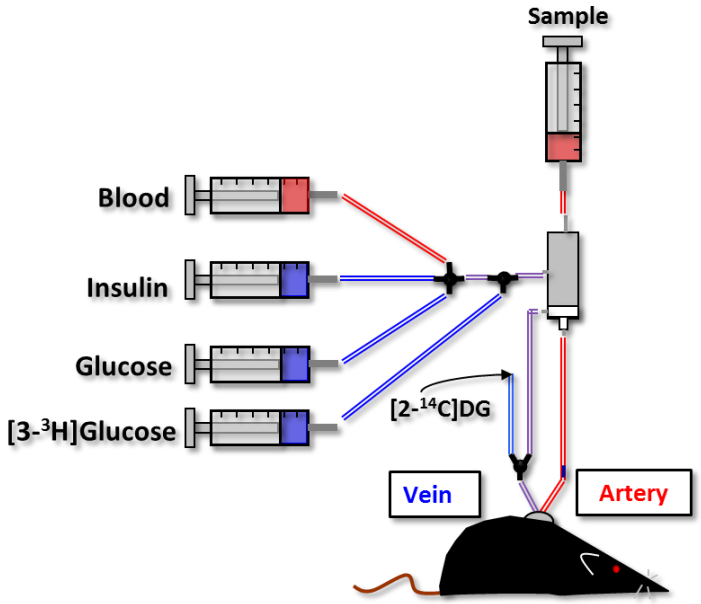

Modified from *Glucose Clamping the Conscious Mouse* by Vanderbilt MMPC 2005

Figure 2.1 – Experimental setup for the hyperinsulinemic-euglycemic clamp

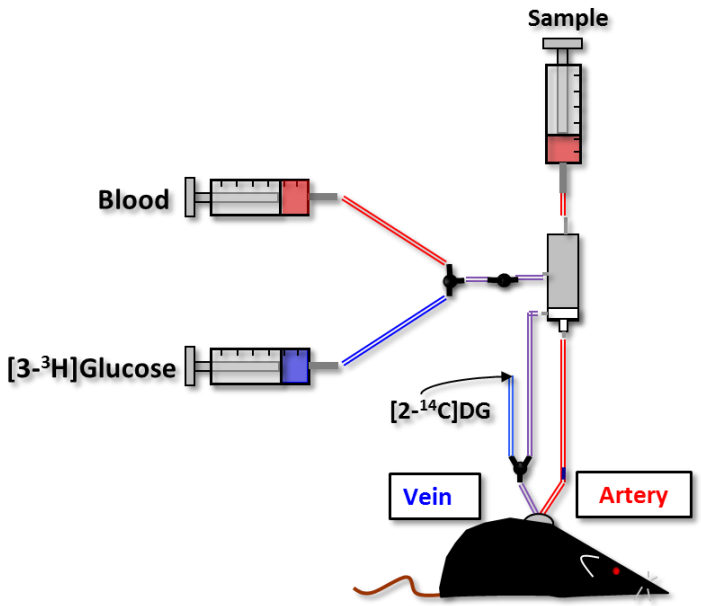

Modified from *Glucose Clamping the Conscious Mouse* by Vanderbilt MMPC 2005

Figure 2.2 – Experimental setup for the saline clamp

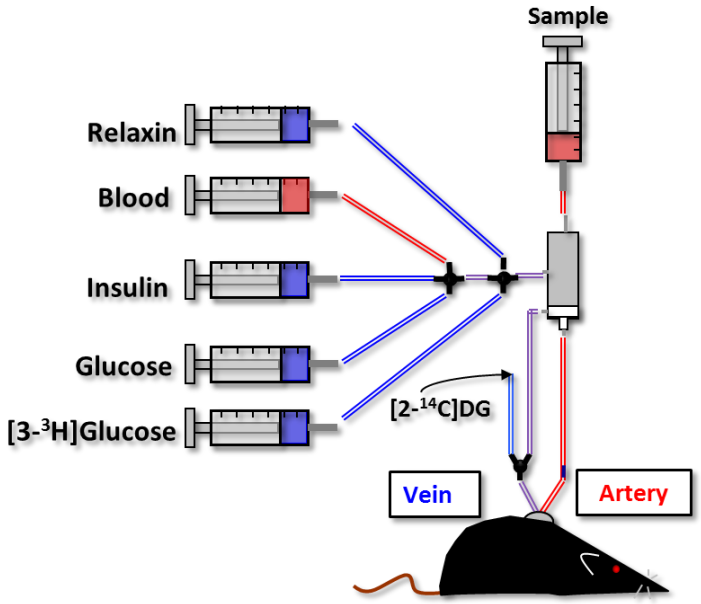

Modified from *Glucose Clamping the Conscious Mouse* by Vanderbilt MMPC 2005

Figure 2.3 – Experimental setup for the hyperinsulinemic-euglycemic clamp with acute relaxin infusion

Chapter III

LOSS OF VASCULAR FUNCTION: CAPILLARY RAREFACTION IS SIGNIFICANT TO THE PATHOGENESIS OF SKELETAL MUSCLE INSULIN RESISTANCE

Aims

The goal of Chapter III was to determine whether capillary rarefaction is a cause or a consequence of muscle insulin resistance. The microvascular adaptations that are present in insulin resistance have been well established. However, previous studies rely on correlative data that suggests a causative relationship between capillary rarefaction and skeletal muscle insulin resistance. The current Aim investigated whether a decrease in the number of capillaries that perfuse skeletal muscle directly impairs insulin-stimulated MGU in otherwise healthy mice. To address this Aim, mice with muscle-specific genetic deletion of vascular endothelial growth factor-A were utilized to induce muscle capillary rarefaction in low fat chow-fed mice. This genetic mouse model permits the investigation into the specific consequence of reducing capillary number to insulin-stimulated MGU. The hypothesis tested within Chapter III was that capillary rarefaction specifically impairs insulin-stimulated MGU by increasing the resistance to the delivery component of MGU.

Introduction

Insulin resistance is closely associated with cardiovascular disease and together are central to the metabolic syndrome (126). Skeletal muscle contributes ~80% of insulin-mediated glucose disposal, thus impairments in insulin-stimulated MGU are critical to the pathogenesis of insulin resistance. Pharmacologically limiting glucose and insulin delivery to the muscle impairs insulin-stimulated MGU (59). Moreover, there is a correlation between reduced blood flow to the muscle and insulin resistance (17, 18, 31, 47). Recent studies have linked diet-induced extramyocellular adaptations to insulin resistance in rodent models (53, 87, 127) and humans (111). The number of capillaries perfusing the muscle is positively related to peripheral insulin action - independent of age, body composition, energy expenditure, and lipid status (128). The important question that remains to be answered is whether the reduction in capillaries is a cause or consequence of muscle insulin resistance.

Insulin recruits unperfused capillaries which enhances nutrient blood flow to metabolically active muscle. The augmented microvascular blood volume precedes insulin-stimulated MGU (45). Studies estimate that 40% of insulin-stimulated MGU results from increased muscle perfusion and this hemodynamic response is absent in patients with type 2 diabetes (36, 37, 47, 48, 50, 57, 59). Muscle capillarity is an important predictor of insulin-mediated glucose disposal and, accordingly, insulin resistant humans and rodents exhibit capillary rarefaction (51, 53-55, 80). Pharmacological agents that target the vasculature to increase tissue perfusion also improve skeletal muscle insulin resistance and augment muscle microvascular density

(53, 86, 87). This affirms the importance of restoring skeletal muscle perfusion in ameliorating insulin resistance (53, 86, 87, 129).

The vascular endothelial growth factor (VEGF) family of proteins regulate vasculogenesis, angiogenesis, and lymphanogenesis (130). In particular, VEGF-A stimulates the formation of new vascular networks by recruiting and differentiating endothelial progenitor cells in addition to inducing endothelial cell proliferation and migration (130). Insulin resistant states are characterized by impaired VEGF-A action in the vascular beds of cardiac and skeletal muscle triggering capillary regression (51, 79, 82, 131). Cardiac and skeletal myocellular VEGF-A production regulates capillarity by paracrine signaling to the endothelium (75, 76). Capillary density correlates with the severity of insulin resistance in obesity; however, the specific effect of capillary rarefaction to the pathogenesis of skeletal and cardiac muscle insulin resistance has not been elucidated (53, 54, 127, 128).

The experiments described herein test the hypothesis that skeletal and cardiac muscle capillary rarefaction, in lean, otherwise healthy mice impairs muscle insulin action. Genetic deletion of skeletal and cardiac muscle VEGF-A (referred to as VEGF in subsequent sections) was used to selectively reduce muscle capillarity in lean mice to determine the specific consequence of capillary rarefaction on insulin-stimulated MGU.

Experimental Design

Mice with genetic deletion of skeletal and cardiac muscle VEGF-A ($mVEGF^{-/-}$) and wild-type ($mVEGF^{+/+}$) were studied as a genetic model of capillary rarefaction. This

model permits the investigation of the direct effects of microvascular density, independent of another known insulin resistant insult (e.g. diet), in the pathogenesis of muscle insulin resistance. Mice were fed a low fat chow diet for 9 weeks and glucose regulatory effects were studied at 12 weeks of age. To determine the effects of capillary rarefaction on glucose kinetics mice either underwent an insulin clamp (Figure 3.1), saline clamp (Figure 3.2), or glucose tolerance test (Figure 3.3). Cardiac function was assessed by echocardiography. See Chapter II for detailed methods.

Results

Adaptations to genetic ablation of skeletal and cardiac muscle VEGF

There were no differences in total body, fat, or lean masses at 12 weeks of age (Table 3.1). VEGF levels in cardiac and skeletal muscle of *mVEGF*$^{-/-}$ mice were undetectable, compared to ~30 pg/mg protein in cardiac and skeletal muscle of *mVEGF*$^{+/+}$ littermates (Figure 3.4A; $p \leq 0.001$). The reduction in VEGF protein corresponded to 60% and 50% decreases in capillary density in skeletal and cardiac muscle respectively (Table 3.1; $p \leq 0.05$). Plasma VEGF levels were similar in both groups (Figure 3.4B). Cardiac output was equal between genotypes (Table 3.1) as heart rate and stroke volume, calculated from the echocardiography, did not differ (data not shown). Furthermore, mean arterial pressure was similar between genotypes (Table 3.1). Left ventricular (LV) volume and LV mass were significantly increased in the *mVEGF*$^{-/-}$ mice but, ejection fraction and fractional shortening were 2 and 2.5-fold lower (Table 3.1; $p \leq 0.05$).

$mVEGF^{-/-}$ mice have impaired insulin-stimulated glucose disposal and augmented fasting hepatic glucose turnover

Basal (5 h fasting) and insulin clamp arterial glucose and insulin did not differ between genotypes (Table 3.2). The basal circulating FFA concentrations and the suppression of FFA by insulin were similar between genotypes (Table 3.2). The steady-state GIRs were equal (Figure 3.5B). Fasting endogenous glucose production ($EndoR_a$) and glucose disappearance (R_d) were 1.6-fold greater in $mVEGF^{-/-}$ mice (Figure 3.5C and D; $p \leq 0.05$). The relative gene expression for phosphoenolpyruvate carboxykinase (PEPCK; Figure 3.6D) was not different between genotypes, however, glucose-6-phosphatase (G6Pase; Figure 3.6D; $p \leq 0.05$) was higher in $mVEGF^{-/-}$ mice and may have contributed to the augmented fasting $EndoR_a$. The suppression of $EndoR_a$ and the absolute whole-body R_d during insulin stimulation were similar between groups (Figure 3.5C and D). Notably, the increase in insulin-stimulated glucose disposal was blunted by 56±16% in the $mVEGF^{-/-}$ mice suggesting an impairment in peripheral insulin action (Figure 3.5E; $p \leq 0.05$). The results from the GTTs (Figure 3.6A) indicated that $mVEGF^{-/-}$ mice were less glucose tolerant than their wild-type littermates. The area under the curve for the first 30 min (Figure 3.6C; $p \leq 0.05$) of the GTT was greater in the $mVEGF^{-/-}$ mice and the insulin response did not differ except for the 60 min time point (Figure 3.6B).

Consistent with the impairment in insulin-stimulated whole-body R_d, insulin-stimulated R_g in skeletal and cardiac muscle in $mVEGF^{-/-}$ mice was also abated compared to $mVEGF^{+/+}$ littermates (Figure 3.7A and B; $p \leq 0.05$). Insulin-stimulated R_g is the difference between the R_g during the insulin clamp and an average R_g from the saline-infused cohort of mice. The data obtained from these saline-infused time controls permit

the quantification of the specific effect of insulin on R_g. Furthermore, *in vivo* insulin signaling in skeletal muscle was attenuated during the insulin clamp evident by a decrease in the association of the p85 subunit of PI 3-kinase with phospho-IRS-1 (Figure 3.8B; $p \leq 0.05$). Interestingly, downstream Akt activation, which is central to multiple signaling pathways in muscle, was unaffected during the insulin clamp (Figure 3.8D).

Muscle Insulin action is decreased in *mVEGF*$^{-/-}$ mice *in vivo,* but not *in vitro*

Glucose uptake was analyzed on isolated muscle, thus removing the extramyocellular barriers to MGU. Isolated MGU was determined in the soleus (slow-twitch) and extensor digitorum longus (EDL) (fast-twitch) muscles. The basal and insulin-stimulated glucose uptake in isolated skeletal muscles were equal between genotypes (Figure 3.9) suggesting no direct impairment of insulin action at the myocyte. The data in isolated muscle contrasts with the muscle glucose uptake and insulin signaling data from the insulin clamp, which were diminished as described above. These data indicate insulin action was impaired by muscle VEGF deletion in the whole organism where extramyocellular factors are present, but not in isolated muscle where they are not. This strongly suggests that muscle VEGF deletion results in resistance to insulin because of an impaired capacity to deliver insulin to the sarcolemma.

Liver glycogen content was greater in *mVEGF*$^{-/-}$ mice after the insulin clamp

Whole-body R_d was elevated in the basal state of *mVEGF*$^{-/-}$ mice and equal during the insulin clamp. Liver glycogen content was assessed after the insulin clamp to test the possibility that liver glucose uptake was compensating for the impaired insulin-stimulated

MGU. Consistent with this possibility *mVEGF*$^{-/-}$ mice had a ~two-fold increase in liver glycogen concentrations compared to *mVEGF*$^{+/+}$ littermates (Table 3.2; $p \leq 0.05$). During the time control experiment, where saline was infused in lieu of insulin, fasting (7.5 h) liver glycogen levels (Table 3.2) were minimal and there was no significant difference between genotypes. The greater hepatic glycogen concentration in the *mVEGF*$^{-/-}$ mice was independent of changes in phosphorylation of Akt in the liver (Figure 3.8F) during the insulin clamp. Hepatic glycogen synthase activity was assessed after the insulin clamp. *mVEGF*$^{-/-}$ mice tended to have greater glycogen synthase activity (Table 3.2; $p = 0.08$) which likely contributes to the greater liver glycogen content after the insulin clamp. Thus, indirect adaptations at the liver may counterbalance the diminished insulin-stimulated MGU and explain the similar total glucose utilization between the two genotypes during insulin stimulation (Figure 3.5B).

Discussion

These studies demonstrate that capillary rarefaction impairs muscle insulin action *in vivo*. Our data support the paradigm that capillary regression contributes to the pathogenesis of skeletal muscle insulin resistance. Diabetic states are characterized by muscle capillary regression which results from impaired VEGF action (75, 80). Here we show that local VEGF deletion is sufficient to cause muscle insulin resistance due to diminished muscle capillary density. Although the decrease in muscle capillaries is substantive it is also possible that an alteration in the vessel wall that affects permeability to insulin occurs. Previous studies have shown muscle capillarity strongly correlates with insulin-sensitivity (54, 55). Furthermore, serveral therapeutic treatments that reverse

muscle insulin resistance in mice augment capillary density (53, 87). Our data illustrates that attenuating capillarity specifically in muscle blunts insulin-stimulated R_d due to diminished muscle R_g, without directly affecting myocellular insulin action. Additionally, *mVEGF*$^{-/-}$ mice were less glucose tolerant than their wild-type littermates despite similar insulin responses to a glucose load. These data emphasize the importance of increased muscle blood volume and capillary surface area for the delivery of insulin and glucose to skeletal muscle during hyperinsulinemia (37, 45, 59).

The reduced insulin-stimulated MGU in *mVEGF*$^{-/-}$ mice was not attributable to impaired insulin action directly at the myocyte; however, *in vivo* insulin signaling during hyperinsulinemia was blunted in *mVEGF*$^{-/-}$ mice suggesting a defect in insulin delivery. There was no difference in *ex vivo* insulin-mediated glucose uptake in isolated muscles. Measuring glucose uptake in isolated muscle removes the vascular delivery component of MGU eliminating the difference between genotypes evident during the insulin clamp. Skeletal muscle does not express VEGF receptors indicating the decrease in muscle VEGF does not have direct effects at the myocyte (132). The association of the p85 subunit of PI 3-kinase with phospho-IRS-1 during the insulin clamp was attenuated in *mVEGF*$^{-/-}$ mice, though skeletal muscle Akt activation was preserved. Kim et al. demonstrated that insulin stimulated phosphorylation of Akt in diabetic muscle was normal and the primary deficiency in insulin signaling was attributed to a decrease in PI 3-kinase association with IRS-1 (133). Our data are consistent with studies that showed the critical role of glucose and insulin delivery to insulin-stimulated MGU (17, 18, 27, 36, 86). Moreover, in genetic- and diet-induced models of muscle insulin resistance the physiological actions of insulin to increase muscle microvascular recruitment and nutrient

blood flow are impaired resulting in an abatement in insulin and glucose delivery to the myocyte (18, 35, 47, 48, 134). The present data demonstrate that the attenuation in muscle capillary density associated with insulin resistance, in the absence of other primary defects, is capable of seriously diminishing insulin-stimulated MGU due to decreases in insulin and, likely, glucose delivery to the myocyte. It is also possible that other nutritional or endocrine factors that are deficient with poor muscle perfusion are necessary for the full response to insulin *in* vivo. These studies clearly demonstrate that a loss in muscle capillaries causes a marked impairment in muscle insulin action, thus, supporting the paradigm that capillary rarefaction in insulin resistant human skeletal muscle is not simply a consequence of the disease but central to the pathogenesis of muscle insulin resistance.

At rest ~30% of capillaries are required to maintain the demand for skeletal muscle perfusion (135, 136). As a result of the low number of capillaries necessary to maintain nutrient blood flow, there was no defect in fasting MGU in *mVEGF*$^{-/-}$ mice (data not shown). Physiological hyperinsulinemia recruits unperfused capillaries doubling the microvascular blood volume in the muscle (35, 137). The augmented insulin and glucose delivery to the muscle interstitium during hyperinsulinemia is dependent on the increased surface area for substrate exchange induced by insulin-mediated capillary recruitment (27, 35, 137). The ~60% attenuation in skeletal muscle capillary density in *mVEGF*$^{-/-}$ mice resulted in an impairment in glucose uptake during steady-state hyperinsulinemia. This effect is similar to the decrease in capillary recruitment that prevents an increase in muscle blood volume and impairs muscle insulin action in obese, type 2 diabetic individuals (35).

In our model of muscle specific VEGF deletion, cre-recombinase is under the MCK promoter which is not expressed until fetal day 16 and then is upregulated post-birth (138). This time course of VEGF ablation limits developmental abnormalities. VEGF expression is critical for embryonic development and the loss of a single VEGF allele in the whole organism causes embryonic lethality with developmental abnormalities evident by day 9.5 of gestation (71, 72). Furthermore, endothelial-specific deletion of VEGF results in endothelial apoptosis and sudden death in 55% of mutant mice by 25 weeks of age which indicates the importance of autocrine VEGF signaling in the maintenance of endothelial integrity in the adult animal (78). Olfert et al. showed in muscle-specific VEGF deficient mice that the attenuation in skeletal muscle capillary density occurs as early as at 1 month of age (76). The myocellular paracrine signaling of VEGF is essential for the spatial branching of the capillary network and is necessary for muscle capillary architectural organization (75, 77, 139). The capillaries present in *mVEGF*$^{-/-}$ mice are likely a combination of refractory capillaries, VEGF independent capillaries, and vessels present prior to MCK expression that are maintained by autocrine endothelial VEGF signaling.

Diabetic states are characterized by cardiac muscle capillary regression and impaired VEGF action (82, 131). Severe hyperglycemia downregulates VEGF expression, which is seminal in the pathology of diabetic cardiomyopathy (81). Endothelial cells are particularly sensitive to changes in plasma glucose because they are very permeable to glucose. VEGF ablation in our model resulted in a 50% decrease in cardiac capillary density. Notably, compensatory mechanisms kept cardiac output normal. The conserved cardiac output is a mathematical consequence of the decreased

ejection fraction coupled with the increase in left ventricular diastolic volume. The potential relationship of this to the underlying vascular pathology must be speculative at this point. The thinner but larger ventricular cavity might entail less transmural resistance to flow, allowing better capillary perfusion pressure through an attenuated vascular network. Alternatively, the larger endocardial surface area might allow some direct supply of oxygen and nutrients to the immediately adjacent myocardium, a mechanism important in the right ventricle, but potentially significant for the left ventricle in *mVEGF*$^{-/-}$ mice. While the dilation in our model is common to many cardiomyopathic conditions, the preservation of cardiac output may be a consequence of this specific etiology.

Basal glucose flux was elevated in *mVEGF*$^{-/-}$ mice compared to *mVEGF*$^{+/+}$ littermates. Glucose homeostasis was maintained, despite the elevated glucose fluxes. *mVEGF*$^{-/-}$ mice had greater liver glycogen deposition after the insulin clamp; however, there was no significant difference in fasting hepatic glycogen between the two genotypes. The greater liver glycogen in *mVEGF*$^{-/-}$ mice may offset the reduction in insulin-stimulated muscle R_g, explaining the equal GIRs and absolute whole-body R_d during the insulin clamp. The augmented liver glycogen after the insulin clamp was independent of the phosphorylation status of Akt in the liver. However, glycogen synthase activity tended to be augmented in *mVEGF*$^{-/-}$ mice. The elevated activity of glycogen synthase likely contributes to the higher hepatic glycogen concentrations in *mVEGF*$^{-/-}$ mice after the insulin clamp. The presence of G6Pase in the liver obviates the use of isotopic 2-deoxyglucose to measure R_g in the liver, thus, no precise measurement of hepatic glucose uptake can be determined with the insulin clamp protocol performed in

the current studies. Moreover, the increased basal glucose turnover suggests accelerated hepatic cycling of glucose independent of hepatic insulin action (140). However, this is unlikely with utilizing [3-^{3}H]glucose. The increased fasting EndoR_a may be due to the greater G6Pase expression in the liver of *mVEGF*$^{-/-}$ mice. The mechanism behind the hepatic adaptation is unclear. However, it is notable that untreated insulin resistant humans also have accelerated glucose production.

The compensatory mechanisms in the *mVEGF*$^{-/-}$ mice cannot be attributed to changes in circulating VEGF levels. Thus, the deletion of all VEGF-A variants in muscle is not likely to have direct physiological effects on other tissues. The compensation present in the liver is expected to be a consequence of the impaired insulin-stimulated MGU or perhaps inflammation secondary to heart or skeletal muscle hypoxia resulting from poor perfusion.

These data show for the first time that a reduction in capillary density is sufficient to induce muscle insulin resistance in lean mice. The present investigation is consistent with human data that exhibit a strong relationship between muscle capillary density and insulin-mediated peripheral glucose disposal (51, 52, 55). The results further elucidate the significance of the extramyocellular adaptations present in insulin resistant states, thus, highlighting the importance for novel therapeutic approaches to target the vascular bed of insulin sensitive tissues in the treatment of insulin resistance and type 2 diabetes.

Acknowledgements

This work was supported by National Institutes of Health Grants DK054902 and DK059637 (Mouse Metabolic Phenotyping Center).

The authors thank ZhiZhang Wang of the VMMPC Cardiovascular Pathophysiology Core for performing echocardiography in these studies and thank Melissa B. Downing of the Mouse Pathology Core Laboratory of the Mouse Metabolic Phenotyping Center**.** The authors would also like to thank Dr. Jeffrey N. Rottman for his insightful comments interpreting the echocardiography results.

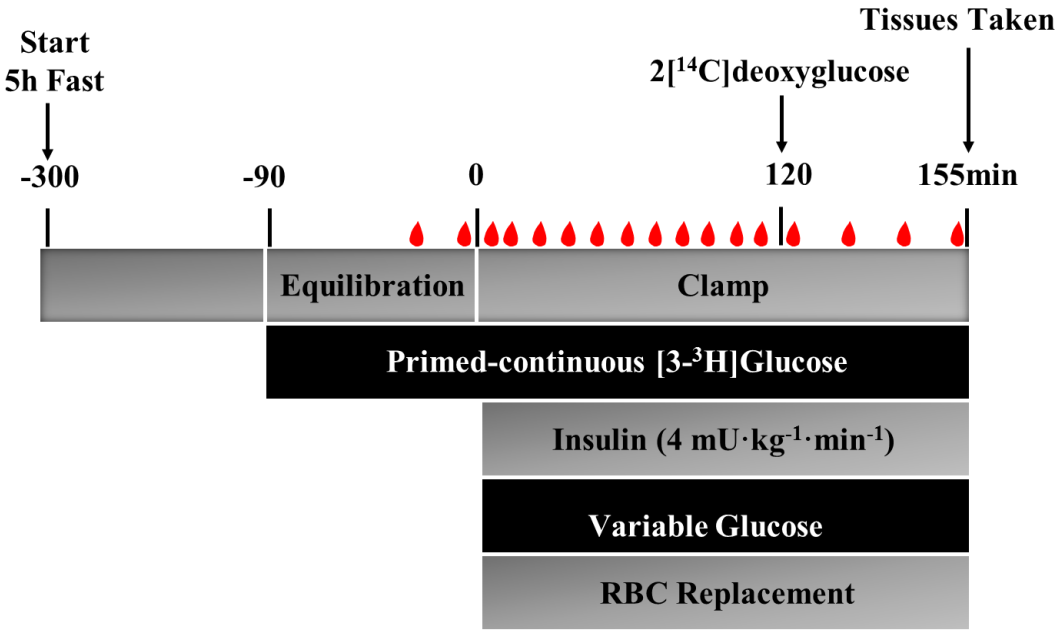

Figure 3.1 – Protocol for the hyperinsulinemic-euglycemic clamps performed in Chapter III. Experiments were performed 7 days after surgical implantation of carotid artery and jugular vein catheters. Mice were fasted for 5 h prior to the onset of the clamp. Primed-continuous infusion of [3-^{3}H]glucose began at *t*= -90 min. At *t*= 0 min insulin was elevated to postprandial levels. Basal blood draws occurred at *t*= -15 and -5 min and blood glucose was measured at 10 min intervals starting at *t*= 0 min. Variable glucose was infused to maintain euglycemia at ~150 mg/dL and red blood cell replacement maintained hematocrit during the study period. 2[^{14}C]glucose was injected intravenously at *t*= 120 min to measure tissue specific glucose uptake.

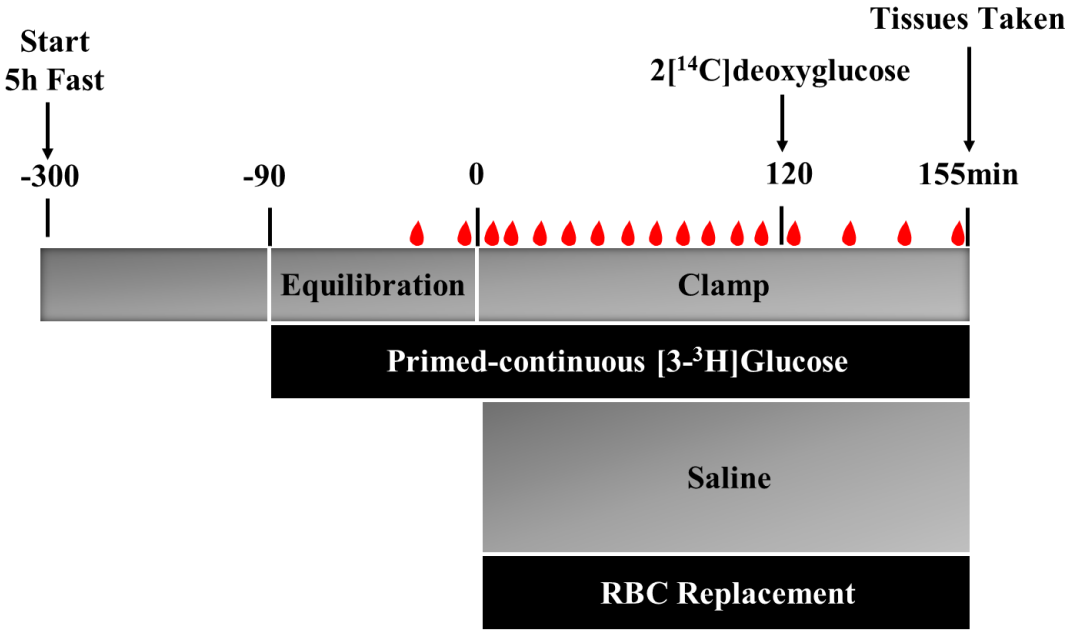

Figure 3.2 – Protocol for the saline clamps performed in Chapter III. Experiments were performed 7 days after surgical implantation of carotid artery and jugular vein catheters. Mice were fasted for 5 h prior to the onset of the clamp. Primed-continuous infusion of [3-^{3}H]glucose began at *t*= -90 min. At *t*= 0 min saline was infused in lieu of insulin. Basal blood draws occurred at -15 and -5 min and blood glucose was measured at 10 min intervals starting at *t*= 0 min. Red blood cell replacement maintained hematocrit during the study period. 2[^{14}C]glucose was injected intravenously at *t*= 120 min to measure tissue specific glucose uptake.

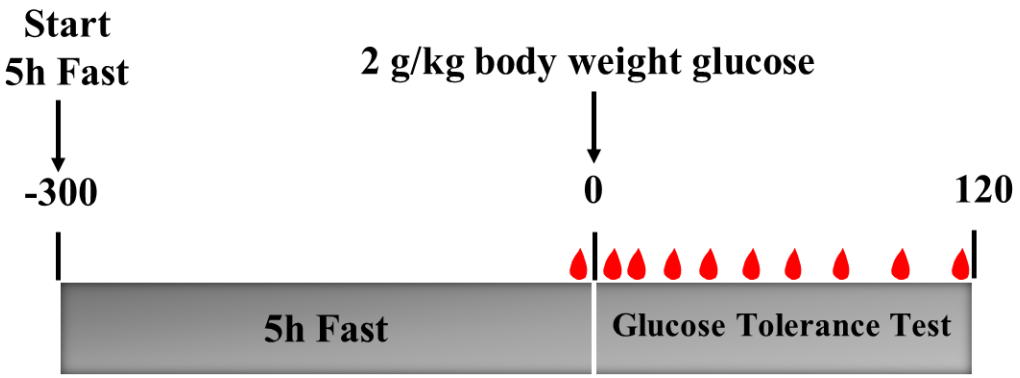

Figure 3.3 – Protocol for the glucose tolerance test performed in Chapter III. Experiments were performed 7 days after surgical implantation of carotid artery and gastric catheters. The gastric catheter permits physiological absorption of glucose without inducing a stress response. Mice were fasted for 5 h prior to the outset. At *t*= 0 min 2g/kg body weight of glucose was administered via the gastric catheter. Blood glucose was assessed at *t*= 5, 10, 15, 20, 30, 45, 60, 90, and 120 min. Plasma insulin was assessed at *t*= 10, 20, 30, 60, and 120 min. Fasting arterial glucose and insulin were measured at t = -5 min.

Table 3.1
Characteristics of muscle specific VEGF deficient mice

	$mVEGF^{+/+}$	$mVEGF^{-/-}$
N	8	9
Weight (g)	26.1 ± 1.5	25.3 ± 0.9
Fat (g)	2.2 ± 0.30	2.1 ± 0.20
Muscle (g)	18.5 ± 1.2	18.0 ± 0.7
Gastrocnemius capillary density†	1.00 ± 0.2	0.41 ± 0.1*
Cardiac capillary density†	1.00 ± 0.06	0.52 ± 0.06*
Mean arterial pressure (mmHg)	117 ± 4.0	108 ± 4.4
Cardiac output (mL/min)	23.9 ± 1.7	21.0 ± 0.6
Fractional shortening (%)	46.6 ± 1.2	18.7 ± 2.0*
Ejection fraction (%)	78.9 ± 1.3	38.5 ± 3.7*
LV diastolic volume (μL)	47.3 ± 4.0	89.5 ± 7.0*
LV mass (mg)	54.6 ± 5.5	66.9 ± 3.4*

Data are expressed as mean ± SE. †Capillary density is quantified by the number of CD 31+ structures normalized to $mVEGF^{+/+}$ mice. LV is the abbreviation for left ventricular. *P-value ≤ 0.05.

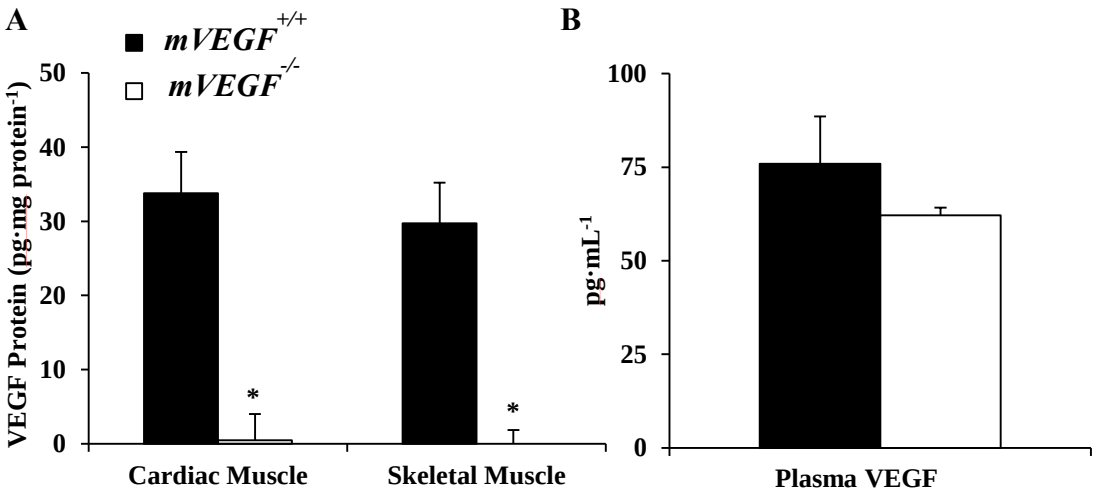

Figure 3.4- (A) VEGF-A protein levels in tissue homogenates from cardiac and skeletal muscle and (B) VEGF-A plasma concentration. Skeletal muscle VEGF levels were quantified in the gastrocnemius. Values are expressed as means ± SE. n = 5, *P-value ≤ 0.05 vs. $mVEGF^{(+/+)}$.

Table 3.2
Fasting and insulin clamp characteristics

	mVEGF$^{+/+}$	*mVEGF*$^{-/-}$
Arterial glucose (mg/dL)		
Basal	119 ± 7	113 ± 5
Insulin clamp	145 ± 3	151 ± 3
Arterial insulin (ng/mL)		
Basal	1.2 ± 0.2	1.6 ± 0.3
Insulin clamp	4.2 ± 0.8	5.2 ± 0.5
Free fatty acids (mmol/L)		
Basal	0.76 ± 0.10	0.76 ± 0.10
Insulin clamp	0.18 ± 0.04	0.17 ± 0.01
Liver glycogen (mg glucose/g liver)	10.0 ± 2.3	18.6 ± 2.1*
Fasting liver glycogen (mg glucose/g liver)	3.90 ± 2.0	8.30 ± 1.9
Glycogen synthase activity†	0.06 ± 0.007	0.09 ± 0.015

Liver glycogen was measured from tissue excised immediately after the insulin clamp and fasting liver glycogen was assessed immediately after the 7.5 h saline infused experiments. †Liver glycogen synthase activity was determined after the insulin clamp and presented as the ratio of glycogen synthase activity in the absence and presence of glucose-6-phosphate. Data are expressed as mean ± SE. n= 7-9, *P-value ≤ 0.05.

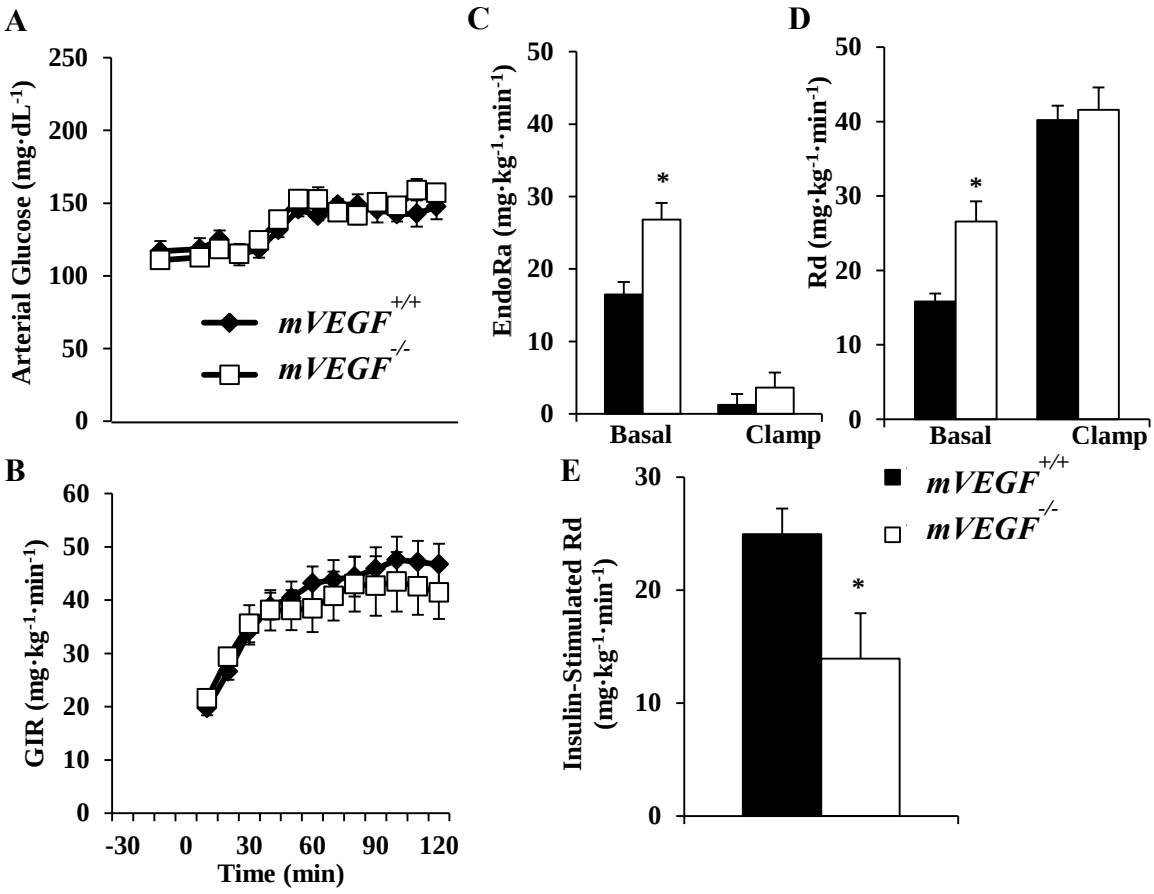

Figure 3.5 - Arterial glucose (A) and glucose infusion rate (B) during the hyperinsulinemic-euglycemic clamp. Mice were fasted 5 h prior to the onset of the clamp. Blood glucose was maintained at ~150 mg/dl during steady-state (80-120 min) and the time course is displayed to demonstrate quality of the clamp. 50% glucose was infused to maintain euglycemia. Endogenous glucose production ($EndoR_a$ - C), whole-body glucose disappearance (R_d - D), and insulin-stimulated glucose disposal (E) determined during the hyperinsulinemic-euglycemic clamp. Basal values were determined from samples at t= -15 and -5 min prior to the onset of the clamp and insulin clamp levels were calculated from steady-state values (80-120 min). Insulin-stimulated R_d was calculated by subtracting the basal R_d from the clamp R_d, which measures the increase in insulin-stimulated glucose disposal. Data are expressed as mean ± SE, n= 7-9,*P-value ≤ 0.05 vs. $mVEGF^{(+/+)}$.

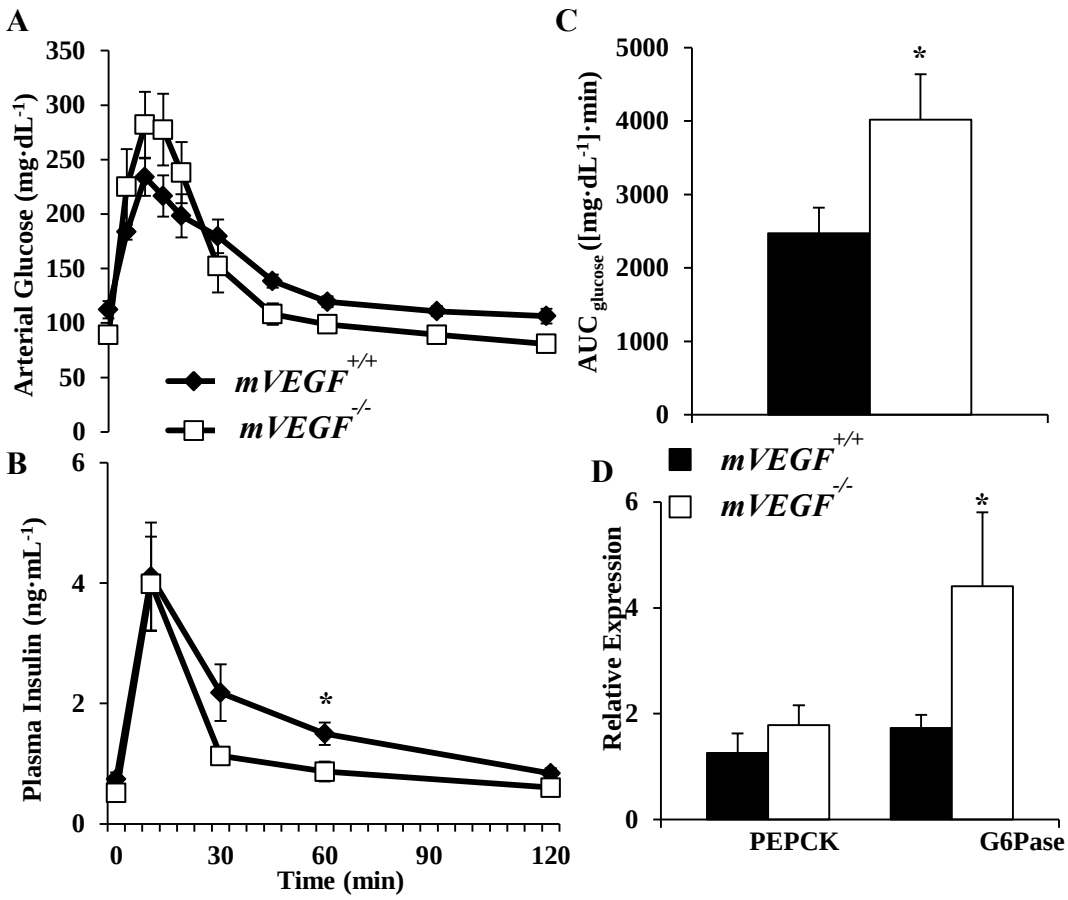

Figure 3.6 - Glucose tolerance was determined (A) and corresponding plasma insulin levels quantified (B) on 5 h fasted mice. The area under the curve (C) was determined from 0-30 min and normalized to fasting arterial glucose concentration. RT-PCR was performed on hepatic RNA extracts from mice fasted for 5 h for the relative expression of the gluconeogenic genes PEPCK and G6Pase (D). Values are expressed as mean ± SE. n=5-6, *P-value ≤ 0.05 vs. $mVEGF^{(+/+)}$.

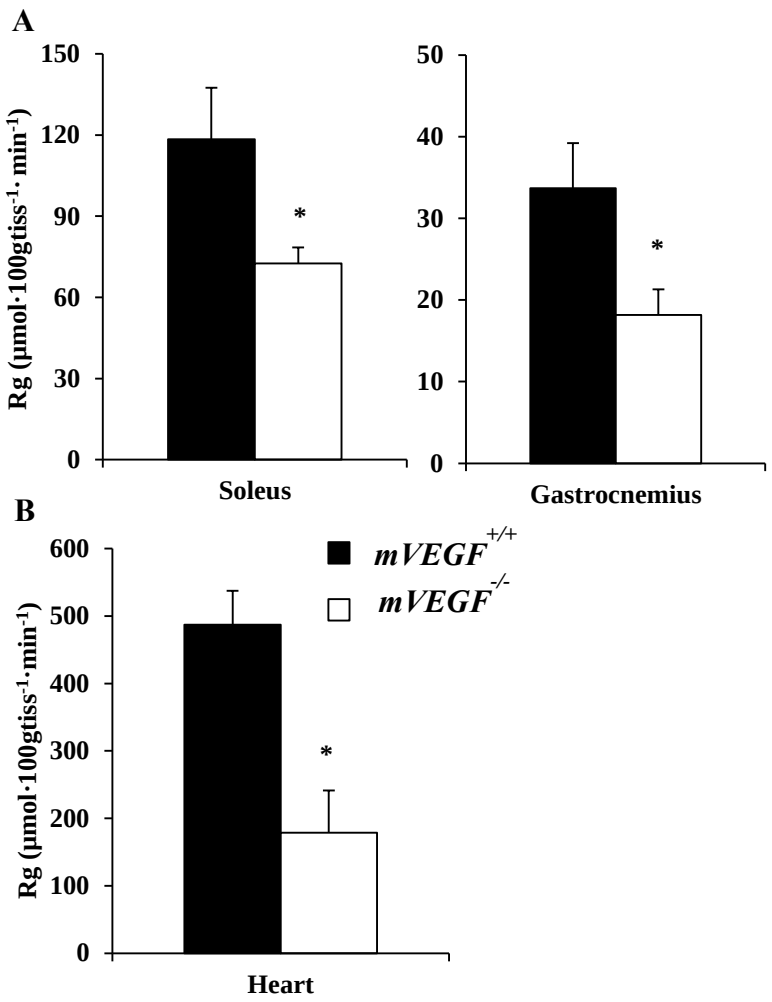

Figure 3.7 - Insulin-stimulated metabolic index (R_g) in skeletal (A) and cardiac (B) muscle. To quantify insulin-stimulated R_g, we performed a time control in a cohort of *mVEGF*$^{(+/+)}$ and *mVEGF*$^{(-/-)}$ mice in which saline was infused in lieu of insulin to quantify basal R_g. The R_g values from the saline infusion were averaged and subtracted from the R_g values during the insulin clamp. Data are expressed as mean ± SE. n= 7-9, *P-value ≤ 0.05 vs. *mVEGF*$^{(+/+)}$.

Table 3.3
Fasting Muscle Glucose Uptake during the Saline Clamp

	mVEGF$^{+/+}$	*mVEGF*$^{-/-}$
Soleus R_g ($\mu mol \cdot 100_{gtissue}^{-1} \cdot min^{-1}$)	9.5	7.6
Gastrocnemius R_g ($\mu mol \cdot 100_{gtissue}^{-1} \cdot min^{-1}$)	5.4	3.4
Heart R_g ($\mu mol \cdot 100_{gtissue}^{-1} \cdot min^{-1}$)	127.5	260.5

Mice were fasted 5 h prior to the onset of the saline clamp. Tissues were collected after 2.5 h saline infusion. Data are expressed as mean ± SE and n= 7-9.

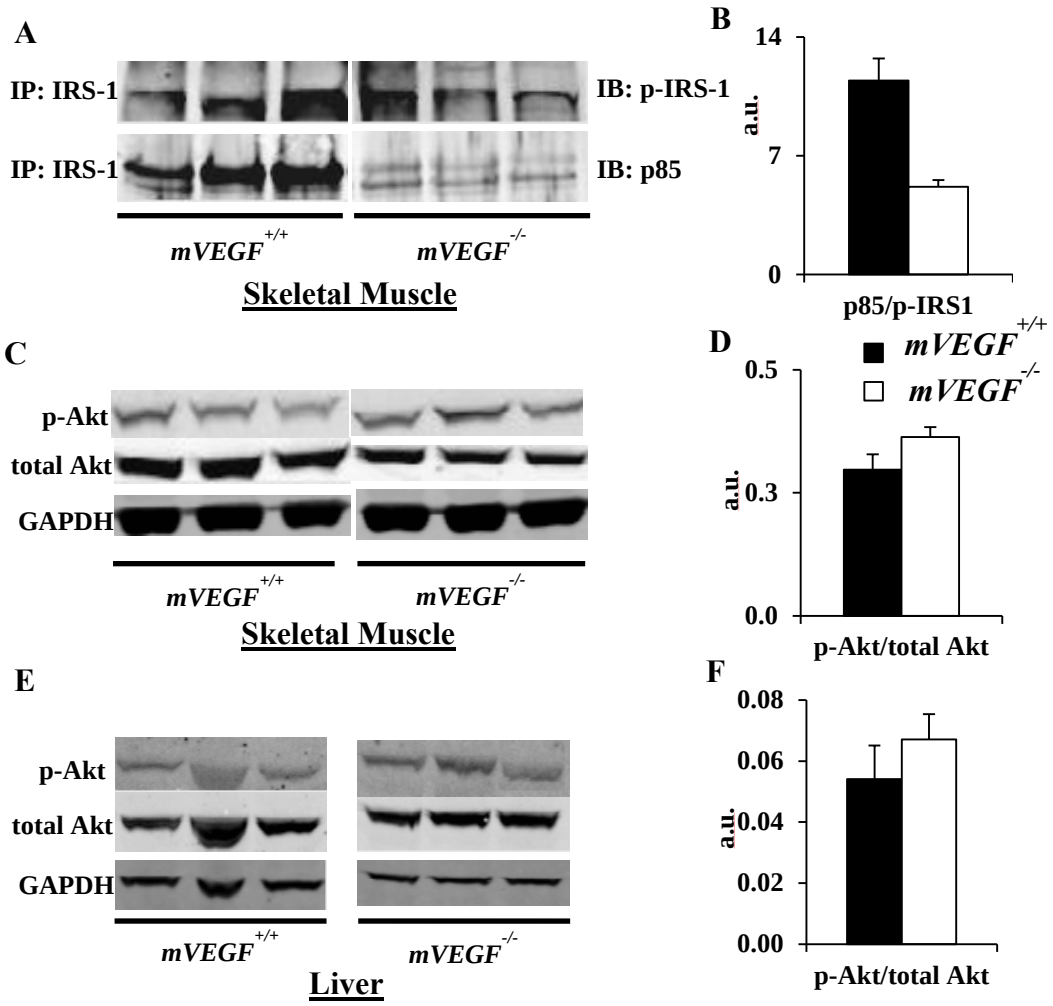

Figure 3.8 - Skeletal muscle and hepatic insulin signaling after the hyperinsulinemic-euglycemic clamp. Western blot analysis was performed on extracts of the gastrocnemius and liver for the phosphorylation of Akt at Ser473 and total Akt. Infrared imaging was performed on 4-12% SDS-PAGE gel in skeletal muscle (A and C) and liver (E). Immunoprecipitation (IP) from gastrocnemius extracts were performed with total IRS-1 then immunoblots (IB) were completed for phospho-IRS-1 at Tyr612 and the p85 subunit of PI 3-kinase (A). Insulin-stimulated p85 association with phospho-IRS-1 was quantified as the ratio of p85 to phospho-IRS-1 (B). Insulin activation of Akt (C and E) was quantified as the ratio of phospho-Akt to total Akt in skeletal muscle (D) and liver (F). GAPDH was used as a loading control. Data are expressed as mean ± SE, n= 5-6, *P-value ≤ 0.05 vs. $mVEGF^{(+/+)}$.

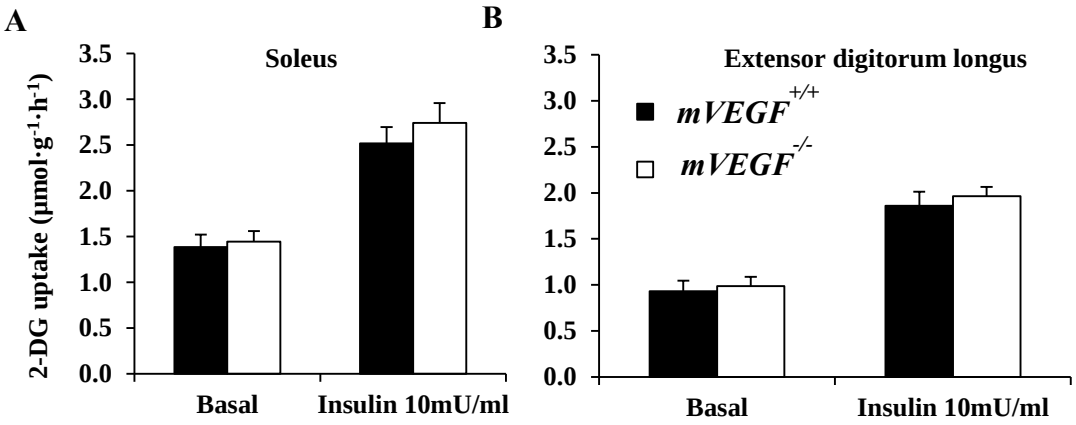

Figure 3.9 - Skeletal muscle insulin action was assessed in the isolated soleus (A) and extensor digitorum longus (B). Mice were fasted for 5 h prior to the excision of the muscles. Values are expressed as mean ± SE, n= 6.

Chapter IV

GAIN OF VASCULAR FUNCTION: PHARMACOLOGICALLY TARGETING THE EXTRAMYOCELLULAR BARRIERS TO MUSCLE GLUCOSE UPTAKE WITH THE HORMONE RELAXIN

Aims

The goal of Chapter IV was to determine whether pharmacologically targeting the extramyocellular barriers to MGU with the hormone relaxin rescues HF diet-induced skeletal muscle insulin resistance. Previous work has established a critical role for glucose and insulin delivery in the regulated process of insulin-stimulated MGU. Furthermore, extracellular matrix remodeling and vascular dysfunction are involved in the pathogenesis of insulin resistance and the greater metabolic syndrome. There is a need for therapeutic options to treat insulin resistance with a physiological approach that has the potential to improve both metabolic and vascular dysfunction associated with obesity. To address this, lean and HF-fed C57BL/6J mice were studied to determine the hemodynamic and metabolic effects of relaxin during a insulin clamp. To investigate the therapeutic potential of relaxin C57BL/6J mice were fed a HF diet for 13 weeks with the final 3 weeks of the diet mice received a continuous infusion of relaxin or vehicle via osmotic minipumps. The hypothesis tested was that a chronic intervention with relaxin will reverse the extramyocellular adaptations to a HF diet, thus ameliorating diet-induced skeletal muscle insulin resistance.

Introduction

Insulin resistance precedes the development of type 2 diabetes and it is associated with cardiovascular disease. Recent evidence suggests that muscle insulin resistance coincides with extramyocellular adaptations including extracellular matrix (ECM) remodeling and capillary rarefaction (51, 82, 87, 111). Kang et al. established that the accumulation of ECM proteins and lower capillary number correspond to muscle insulin resistance in HF-fed mice (87, 111). The vascular and ECM abnormalities associated with obesity provide novel therapeutic targets to simultaneously treat insulin resistance and its co-aggregates.

The hemodynamic action of insulin is fundamental to skeletal muscle metabolism during insulin stimulation (141, 142). Hyperinsulinemia increases skeletal muscle microvascular blood volume, thus, enhancing nutrient and hormone flux to this tissue (37, 45, 84). Previous studies estimated that 40% of insulin-stimulated MGU was a result of increased muscle perfusion and that this hemodynamic response is diminished in insulin resistant individuals (36, 57). Studies applying metabolic control analysis demonstrated that the vascular delivery of glucose to the muscle is a major limitation to insulin-stimulated MGU (14, 17). HF-fed mice have attenuated vascular insulin signaling that precedes the impairment in insulin responsive tissues such as skeletal muscle, liver, and adipose tissue (50). Kubota et al. showed that impaired endothelial insulin signaling, in mice lacking endothelial insulin receptor substrate 2, prevented eNOS activation and resulted in decreased muscle perfusion, substrate delivery, and MGU during steady-state hyperinsulinemia (48).

Relaxin (Rlx), a 6-kDa protein hormone, has potent vasodilatory and antifibrotic actions (101, 102, 143-145). Rlx augments circulating vascular endothelial growth factor-A (VEGF) concentrations, which is essential to the vasodilatory response (95). Furthermore, Rlx induced VEGF expression stimulates the integration of bone-marrow derived endothelial cells into sites of vasculogenesis to enhance vessel growth (104, 105). In experimental models of type I diabetes and hypertension, Rlx attenuated the fibrotic response in cardiac and renal tissues respectively (101, 102). An important mechanism for the antifibrotic actions of Rlx is blunted TGFβ signaling, which can reduce collagen (Col) deposition (96-99). Rlx regulation of matrix metalloproteinases (MMP) -2 and -9 activities has been shown to be important to the ECM remodeling mechanism of Rlx and the acute vasodilatory response (94, 96, 99). The pleiotropic actions of Rlx provide an intriguing therapeutic candidate for insulin resistance.

The goal of the current investigation was to determine the viability of Rlx intervention in rescuing muscle insulin resistance. The hypotheses tested herein are: (1) acute Rlx infusion will enhance skeletal muscle perfusion and insulin action in lean but not HF-fed mice; and chronic Rlx intervention in HF-fed mice will (2) reverse muscle insulin resistance and (3) enhance endothelial reactivity and augment skeletal muscle capillarity.

Experimental Design

Male 6-week old C57BL/6J mice (Jackson Laboratory) were either placed on a chow or HF diet containing 5.5% or 60% calories as fat respectively. In Protocol 1 (Figure 4.1), 13 week chow-fed and HF-fed mice had a primed (10µg) continuous

infusion (15µg/h) with recombinant H-2 Rlx (15µg/h; H2-relaxin, Corthera, Inc, a subsidiary of Novartis Pharmaceuticals Corp.) or Vehicle (20mM sodium acetate, pH 5.0) for 6.5 h total. The infusion of Rlx or Vehicle began 1 h after the onset of the fast and lasted for the duration of the insulin clamp. In Protocol 2 (Figures 4.2 and 4.3), mice were fed a HF diet for 13 weeks. At week 10 of HF-feeding osmotic minipumps (Alzet models 2001 and 2002; replaced after 2 weeks) were implanted subcutaneously to deliver Rlx at a rate of 1 $mg \cdot kg^{-1} \cdot day^{-1}$ or Vehicle. The HF-fed cohort in Protocol 1 permitted a control for any potential acute actions of relaxin in Protocol 2 during the insulin clamps. In all protocols, insulin clamps were performed to assess insulin action (Figures 4.1 and 4.3) and aortic ring reactivity tests to assess vascular function. See Chapter II for detailed methods.

Results

Protocol 1: Acute Rlx infusion enhances insulin-stimulated MGU in chow-fed but not HF-fed mice.

Glucoregulatory: To test the hypothesis that a 6.5 h Rlx infusion enhances insulin-stimulated MGU in chow-fed mice, insulin clamps were performed in 5 h fasted mice. There was no difference in body weight between treatment groups (Table 4.1). The acute chow-fed Rlx group had greater fasting arterial insulin; however, no change in fasting arterial glucose was present (Table 4.1). Insulin clamps were performed to determine *in vivo* muscle insulin action in conscious unrestrained mice (15). During the steady-state period of the insulin clamp (80-120 min), Rlx treated mice required a higher GIR to maintain euglycemia compared to Vehicle infused mice ($p \leq 0.05$; Figure 4.4A). The

increase in GIR was independent of changes in the suppression of endoR_a (Figure 4.4B). The enhanced GIR in the Rlx group was due to an augmented whole-body glucose disappearance (R_d) during the clamp steady-state period ($p \leq 0.05$; Figure 4.4B). The R_g in the Rlx infusion group was greater in the gastrocnemius, superior vastus lateralis (SVL), and heart ($p \leq 0.05$; Figure 4.4C). The *in vivo* muscle glucose flux data coincided with augmentation of the ratio of phospho-Akt to total Akt in the gastrocnemius ($p \leq 0.05$; Figure 4.5B).

The acute Rlx infusion of Protocol 1 was repeated in HF-fed mice. In contrast to the chow-fed mice, there was no difference in insulin action and glucose fluxes between the Vehicle and Rlx infused groups. There was no difference in body weight or arterial glucose and insulin levels in the fasted and clamp states (Table 4.1). The GIR during the insulin clamps were equal (Figure 4.6A). The endoR_a and R_d were comparable between groups in the basal and insulin clamp states (Figure 4.6B). The R_g data corresponded to the flux analysis with no difference in the gastrocnemius, SVL, or heart (Figure 4.6C). HF-fed mice are resistant to the acute effects of Rlx.

Ex vivo glucose uptake was determined in isolated muscle from chow-fed mice that underwent a 6.5 h Rlx infusion (Protocol 1) identical to the insulin clamp cohorts. Isolated glucose uptake was performed only in the chow-fed mice due to the enhanced insulin clamp R_g. Glucose uptake in isolated muscle removes the vascular delivery barrier of MGU during hyperinsulinemia. There was no difference in basal or insulin-stimulated glucose uptake in isolated soleus or extensor digitorum longus (EDL) muscles between groups (Figure 4.5A).

Vascular: The 6.5 h Rlx infusion enhanced the hemodynamic response to insulin in chow-fed mice. Endothelial-dependent aortic ring relaxation in the Rlx group was amplified with no difference in smooth muscle-dependent relaxation ($p \leq 0.05$; Figure 4.4D). The acute enhancement in endothelial specific vascular reactivity was absent in the HF-fed cohort (Figure 4.6D). Muscle blood flow was increased in the Rlx group as indicated by a 2.5-fold increase in gastrocnemius microsphere content ($p \leq 0.05$; Figure 4.5C). The 6.5 h Rlx infusion resulted in a 2.5-fold increase in MMP-9 and pro-MMP-2 activities ($p \leq 0.05$; Figure 4.5D).

Protocol 2: Rlx intervention reverses diet-induced insulin resistance and the associated extramyocellular adaptations.

Glucoregulatory: To test the hypothesis that intervention with Rlx can reverse muscle insulin resistance and the extramyocellular adaptations to a HF diet, mice were treated with Rlx or Vehicle for the final 3 weeks of a 13 week HF diet. Rlx intervention did not alter body weight or composition (Table 4.2). Furthermore, the 3 week Rlx treatment did not result in differences in mean arterial blood pressure or cardiac morphology (Table 4.2). Insulin clamps were performed after the 3 week intervention. Fasting (5 h) arterial glucose was lower in the Rlx treated mice ($p \leq 0.05$; Table 4.2). During the steady-state period of the insulin clamp, the Rlx group required a higher GIR to maintain euglycemia at ~150 mg/dL ($p \leq 0.05$; Figure 4.7A). Rlx did not affect fasting glucose fluxes. Insulin suppressed endoR_a during the steady-state period to a greater extent with Rlx intervention ($p \leq 0.05$; Figure 4.7B), suggesting improved hepatic insulin action. The greater GIR in the Rlx treated group corresponded to enhanced whole-body R_d during the steady-state

period of the insulin clamp ($p \leq 0.05$; Figure 4.7B). R_g was elevated in the gastrocnemius and SVL in the Rlx group compared to Vehicle during hyperinsulinemia ($p \leq 0.05$) and cardiac muscle R_g tended to be higher ($p=0.1$; Figure 4.7C). Skeletal muscle and hepatic phospho-Akt to total Akt ratio tended to be higher after the Rlx intervention but differences were not significant (Figure 4.8A).

Ex vivo glucose uptake in isolated soleus and EDL showed no difference between the Vehicle or Rlx groups (Figure 4.7D). This suggests that the extramyocellular effects of Rlx are key to the effectiveness of Rlx intervention in HF-fed mice.

Extracellular Matrix Remodeling: Col-III and -IV levels were equivalent in skeletal muscle between treatment groups (Figure 4.8B and C). The improvement in hepatic insulin action with Rlx treatment was associated with reduced col-III ($p \leq 0.05$; Figure 4.8D). Cardiac col-III and -IV were increased in response to the HF diet, but were reduced by ~50% and ~65% respectively after the 3 week Rlx intervention ($p \leq 0.05$; Figure 4.9A and B). This effectively normalized these ECM proteins to levels of lean mice. The abatement in cardiac ECM protein associated with a reduction in SMAD2 phosphorylation ($p \leq 0.05$; Figure 4.9C), which is a marker of TGFβ receptor downstream activation.

Vascular: The enhanced muscle insulin action in Rlx treated mice was associated with a 2-fold expansion of skeletal muscle capillary density ($p \leq 0.05$; Figure 4.10A). Improved vascular reactivity was present after the Rlx intervention as indicated by an augmented endothelial-dependent aortic relaxation ($p \leq 0.05$; Figure 4.10C). There was no difference in smooth muscle-dependent relaxation in response to sodium nitroprusside and no significant change in the vasculature response to phenylephrine (PE) (Figure 4.10C and

D). A potential common mechanism for the changes in skeletal muscle capillary density and endothelial-dependent relaxation is the elevated arterial VEGF concentrations after 3 weeks of continuous Rlx administration ($p \leq 0.05$; Figure 4.10B).

Discussion

These studies demonstrate for the first time that infusion of the hormone Rlx acutely augments muscle perfusion and insulin-stimulated MGU in lean, healthy C57BL/6J mice. There is no such acute Rlx effect in HF-fed mice. However, results show that a 3 week Rlx intervention in HF-fed ameliorates the metabolic and cardiovascular dysfunction. It is important to recognize that the potent metabolic effects of Rlx were absent in isolated muscle fibers, regardless of whether Rlx was administered acutely in lean mice or as a chronic intervention in HF-fed mice. The data from isolated muscle support the hypothesis that Rlx diminishes the extramyocellular barriers to MGU during hyperinsulinemia.

Baron et al. demonstrated that the co-infusion of insulin and a vasodilator in healthy subjects resulted in a synergistic effect to enhance limb blood flow and muscle glucose uptake (84). In congruence with this clinical study, the acute Rlx infusion in the chow-fed mice of Protocol 1 increased steady-state R_d and muscle R_g during the insulin clamp. The Rlx infused mice had greater muscle microsphere deposition at the termination of the insulin clamp and enhanced aortic ring relaxation suggesting a greater hemodynamic response to insulin. The amplified muscle blood flow increases insulin and glucose access to the muscle interstitium. This would predictably enhance insulin action as supported by augmented *in vivo* skeletal muscle insulin signaling. The increased pro-

MMP-2 and MMP-9 activities were consistent with the acute vasodilatory mechanisms of Rlx (94).The equivalent basal and insulin-stimulated glucose uptake in isolated muscle suggests that the primary mechanism for the enhanced muscle R_g was independent of direct actions of Rlx on the myocyte.

The 3 week Rlx intervention in Protocol 2 was effective in improving insulin action in HF-fed mice. The improvement in glucose homeostasis in both the fasted and insulin-stimulated state is speculated to be a result of the actions unique to Rlx that improve vascular adaptations to the HF diet. The isolated MGU data support this conclusion. Potentially other extramyocellular factors that require long-term treatment, such as an increase in plasma VEGF, could be necessary for the *in vivo* glucoregulatory effects of Rlx that are absent *ex vivo*. Furthermore, Rlx has been shown to antagonize angiotensin II action (146) and the renin-angiotensin system has been implicated in the pathogenesis of skeletal muscle capillary rarefaction and insulin resistance (53). The glucoregulatory and vascular adaptations that are present with the chronic Rlx administration are notably absent in the HF-fed cohort of Protocol 1. This may provide insight into the mechanism of Rlx action in HF-fed mice. It would suggest that an adaptive process, rather than acute activation, is required to overcome the impairments in insulin action in HF-fed mice. Rlx intervention has previously been shown to ameliorate endothelial dysfunction in models of hypertension (95, 145, 147). In the current model of HF diet-induced insulin resistance, Rlx improved endothelial function. The improvement in endothelial reactivity did not occur in HF-fed mice that underwent an acute Rlx infusion, suggesting long-term administration is necessary to overcome the vascular impairment associated with a HF diet (148). Rlx acts through an eNOS dependent

pathway to cause vascular relaxation. It is speculated that the vascular remodeling and impaired eNOS function present in HF-fed mice nullifies the acute Rlx effect in the HF-fed mice in Protocol 1 (149). Consistent with this finding, acute administration of Rlx does not ameliorate hypertension in spontaneously hypertensive rats (146). Additionally, Rlx treated mice had a ~2-fold increase in skeletal muscle capillary density. Capillary rarefaction and endothelial dysfunction associated with obesity are critical to the pathogenesis of skeletal muscle insulin resistance (38, 54, 55, 150). The actions of Rlx on the vasculature may enhance the hemodynamic response to hyperinsulinemia, thus augmenting microvascular perfusion. An increase in muscle blood volume would increase the surface area for insulin and glucose diffusion, in addition to other hormones and nutrients (14, 45, 48, 59). The likely mechanism for the improved endothelial function and expansion of skeletal muscle capillary density is the elevation in circulating VEGF, which has been shown to be critical to the sustained vasodilatory and angiogenic actions of Rlx (95, 104, 105).

The efficacy of Rlx to enhance MGU during hyperinsulinemia acutely in lean and chronically in HF-fed mice was independent of an interaction directly with the insulin receptor. Originally, Rlx was characterized to be part of the insulin family of proteins due to their common two-chain structure. More recent data demonstrated that Rlx diverged from the insulin family early in vertebrate evolution forming a separate protein and receptor family (151). There is no evidence to support the cross-reactivity of Rlx with the insulin receptor, as Rlx does not activate protein kinase receptors (152). The metabolic effects demonstrated in the current study were likely due to extramyocellular and

extrahepatic adaptations to Rlx. Notably, the specific receptor for Rlx, RXFP1, has not been identified in skeletal myocytes or hepatocytes (152).

ECM deposition occurs in skeletal muscle, liver, and cardiac tissue of HF-fed rodents (87, 153, 154) and insulin resistant humans (111, 153, 155, 156). The interaction of collagen proteins with the integrin receptors has been linked to the development of hepatic and skeletal muscle insulin resistance (87). In the current studies, Rlx reversed the deposition of hepatic col-III, though there was no difference in hepatic col-IV (data not shown). It is speculated that the improved hepatic insulin action was related to the reduction in col-III and the potential interaction with the hepatic integrin receptors. Nonalcoholic fatty liver disease and nonalcoholic steatohepatitis are associated with the development and progression of fibrosis in type 2 diabetes and subsequent impairments in hepatic insulin action (153, 157). Previously, col-III and –IV have been shown to be elevated in muscle of HF-fed mice and humans (87, 111); however, there was no difference in these collagen species in skeletal muscle in the current model, perhaps relating to differences in diet duration. Although col-III and -IV are major components of the extracellular matrix there are other distinct matrix proteins that could have been altered.

Rlx intervention diminished col-III and -IV accumulation in the heart, which is consistent with the antifibrotic effects of long-term Rlx treatment shown in rodent models of type 1 diabetes (101) and hypertension (102). The decreased cardiac ECM proteins after the Rlx treatment was likely a consequence of Rlx inhibiting the downstream activation of SMAD2 by transforming growth factor-β (TGFβ) (96, 97, 99). The diminished cardiac col-III and –IV and ameliorated endothelial dysfunction in Protocol 2

emphasizes that Rlx may be efficacious in the treatment of the broader dysfunction associated with the metabolic syndrome.

Macro- and microangiopathies correlate with insulin resistance (158, 159) leading to impaired tissue perfusion, which is a key component of the etiology of diabetes-related tissue and organ damage (46). Furthermore, endothelial dysfunction and capillary rarefaction contribute to hypertension and insulin resistance, both of which are components of the metabolic syndrome and increase the risk of cardiovascular mortality (46, 150, 160). Thus, it is critical to consider the common underlying vascular pathologies to develop novel intervention strategies to treat the metabolic syndrome. However, a critical consideration for the long-term clinical administration of a vascular proliferative compound is the potential exacerbation of tumor development and metastasis. This is particularly important because there is a positive association between insulin resistance and many types of cancers (161). It is possible that chronic exposure to Rlx for the treatment of insulin-resistance may exacerbate outcomes in cancer patients. Notably, Rlx is expressed at higher levels in prostate cancer and correlates to metastatic potential and diminished survival (162) and the inhibition of RXFP1 has been investigated as a potential therapeutic target (163).

These studies demonstrate the effectiveness of Rlx in targeting the extramyocellular barriers to MGU for the treatment of insulin resistance. Intervention with the hormone Rlx targets multiple physiological systems to ameliorate cardiac and hepatic collagen accumulation, increase skeletal muscle capillary density, and improve diet-induced endothelial dysfunction. These effects contribute to the enhancement of *in vivo* insulin action in HF-fed mice and require an extended treatment period to mitigate

these extramyocellular barriers to insulin-stimulated MGU. The results not only highlight the efficacy of Rlx in the correction of muscle insulin resistance, but also demonstrate the potential therapeutic value of Rlx in reversing fibrosis and vascular dysfunction associated with a HF diet.

Acknowledgements

This work was funded by National Institutes of Health Grants DK054902 andDK059637 (Mouse Metabolic Phenotyping Center). The Diabetes Research and Training Center (DK20593) also provided support for this work.

I am thankful for ZhiZhang Wang of the VMMPC Cardiovascular Pathophysiology Core for performing echocardiography in these studies, the Brophy Laboratory particularly Kyle Hocking for performing aortic relaxation experiments, and Melissa B. Downing of the Vanderbilt University Mouse Pathology Core Laboratory of the Mouse Metabolic Phenotyping Center. I kindly thank Dr. Dennis Stewart of Corthera, Inc, a subsidiary of Novartis Pharmaceuticals Corp., for supplying recombinant H-2 relaxin and for his helpful insight.

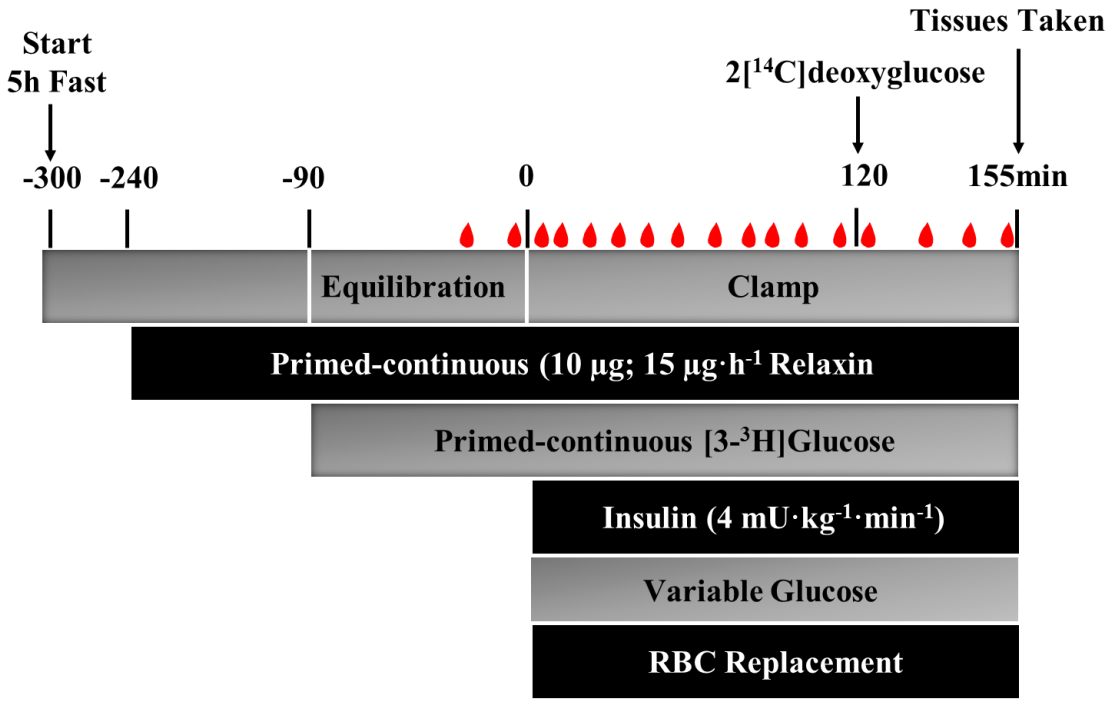

Figure 4.1 – Protocol 1: Experimental setup for the hyperinsulinemic-euglycemic clamps performed in Chapter IV. Experiments were performed 7 days after surgical implantation of carotid artery and jugular vein catheters. Mice were fasted for 5 h prior to the onset of the clamp. A primed-continuous infusion of relaxin began at *t*= -240 min. Primed-continuous infusion of [3-^{3}H]glucose began at -90 min. At *t*= 0 min insulin was elevated to postprandial levels. Basal blood draws occurred at *t*= -15 and -5 min and blood glucose was measured at 10 min intervals starting at *t*= 0 min. Variable glucose was infused to maintain euglycemia at ~150 mg/dL and red blood cell replacement maintained hematocrit during the study period. 2[^{14}C]glucose was injected intravenously at *t*= 120 min to measure tissue specific glucose uptake.

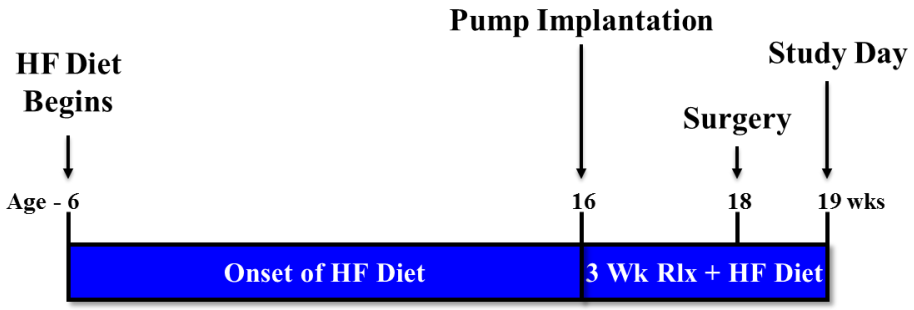

Figure 4.2 – Protocol 2: Diet and treatment time-course for the chronic relaxin intervention in high-fat fed C57BL/6J mice. The onset of the high-fat diet began at 6 weeks of age and lasted for 13 weeks. Relaxin or Vehicle was administered at a rate of 1 $mg \cdot kg^{-1} \cdot day^{-1}$ and began at week 10 of the high fat diet. Relaxin and Vehicle were administered continuously for the final 3 weeks of high fat-feeding, at which time hyperinsulinemic-euglycemic clamps were performed.

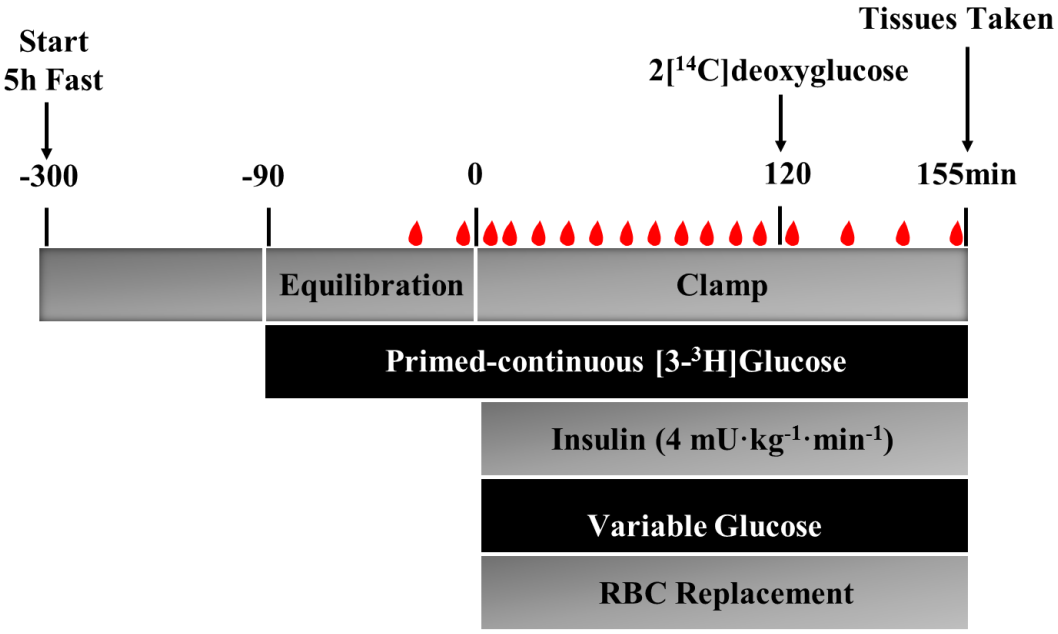

Figure 4.3 – Protocol 2: Experimental setup for the hyperinsulinemic-euglycemic clamps performed in Chapter IV. Experiments were performed 7 days after surgical implantation of carotid artery and jugular vein catheters. Mice were fasted for 5 h prior to the onset of the clamp. Primed-continuous infusion of [3-^{3}H]glucose began at *t*= -90 min. At *t*= 0 min insulin was elevated to postprandial levels. Basal blood draws occurred at *t*= -15 and -5 min and blood glucose was measured at 10 min intervals starting at *t*= 0 min. Variable glucose was infused to maintain euglycemia at ~150 mg/dL and red blood cell replacement maintained hematocrit during the study period. 2[^{14}C]glucose was injected intravenously at *t*= 120 min to measure tissue specific glucose uptake.

Table 4.1
Insulin Clamp Characteristics in Protocol 1

		Vehicle	Relaxin
Protocol 1: Chow-fed Mice	*n*	9	8
	Weight (g)	30.0 ± 0.3	29.5 ± 0.3
	Arterial glucose (mg/dL)		
	Basal	130 ± 7	129 ± 3
	Clamp	148 ± 2	149 ± 3
	Arterial insulin (ng/mL)		
	Basal	0.8 ± 0.1	1.2 ± 0.1*
	Clamp	4.6 ± 0.3	4.6 ± 0.3
Protocol 1: HF-fed Mice	*n*	5	5
	Weight (g)	38.6 ± 2	40.1 ± 1
	Arterial glucose (mg/dL)		
	Basal	132 ± 9	126 ± 11
	Clamp	148 ± 3	146 ± 4
	Arterial insulin (ng/mL)		
	Basal	5.2 ± 1	7.1 ± 2
	Clamp	10.9 ± 2	12.6 ± 2

Mice were fasted 5 h prior to the onset of the insulin clamp. The Rlx infusion occurred for a duration of 6.5 h through the insulin clamp. Insulin clamp arterial glucose was an average of 80-120 min and arterial insulin was an average of t= 100 and 120 min. Data are expressed as mean ± SE. *P-value ≤ 0.05

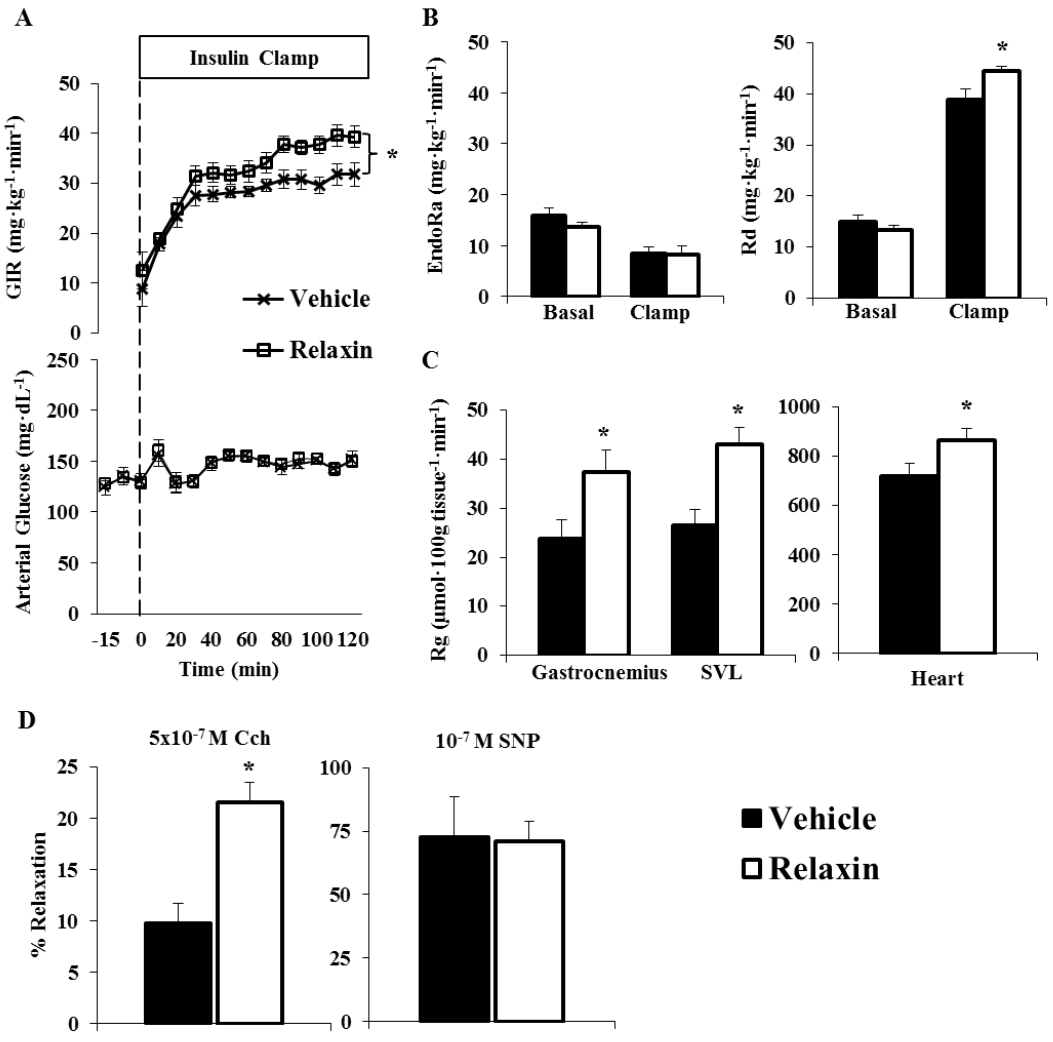

Figure 4.4 - Protocol 1, chow-fed: Hyperinsulinemic-euglycemic clamps, glucose flux analysis, and vascular reactivity after a 6.5 h Rlx or Vehicle infusion in lean mice. (A) Glucose infusion rate (top) and arterial glucose (bottom) during the insulin clamp. Mice were fasted 5 h prior to the onset of the clamp. Blood glucose was maintained at ~150 mg/dL during steady-state (80-120 min) and the time course is displayed to demonstrate quality of the clamp. 50% glucose was infused to maintain euglycemia. Endogenous glucose production and whole-body glucose disposal (B-EndoRa and Rd) during the insulin clamp. Basal values are an average of *t*= -15 and -5 min and the insulin clamp values are an average of 80-120 min (steady-state). (C) Glucose metabolic index (Rg) after the insulin clamp in the gastrocnemius, SVL (superior vastus lateralis), and heart. Endothelial and smooth muscle dependent relaxation (D) in aortas excised from mice after the insulin clamp in response to carbachol (Cch) and sodium nitroprusside (SNP) respectively. Data are expressed as mean ± SE, n= 8-9,*P-value ≤ 0.05.

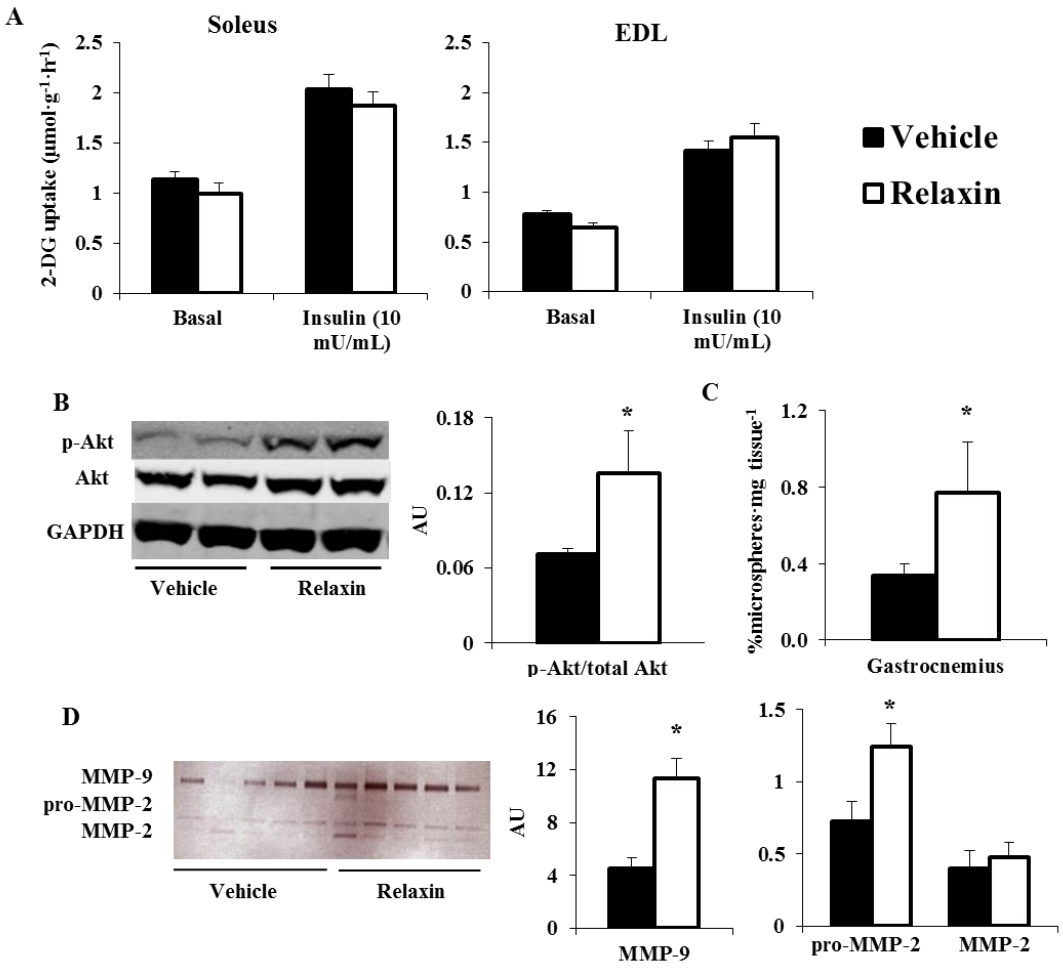

Figure 4.5 - Protocol 1, chow-fed: Isolated MGU, insulin signaling, muscle perfusion, and MMP activation after the 6.5 h Rlx or Vehicle infusion. Isolated muscle glucose uptake (A) on the soleus and EDL (extensor digitorum longus). Mice were fasted for 5 h and muscles excised after the 6.5 h Rlx infusion. Western blot analysis of the activation status of Akt (B) after the insulin clamp analyzed as the ratio of phosphorylated Akt to total Akt. Microsphere content in the gastrocnemius (C) after the insulin clamp. Gelatin zymogram to determine matrix metalloproteinase-2 and -9 activitity (D) in gastrocnemius muscle after the insulin clamp. AU represents arbitrary units. AU represents arbitrary units. Data are expressed as mean ± SE, n= 5.

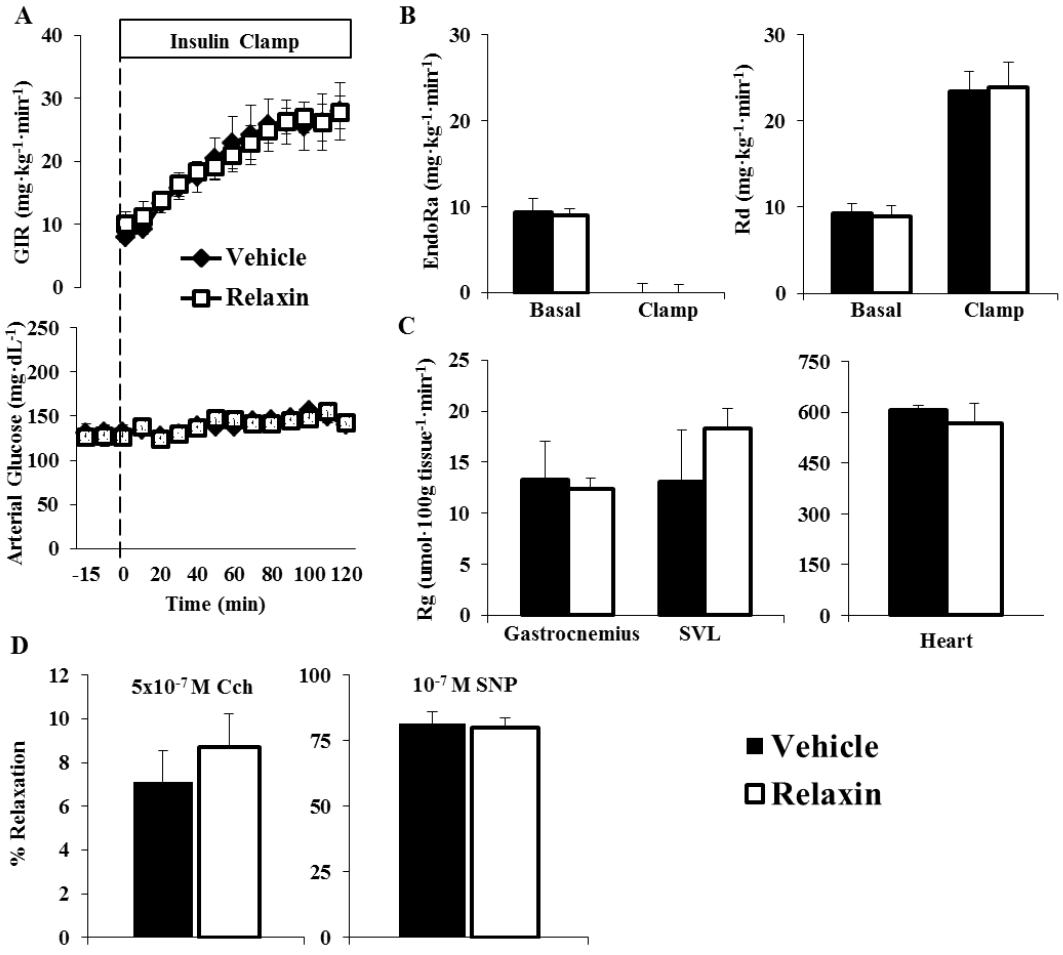

Figure 4.6 - Protocol 1, high fat-fed: Hyperinsulinemic-euglycemic clamps, glucose flux analysis, and vascular reactivity after a 6.5 h Rlx or Vehicle infusion in HF-fed mice. (A) Glucose infusion rate (top) and arterial glucose (bottom) during the insulin clamp. Mice were fasted 5 h prior to the onset of the clamp. Blood glucose was maintained at ~150 mg/dL during steady-state (80-120 min) and the time course is displayed to demonstrate quality of the clamp. 50% glucose was infused to maintain euglycemia. Endogenous glucose production and whole-body glucose disposal (B-EndoRa and Rd) during the insulin clamp. Basal values are an average of *t*= -15 and -5 min and the insulin clamp values are an average of 80-120 min (steady-state). (C) Glucose metabolic index (Rg) after the insulin clamp in the gastrocnemius, SVL (superior vastus lateralis), and heart. Endothelial and smooth muscle dependent relaxation (D) in aortas excised from mice after the insulin clamp in response to carbachol (Cch) and sodium nitroprusside (SNP) respectively. Data are expressed as mean ± SE, n= 5.

Table 4.2
Treatment Group Characteristics in Protocol 2

	Vehicle	Relaxin
n	13	11
Weight (g)	34.8 ± 0.8	34 ± 1.0
Fat (%)	16.5 ± 1.3	15.6 ± 2.5
Muscle (%)	65.1 ± 0.7	65.7 ± 1.5
Arterial glucose (mg/dL)		
Basal	145 ± 6	130 ± 5*
Clamp	151 ± 2	148 ± 3
Arterial insulin (ng/mL)		
Basal	1.8 ± 0.3	2.1 ± 0.4
Clamp	6.2 ± 0.9	7.5 ± 0.9
Free fatty acids (mmol/L)		
Basal	1.10 ± 0.08	0.80 ± 0.10
Clamp	0.44 ± 0.05	0.42 ± 0.03
Mean arterial pressure (mmHG)	126 ± 3	131 ± 3
Cardiac output (mL/min)	21 ± 1	21 ± 2
Ejection fraction (%)	81 ± 1	77 ± 2
Fractional shortening (%)	48 ± 0.6	45 ± 0.1*
LV mass (mg)	62.5 ± 3	63.9 ± 5
LV diastolic volume (µL)	41 ± 3	43 ± 5

Mice were fasted 5 h prior to the onset of the insulin clamp. Insulin clamp arterial glucose was an average of 80-120 min. Arterial insulin and free fatty acids were an average of t= 100 and 120 min. LV is the abbreviation for left ventricular. Data are expressed as mean ± SE. *P-value $\leq$ 0.05

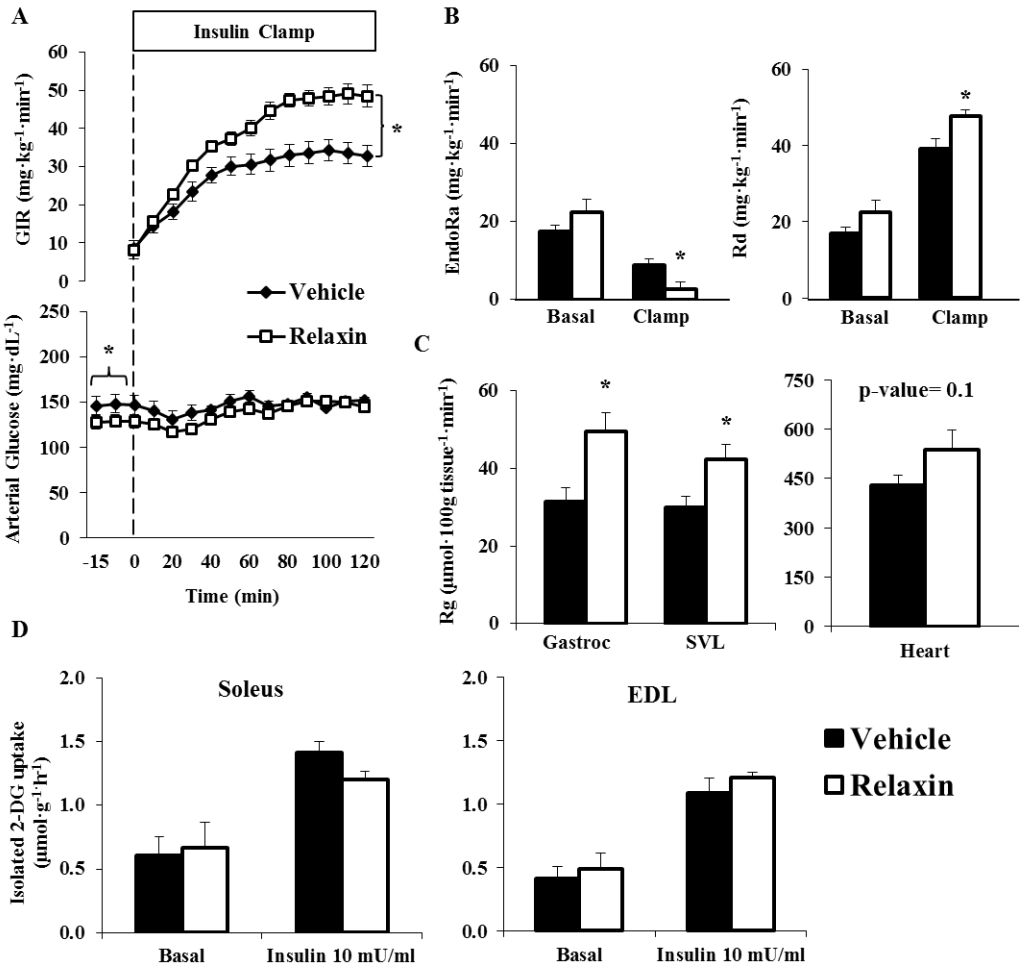

Figure 4.7 - Protocol 2: Hyperinsulinemic-euglycemic clamps, glucose flux analysis, and isolated muscle glucose uptake after the 3 week Rlx or Vehicle intervention in HF-fed mice. (A) Glucose infusion rate (top) and arterial glucose (bottom) during the insulin clamp. Mice were fasted 5 h prior to the onset of the clamp. Blood glucose was maintained at ~150 mg/dL during steady-state (80-120 min) and the time course is displayed to demonstrate quality of the clamp. 50% glucose was infused to maintain euglycemia. Endogenous glucose production and whole-body glucose disposal (B-EndoRa and Rd) during the insulin clamp. Basal values are an average of *t*= -15 and -5 min and the insulin clamp values are an average of 80-120 min (steady-state). (C) Glucose metabolic index (Rg) after the insulin clamp in the gastroc (gastrocnemius), SVL (superior vastus lateralis), and heart. Isolated muscle glucose uptake (D) on the soleus and EDL (extensor digitorum longus). Mice were fasted for 5 h prior to muscles being excised. Data are expressed as mean ± SE, n= 11-13,*P-value ≤ 0.05.

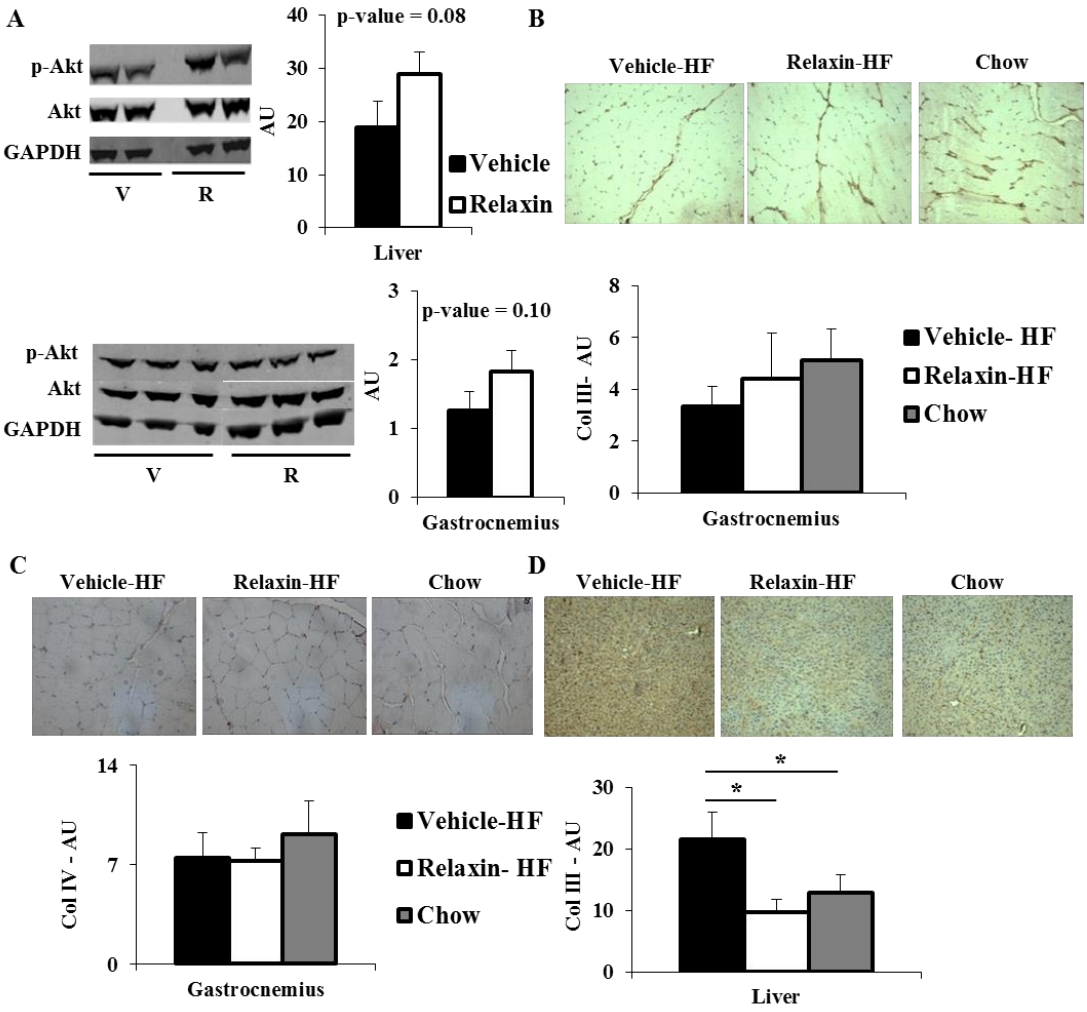

Figure 4.8 - Protocol 2: Insulin signaling and immunohistochemical stain of skeletal muscle and liver. Western blot analysis of the activation status of Akt (A) analyzed as the ratio of phosphorylated Akt to total Akt in liver (top) and skeletal muscle (bottom) from protein extracted from mice after the insulin clamp (V-vehicle and R-relaxin). Immunohistochemical detection of skeletal muscle collagen-III (B) and collagen-IV (C) from the gastrocnemius muscle. Immunohistochemical detection of hepatic collagen-III (D). Immunohistochemical analysis was performed on tissues fixed immediately following the insulin clamp. AU represents arbitrary units. Data are expressed as mean ± SE, n= 5-6,*P-value ≤ 0.05.

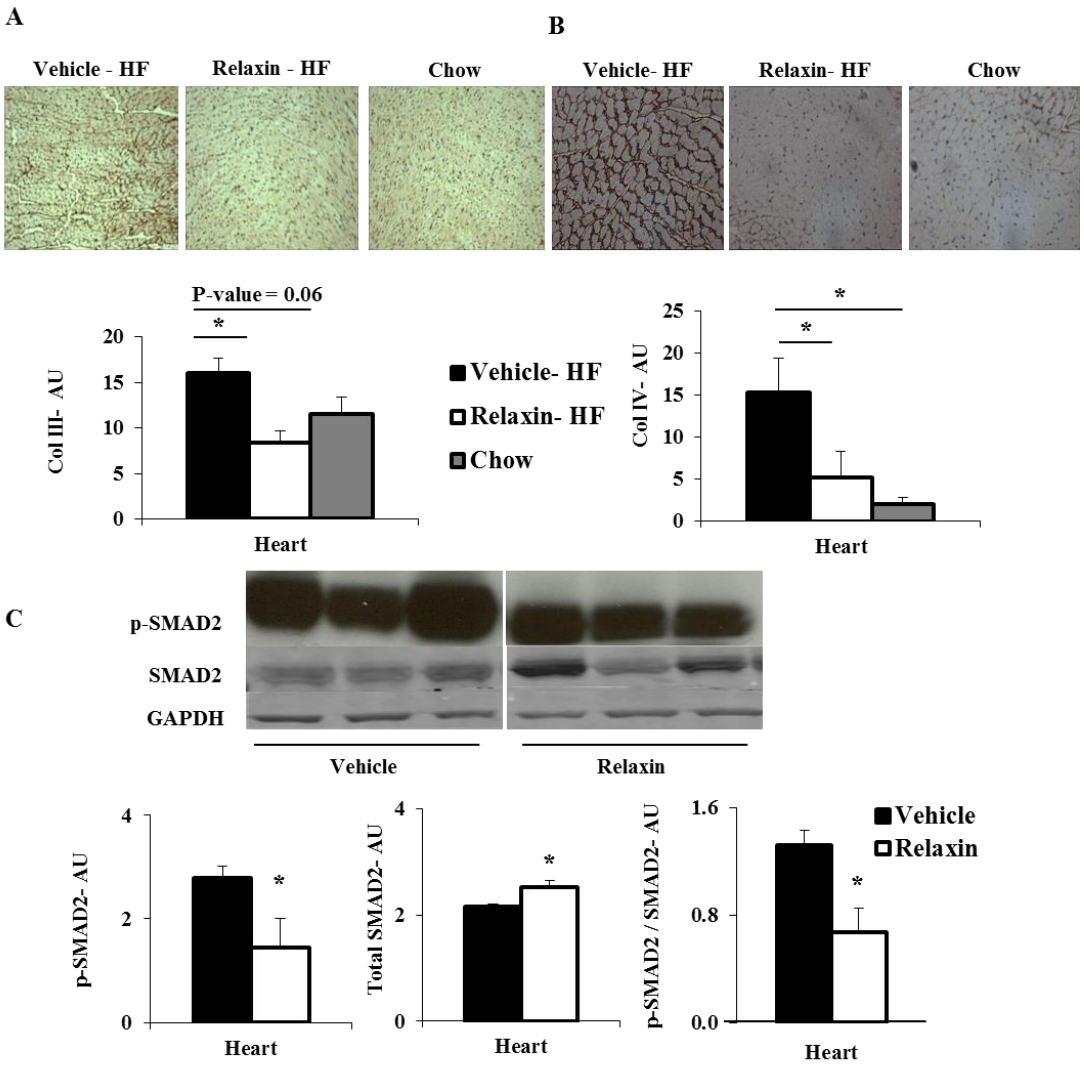

Figure 4.9 - Protocol 2: Collagen protein levels and SMAD2 signaling in cardiac muscle. Immunohistochemical detection of collage-III (A) and –IV (B) from hearts fixed after the insulin clamp. Western blot analysis of phospho-SMAD2, total SMAD2, and the ratio of phospho to total SMAD2 (C) from cardiac protein extracts after the insulin clamp. AU represents arbitrary units. Data are expressed as mean ± SE, n= 5-6,*P-value ≤ 0.05.

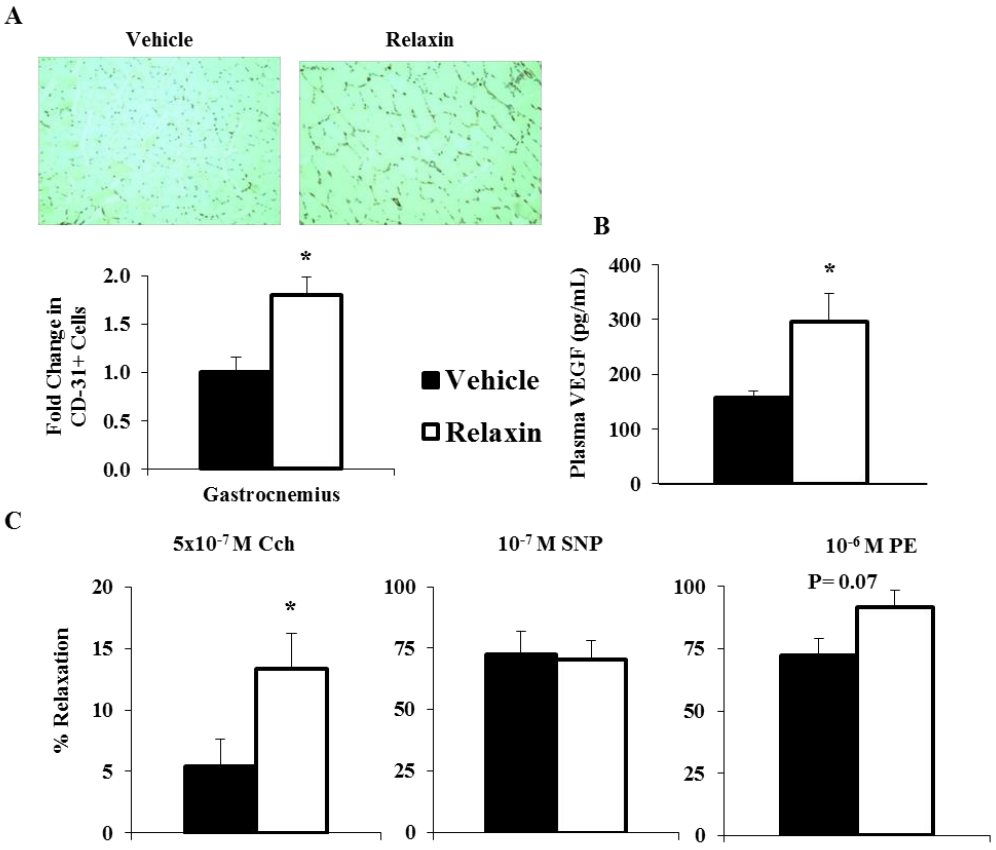

Figure 4.10 - Protocol 2: Capillarity density and vascular reactivity in response to the Rlx intervention. Capillary density (A) quantified with immunohistochemical staining of CD-31. Capillary density is quantified as the number of CD-31+ cells. Plasma vascular endothelial growth factor (VEGF) concentration (B) after the insulin clamps. Vascular reactivity (C) from excised aortas after the insulin clamps. Endothelial-dependent relaxation (left; carbachol), smooth muscle-dependent relaxation (middle; sodium nitroprusside), and stress generated from phenylephrine (right; PE). Responses represented as a percent of maximal tension from KCl stimulation. Data are expressed as mean ± SE, n= 5-8,*P-value $\leq$ 0.05.

Chapter V

CELLULAR BASIS FOR IMPAIRED ENDOTHELIAL INSULIN TRANSPORT SYSTEM IN THE SKELETAL MUSCLE MICROVASCULATURE OF HIGH FAT-FED C57BL/6J MICE

Aims

Insulin resistance and impaired vascular insulin signaling is associated with a blunted delivery of insulin to the interstitium of skeletal muscle limiting the interaction with the insulin receptor (48). The Barrett Laboratory has investigated the transport mechanisms of insulin across the endothelial capillary barrier (23, 27, 33). These studies have characterized the binding of insulin to the capillary wall, a delayed delivery to the muscle interstitium *in vivo*, dependence of caveolin-1 for transendothelial insulin transport *in vitro*, and shown that stimuli that induce insulin resistance (e.g. TNFα) decrease insulin transport and caveolin-1 expression *in vitro* (33, 34, 164). Cavoelin-1 is the critical protein for the formation of caveolae. The elegant investigations performed by the Barrett Laboratory describe the transport of insulin via a receptor mediated process. However, a limitation to these studies is that the mechanistic work was performed utilizing bovine aortic endothelial cells. It is currently unknown whether stimuli that create skeletal muscle insulin resistance, such as a HF diet, cause structural changes to the capillary wall that may hinder insulin transport. The hypothesis tested in Chapter V was that 16 week HF-fed mice will have a decrease in caveolae number within the endothelial cell layer of skeletal muscle capillaries.

Introduction

The capillary network in skeletal muscle forms tight junctions with an enrichment of caveolae, which contrasts from the liver that is comprised of a discontinuous endothelium that permits greater exchange of macromolecules (27). This suggests that the transport of insulin is specific to the tissue of interest and that transport may be limiting in a tissue such as skeletal muscle (or adipose with a similar capillary architecture), but not in a tissue more adept to transport of large macromolecules such as the liver.

A primary transport mechanism for the movement of macromolecules across tight capillaries is endocytosis and secretion via a caveolae dependent process. Schubert et al. showed that caveolae-deficient endothelial cells are incapable of transporting albumin *in vivo*, as the endothelial cells were unable to endocytose albumin for transport (165). Notably, only one study has comprehensively characterized the role of insulin transport *in vivo*. The study was performed in rat cardiac muscle and established a receptor mediated transendothelial transport mechanism (166). This study has not been expanded to other insulin sensitive tissues. Schutzer et al. demonstrated a decline in caveolin-1with aging, a risk factor for the development of insulin resistance, in a smooth muscle cell line (167). However, the effect of aging on the endothelial caveolae structure was not investigated.

The goal of Chapter V was to visualize the capillary endothelial caveolae architecture *in vivo*. Specifically, Chapter V was designed to determine whether 16 week HF-fed mice (that are insulin resistant) have alterations in caveolae number or size in single endothelial layer capillaries that perfuse skeletal muscle utilizing transmission

electron microscopy (TEM). This study is a first step in bridging the *in vitro* work performed (33, 34, 164) to animal models of insulin resistance suggesting the importance of transendothelial insulin transport to skeletal muscle insulin action. The hypothesis tested was that diet-induced insulin resistant mice have fewer endothelial caveolae compared to low fat chow-fed controls.

Experimental Design

C57BL/6J mice were fed a chow or HF diet for 16 weeks. Mice were studied at 20 weeks of age. At the termination of the diet mice underwent perfused fixation as described in Chapter II and the right red gastrocnemius was excised. The samples were further processed for TEM staining by the Vanderbilt University Cell Imagine Shared Resource Core. Visualization is described in detail in Chapter II.

Results

Mice fed the 16 week HF diet gained significant body weight and fat mass compared to the age-matched, chow-fed controls (Table 5.1). Qualitative analysis of caveolae density has been performed. Micrographs were randomized, labels removed, and then separated based on the caveolae density within the capillary. The micrographs were separated into chow-fed and HF-fed groups. This initial screen permitted the decision to move forward with specific quantification of caveolae area per endothelial cell area with an inclusion criterion of greater than 80% success of the qualitative analysis, which was accomplished. There was a striking reduction in caveolae number in the HF-fed group compared to the chow-fed mice (Figures 5.1 and 5.2).

Discussion

The TEM studies indicate that diet-induced insulin resistant mice have fewer caveolae within the endothelial layer of the capillary compared to chow-fed controls. I speculate this microstructural adaptation in the HF-fed mice provides a low insulin transport capacity environment compared to lean mice with capillaries enriched with caveolae. This low transport state is consistent with the *in vitro* findings from Barrett and colleagues (34) that indicated inflammatory cytokines decrease the expression of caveolin-1 and the transendothelial transport of insulin.

The strength of TEM is that it allows for tissue collection by perfusing a fixative that maintains capillary integrity giving a representation of the *in vivo* capillary architecture. The current data can only be extrapolated and applied to the concept of insulin transport within skeletal muscle. The experiments were not designed to visualize insulin localization within caveolae and future investigation will address this limitation. There is clearly a qualitative reduction in endothelial caveolae in HF-fed mice. The current experiments will be expanded in future studies to be more quantitative so that we may determine whether there are significant differences in caveolae per capillary area in our model.

The paradigm of insulin delivery in skeletal muscle is not without controversy (27). The initial work used bovine aortic endothelial cells or umbilical vein endothelial cells. The caveat to applying transport techniques to venous endothelium is that venous cells are innately leaky when compared to aortic or arterial endothelium, thus the potential for false transport data.

The transport assays performed by Barrett's Laboratory (33, 34, 164) were performed in cell culture without *in vivo* validation. Furthermore, the TEM technique we applied can be expanded by injecting labeled insulin into mice and visualizing whether insulin is specifically endocytosed and localized within caveolae structures. The potential of confocal microscopy in live animals could allow for visualization of insulin transport; however, a caveat to this technique is the visualized muscle is superficial limiting the access to nutrient blood flow. The current state of the insulin transport field is limited and critical data for basic characterization of the mechanisms of insulin transport in skeletal muscle remains to be elucidated.

These preliminary findings suggest a potential link between skeletal muscle insulin resistance, transendothelial insulin transport, and caveolae density. The basic process of tissue specific insulin transport needs further characterization. The understanding of how insulin transverses the capillary barrier to reach skeletal muscle insulin receptors could provide a novel pharmacological target to treat insulin resistance and more complete understanding of the pathogenesis of skeletal muscle insulin resistance.

Acknowledgements

This work was funded by National Institutes of Health Grants DK054902 and DK059637 (Mouse Metabolic Phenotyping Center). The Diabetes Research and Training Center (DK20593) also provided support for this work.

There are many contributors to thank for their efforts in designing experiments and teaching the use of transmission electron microscopy. Particularly I would like to

thank Drs. Jay Jerome and Janice Williams for their assistance in experimental design, analysis, and training. Mary Dawes was invaluable in collecting preliminary imagines and teaching image randomization prior to my work on the microscope. The work presented would not have been possible without the Vanderbilt University Shared Resource Core and the leadership of Drs. Sam Wells and Jay Jerome.

Table 5.1
Mouse body weight and composition

	Chow-Fed	*HF-Fed*
N	3	3
Body Weight (g)	25.8 ± 0.9	47.3 ± 1.5*
Fat Mass (%)	4.9 ± 0.4	35.4 ± 4.0*
Lean Mass (%)	76.4 ± 0.4	53.9 ± 2.9*

Data are expressed as mean ± SE. *P-value ≤ 0.01

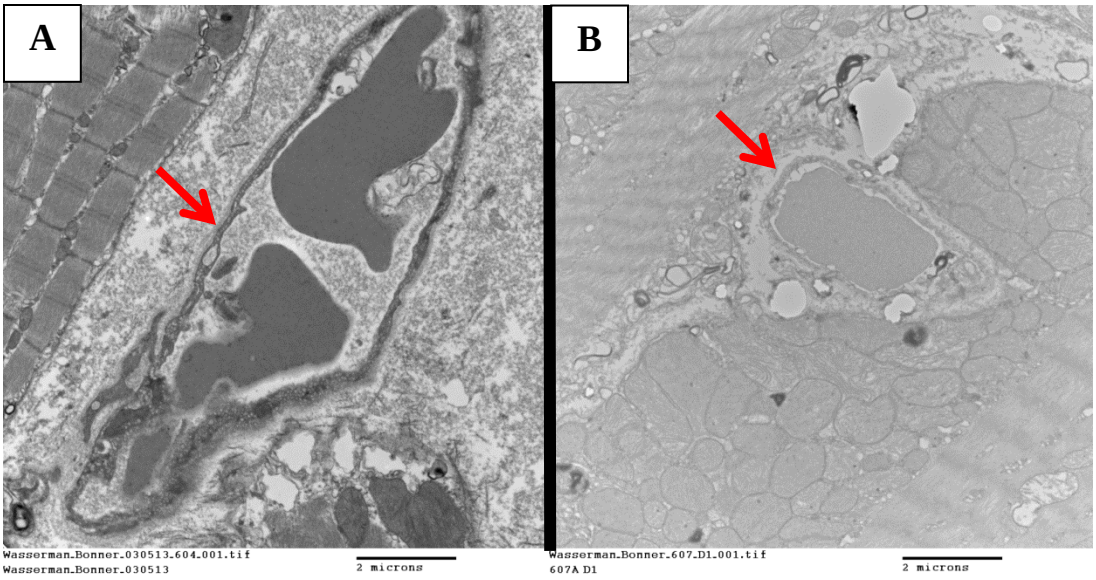

Figure 5.1 – Transmission electron micrograph from the red gastrocnemius of chow-fed (A) and 16 week HF-fed (B) mice. Arrows indicate single endothelial capillary. Images were acquired at a magnification of 11,000x.

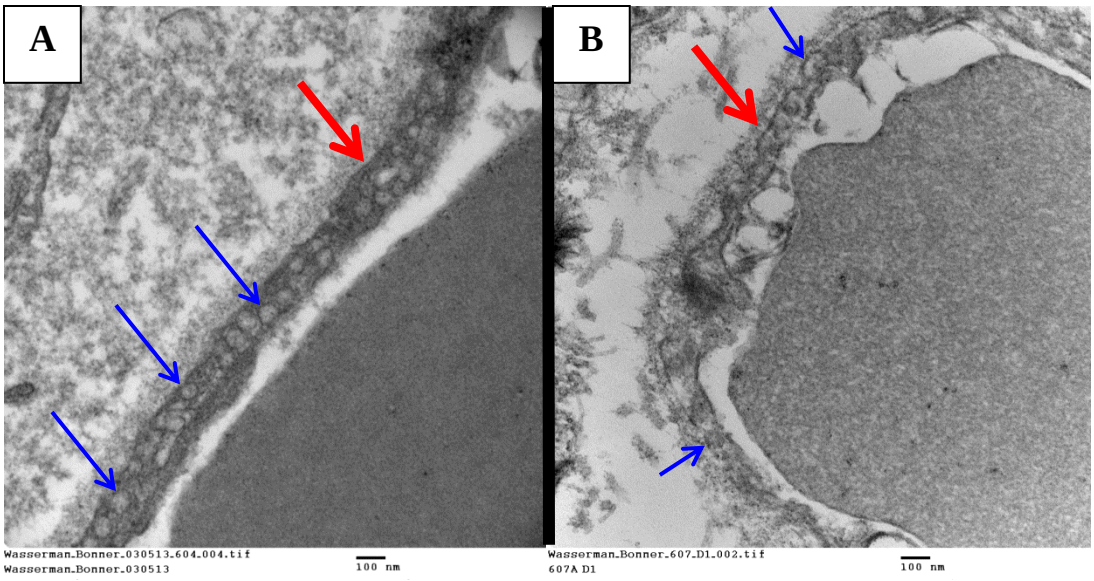

Figure 5.2 – Transmission electron micrograph from the red gastrocnemius of chow-fed (A) and 16 week HF-fed (B) mice. Red arrows indicate single endothelial capillary and blue arrows indicate a single caveolae. Micrographs are the same capillaries from Figure A.1. Images were acquired at a magnification of 67,000x.

Chapter VI

SUMMARY

Collectively the data presented within the Dissertation show the significant contribution of vascular function, capillary density, and capillary architecture to skeletal muscle insulin resistance. The genetic induction of capillary rarefaction in Chapter III showed that the decrease in capillary density within insulin resistant skeletal muscle is a direct cause of the diseased muscle and models that induce muscle capillary proliferation ameliorate skeletal muscle insulin resistance. Furthermore, therapeutic application of the vasoactive and extracellular matrix remodeling hormone relaxin, in Chapter IV, reduced the extramyocellular barriers to insulin-stimulated MGU, which are exacerbated in insulin resistant states. Chapter V demonstrated gross reductions in caveolae density within skeletal muscle endothelium of obese mice. The diminished caveolae number could contribute to the pathogenesis of skeletal muscle insulin resistance; however, the role of caveolae in insulin transport to muscle interstitium needs further investigation. These data provide an opportunity for investigation of novel therapeutic targets to treat the underlying vascular dysfunction with the goal to simultaneously intervene to ameliorate the greater metabolic syndrome associated with obesity.

The correlation between functional and structural capillary rarefaction to skeletal muscle insulin resistance has been well established. To date there has been no evidence directly linking structural capillary rarefaction to the pathogenesis of insulin resistance. These are the first studies to show the causative role of changes in capillary density to the

development of skeletal muscle insulin resistance. Notably, the mouse model investigated within Chapter III took advantage of tissue specific cre-lox recombination technology to specifically ablate VEGF-A from skeletal and cardiac muscle without the complications of a high fat diet (e.g. weight differences, tissue fat accumulation). This mouse model facilitated the direct investigation into the role of capillary rarefaction in the development of skeletal muscle insulin resistance. The phenotype in the VEGF-deficient mice emphasizes the significance of capillary rarefaction to the early progression of skeletal muscle insulin resistance.

The comparison between *in vivo* and *ex vivo* insulin action was important to corroborate that the loss of the vascular delivery component of MGU caused the impairment in insulin-stimulated glucose uptake in Chapter III. This comparison indicated that the phenotype was not driven by an off target effect due to the genetic loss of muscle VEGF directly impairing myocellular insulin action. There are limitations to this conclusion. Indeed assessing insulin action *ex vivo* removes the delivery component of MGU and focuses on the direct effects of the genetic loss of capillaries on myocellular insulin action; however, the absence of blood flow is more complex than uptake that is reliant solely on diffusion. Evidence from our laboratory suggests an important regulatory role of the extracellular matrix-integrin interaction, which may not be active in the *ex vivo* setting. Additionally, endocrine and nutritional factors that may interact with the insulin signaling pathway and glucose uptake are absent in this model. It would be necessary to monitor the plasma to interstitial gradient of glucose and insulin to conclusively determine that there was a detriment in glucose and insulin delivery to skeletal muscle during the insulin clamps. Though unlikely, the *ex vivo* loss of multiple

extramyocellular factors may overemphasize the contribution the capillary density to a decrease in vascular delivery of glucose and insulin to our model.

The muscle creatine kinase promoter driving the expression of cre-recombinase in Chapter III is expressed in skeletal and cardiac muscle. The loss of cardiac VEGF-A induced compensation in the heart to maintain cardiac output. The equivalent cardiac output between genotypes was critical to the interpretations and conclusions of Chapter III. Changes in cardiac output can affect downstream muscle perfusion and delivery of molecules. Delivery is based on muscle blood volume and blood flow velocity, and a detriment in cardiac output would likely cause a subsequent decrease in both. The compensatory mechanisms, present in the skeletal and cardiac muscle VEGF-A deficient mice, to maintain cardiac output are unknown and could potentially contribute to the peripheral impairment in insulin action. Cardiac compensation and failure is associated with insulin resistance. A possible mechanistic link between peripheral insulin resistance and cardiac adaptations are elevated catecholamine levels (168). To optimize our experimental setup a more specific cre-recombinase promoter could be utilized with the VEGF-$A^{lox/lox}$ mice. Recently McCarthy et al. developed a cre-recombinase mouse strain with an inducible human α-skeletal actin promoter that is not active in cardiac muscle (169). This technology would permit the investigation of skeletal muscle specific capillary rarefaction, thus eliminating the potential confounding factor of the cardiac phenotype in my model. Furthermore, the inducible system more closely mimics the pathological state of capillary rarefaction and limits any compensatory mechanisms as the recombination would occur in adult animal.

The influence of capillary density in skeletal muscle insulin action needs further investigation, particularly in different physiological states. The benefits of exercise and lifestyle changes to obesity related insulin resistance has long been established. Moreover, the importance of skeletal muscle capillary supply is critical to exercise capacity. Exercise training induces muscle capillary expansion, which is regulated by muscle VEGF secretion (170). By employing our mouse model, key mechanistic links between exercise, capillary density, and skeletal muscle insulin action could determine whether the metabolic benefits of exercise in skeletal muscle are dependent on an augmentation of capillary density induced by VEGF. This experiment would provide insight into the potential efficacy of treating insulin resistance skeletal muscle with a vascular proliferative agent.

Though lifestyle changes such as exercise and diet are recommended for treatment of obesity related metabolic disease, compliance to this prescription is low. There is demand for comprehensive therapeutic options to combat the low adherence to exercise and diet prescription to treat metabolic and vascular disorders, as these co-morbidities associate with obesity. The pleiotropic hormone relaxin targets multiple physiological systems, including the vasculature and extracellular matrix, to benefit vascular and metabolic dysfunction present in HF-fed mice (Chapter IV). This physiological approach to the treatment of insulin resistance provides a novel avenue to investigate the potential to target the extramyocellular barriers to MGU. Our laboratory and others have demonstrated that genetic and pharmacological interventions targeting the extracellular matrix and vasculature ameliorate diet-induced insulin resistance (86, 87, 171).

The hemodynamic action of relaxin is well established. The data presented in Chapter IV was the first to test the vascular effect in skeletal muscle. An acute administration in lean mice resulted in enhanced skeletal muscle perfusion and insulin-mediated MGU. Notably, the acute vasodilatory and metabolic response to relaxin was absent in HF-fed mice. The complex regulation of the vasoactive response to pharmacological administration of relaxin converges on activation of eNOS and synthesis of nitric oxide (145). However, obese clinical patients and animals models have an impaired response to eNOS activators. This dysfunction is likely the basis of the non-response in the acute relaxin infusion, HF-fed cohort. Importantly the chronic intervention with relaxin proved to be efficacious in improving vascular and metabolic function present in the HF-fed mice (Protocol 2; Chapter IV). The dependence on treatment duration is consistent with hypertensive rat models (146).

The treatment effects of relaxin in our model were dependent on the duration of administration. The expansion in skeletal muscle capillary density and improvement in endothelial specific vasodilation, decreasing the extramyocellular delivery barrier to MGU, are mechanisms that require chronic relaxin exposure. The angiogenic response requires longer than the 6.5 h infusion duration in Protocol 1 of Chapter IV, thus the remodeling effects evident with long-term treatment were necessary for the outcomes in Protocol 2 of Chapter IV. The coupling and phosphorylation state of aortic eNOS in our model, surrogates for the functional state of eNOS, are unknown. The studies performed in Chapter IV utilized aortic ring reactivity to measure endothelial function. Aortic ring reactivity provides a more physiological assessment of eNOS function than the biochemical analysis of eNOS coupling and phosphorylation. The analysis of the

coupling and phosphorylation state of eNOS before and after treatment could be an important next step in understanding the mechanisms by which relaxin improves endothelial-dependent relaxation.

The improvement in glucose flux during the insulin clamps (Protocol 2; Chapter IV) was not limited to skeletal muscle. Hepatic glucose production was suppressed to a greater extent in response to hyperinsulinemia after the 3 week relaxin treatment. This is an important result as hepatic insulin resistance and excessive glucose production contributes to the pathogenesis of type 2 diabetes. The mechanism of action for the enhancement in hepatic insulin action is not fully elucidated. The glucoregulatory effects of the relaxin intervention at the liver and skeletal muscle are likely independent mechanisms. The liver is composed of a highly perfused, discontinuous capillary network facilitating rapid and efficient exchange of hormones and macromolecules. However, the extracellular matrix remodeling phenotype in the liver is speculated to contribute to the mechanisms for the improvement in hepatic insulin action. Kang et al. has described the significant interaction between collagen and cell surface integrin receptors in regulating insulin action (87). The dichotomous action of relaxin on liver and skeletal muscle glucose flux highlights the pleiotropic effects of the hormone on multiple physiological systems. The broad actions of relaxin make it a possible candidate to treat metabolic and cardiovascular dysfunction induced by obesity.

The studies performed in Chapter III and IV could have benefited from a direct measurement of skeletal muscle blood volume and muscle interstitial insulin concentration. The insulin clamp technique relies on a constant rate of insulin infusion for 2.5 h to maintain postprandial plasma concentrations. The subsequent rise in plasma

insulin concentration during the clamp recruits unperfused capillaries and increases total limb blood flow (45, 84, 137, 141, 142, 172). Microvascular recruitment and skeletal muscle blood volume are affected by capillary density and the response in total limb blood flow is dependent on insulin induced eNOS activation (37, 44, 49, 58, 59, 67). Kubota et al. demonstrated in models of impaired endothelial insulin signaling and diet-induced insulin resistance that mice have a blunted increase in muscle blood volume and interstitial insulin concentration during an insulin clamp (48). Notably, the detriment in muscle capillary blood volume, interstitial insulin, and subsequent impaired peripheral glucose disposal was reversed by chronic infusion of an eNOS dependent vasodilator (48). Moreover, insulin clamps in normal conscious dogs revealed that lymph insulin, a marker for the interstitial concentration, remained lower through the duration of the clamp at a ratio of 3:2 (28). Together these studies provide evidence for the importance of insulin delivery to the muscle and that impairments in the hemodynamic action of insulin can delay or attenuate the rise in interstitial insulin during an insulin clamp. Interstitial insulin more strongly correlates to the onset of peripheral glucose uptake than plasma insulin. One can postulate that the loss of vascular function in Chapter III may hinder the rise in interstitial insulin and that the gain of function in Chapter IV may have enhanced it.

Skeletal muscle angiogenesis is a complexly regulated process involving several growth factors. The primary stimulus and driver for capillary growth and sprouting is VEGF. The tightly regulated process becomes abnormal in obesity and diabetic states. Though many report an elevation of VEGF expression in diabetes, there is a concordant elevation of anti-angiogenic factors such as the adipokine thrombospondin-1,

dysregulation of soluble VEGFR1 secretion, vasohibin-1, and impaired VEGFR2 signal transduction (173-175). The imbalance of pro- and anti-angiogenic factors associated with diabetes results in a weakened response to cardiac and peripheral ischemia that may culminate in heart disease, limb amputation, and other disorders. Vasoactive compounds that can overcome this angiogenic dysregulation may reduce mortality and morbidity associated with diabetes. Relaxin elevated plasma VEGF, shown in Chapter IV, and may switch the balance towards a pro-angiogenic environment leading to skeletal muscle capillary preservation and expansion. It is important to note that excessive VEGF signaling can be detrimental to skeletal muscle morphology. Viral delivery of VEGF in a rabbit model of hindlimb ischemia promoted long-term angiogenesis and increased muscle perfusion; however, the unregulated angiogenic stimulus induced skeletal muscle fibrosis and increased skeletal muscle macrophage intravasation (176). A potential approach to combat the aberrant angiogenesis in the setting of excessive VEGF is the co-expression of angiopoietin-1 (ang-1). Ang-1 is critical for capillary maturation and integrity. The administration of VEGF and ang-1 directly into ischemic skeletal muscle resulted in greater collateral vessel development, capillary density, and a decrease in the incidence of necrosis compared with either VEGF or ang-1 alone (177). The application of pro-angiogenic therapeutic agents to skeletal muscle must take into account the coordinated regulation and maturation of capillary development.

A contrast in circulating VEGF existed between the results of Chapter III and IV. The diet-induced insulin resistant mice in Chapter IV had greater plasma VEGF levels compared with the lean mice in Chapter III, consistent with previous investigations (175). The capillary rarefaction present in the muscle-specific VEGF knockout animals was

induced by the absence of muscle tissue VEGF expression. Tissue expression of VEGF is essential for normal capillary development and maintenance. The genetic deletion of VEGF occurred at gestational day 16. The *mVEGF*$^{-/-}$ mice of Chapter III likely were born with fewer capillaries perfusing skeletal muscle that was conserved through adulthood. Interestingly there was no difference in circulating VEGF; however, there was an elevation in circulating VEGF after the relaxin intervention that likely contributed to the expansion of capillary density (Protocol 2; Chapter IV). The equivalent plasma VEGF in the genetic models in Chapter III provides a survival signal for the vascular networks present (78), whereas the increased plasma VEGF after the 3 week relaxin intervention provides a pro-angiogenic environment for the expansion and preservation of skeletal muscle capillary density in HF-fed mice.

The transport of insulin to the skeletal muscle interstitium and the contribution of caveolae to capillary transendothelial transport is a poorly understood phenomenon. Barrett and colleagues (33, 34, 164) showed promising *in vitro* work indicating the critical role of caveolae to insulin delivery and localization of the insulin receptor within these microstructures of the endothelial wall. The novel aspect of the studies performed in Chapter V were the comparison between a lean, healthy mouse and an obese, insulin resistant mouse while using a perfused fixation technique to maintain *in vivo* capillary architecture. The results of Chapter V support previous *in vitro* work performed that implicated insulin resistant inducing stimuli, such as proinflammatory cytokines, to the blunted transport of insulin across the endothelium and the decreased expression of the essential protein for caveolae formation, cavoelin-1 (34). The characterization of skeletal muscle capillary structure and potential transport capacity is important to the

development and progression of the pathogenesis of skeletal muscle insulin resistance. Further investigation needs to corroborate the dependence of transcellular transport of insulin across skeletal muscle capillary endothelial cells for delivery. This is the first characterization of capillary caveolae content in lean and obese mice and supports the need for further research to the mechanism of insulin delivery.

A strength of the work presented in this Dissertation is the emphasis on *in vivo* analyses and the use of animal models of disease. The components of insulin-mediated glucose and insulin delivery are impossible to examine with *ex vivo* and *in vitro* experimental approaches. These experiments over emphasize the role of insulin action specifically at the myocyte, which include the steps for glucose transport and phosphorylation. The current work comprehensively addresses the significant contribution of skeletal muscle capillary density to the etiology of insulin resistance and the potential for targeting the extramyocellular barriers to MGU to rescue diet-induced insulin resistance. The data presented is consistent with previous reports from our laboratory and others that demonstrate a strong relationship between capillary density and insulin action (53, 54, 86, 87, 171). More specifically, pharmacological and genetic interventions that prevent or reverse the onset of diet-induced skeletal muscle insulin resistance also have greater muscle capillary density. The vasodilatory action of insulin and the capillary reserve present in skeletal muscle are viable treatment targets for skeletal muscle insulin resistance.

Chapter VII

CONCLUSIONS AND IMPLICATIONS

The data that comprise this Dissertation support the paradigm that the extramyocellular barriers to insulin-stimulated MGU are essential to the pathogenesis of insulin resistance and provide novel therapeutic targets. These barriers involve the physiological regulation of processes that influence hormone and substrate delivery, such as capillary density, vascular function, extracellular matrix remodeling, and endothelial caveolae density. The fundamental conclusions of the cumulative work include: capillary rarefaction is significant to the pathogenesis of skeletal muscle insulin resistance, the vasoactive and extracellular matrix remodeling hormone relaxin rescues diet-induced insulin resistance, and a deficiency in caveolae microstructure density is present within the endothelial layer of the skeletal muscle capillaries in HF-fed mice.

CURRICULUM VITAE

PERSONAL INFORMATION

Name:	Jeffrey S. Bonner
Address:	1010 Central Avenue, Unit 116 Indianapolis, IN 46202 (937) 470-9467 jsbonner11@gmail.com (e-mail)
Current position:	Scientific Communications Associate Eli Lilly and Company Indianapolis, IN
Date of Birth:	June 17, 1985

EDUCATION

DePauw University, Greencastle, IN
May 2008
BS in Kinesiology

Indiana University, Indianapolis, IN
July 2009
MS in Cellular and Integrative Physiology

Vanderbilt University, Nashville, TN
August 2013
PhD in Molecular Physiology and Biophysics

DISSERTATION TITLE

Muscle Insulin Resistance: Novel Mechanisms and New Treatment Targets

PUBLICATIONS

1. **Bonner JS**, Blevins J, Anderson BM, Kempson SA. Aspirin impairs transport of protective osmolytes in renal inner medullary collecting duct cells. The Open Urology and Nephrology Journal. 2009;2:15-19.

2. Kang L, Lustig ME, **Bonner JS**, Lee-Young RS, Mayes WH, James FD, Lin CT, Perry CG, Anderson EJ, Neufer PD, Wasserman DH. Mitochondrial antioxidative capacity regulates muscle glucose uptake in the conscious mouse: effect of exercise and diet. Journal of Applied Physiology. 2012;113(8):1173-83.

3. **Bonner JS**, Lantier L, Hasenour CM, James FD, Bracy DP, Wasserman DH. Muscle-specific vascular endothelial growth factor deletion induces muscle capillary rarefaction creating muscle insulin resistance. Diabetes. 2013;62:572-580.

4. Lee-Young RS, **Bonner JS**, Mayes WH, Iwuekel I, Barrick BA, Hasenour CM, Kang L, Wasserman DH. AMPKα2 facilitates insulin-mediated glycogen synthesis, as opposed to glucose uptake, in skeletal muscle in vivo. Diabetologia. Epub 2012. PMID: 23224579.

5. Kang L, Lantier L, Kennedy A, **Bonner JS**, Mayes WH, Bracy DP, Bookbinder L, Hasty AH, Thompson C, Wasserman DH. Hyaluronan accumulates with high fat feeding and contributes to insulin resistance. Diabetes. Epub 2013. PMID: 23349492

6. **Bonner JS**, Lantier L, Hocking KM, Kang L, Owolabi M, James FD, Bracy DP, Brophy CM, Wasserman DH. Relaxin treatment reverses insulin resistance in high fat-fed mice. In revisions for Diabetes.

PRESENTATIONS

1. Vanderbilt University Diabetes Day, *Capillary Rarefaction: A Cause or Consequence of Muscle Insulin Resistance?*; Nashville, TN (2012)

2. American Diabetes Association Scientific Sessions Guided Poster Tour Presentation, *Relaxin Intervention Reverses Diet-Induced Insulin Resistance and Cardiovascular Dysfunction*; Philadelphia, PA (2012)

ABSTRACTS AND POSTER PRESENTATIONS

1. **Bonner JS**, Hocking KM, Kang L, James FD, Bracy DP, Brophy CM, Wasserman DH. Relaxin is a novel sensitizer of insulin-mediated muscle glucose uptake in C57BL/6J mice. American Diabetes Association Scientific Sessions 2011; San Diego, CA.

2. **Bonner JS**, Lantier L, Hasenour CM, James FD, Bracy DP, Wasserman DH. Muscle capillary rarefaction by muscle VEGF deletion reduces insulin-stimulated muscle glucose uptake in C57BL/6J mice. American Diabetes Association Scientific Sessions 2012; Philadelphia, PA.

3. **Bonner JS,** Hocking KM, Lantier L, Kang L, James FD, Bracy DP, Brophy CM, Wasserman DH. Relaxin intervention reverses diet-induced insulin resistance and cardiovascular dysfunction. American Diabetes Association Scientific Sessions 2012; Philadelphia, PA.

4. **Bonner JS**, Kang L, James FD, Bracy DP, Wasserman DH. Relaxin treatment reverses cardiac extracellular matrix remodeling in high fat-fed mice. American Diabetes Association Scientific Sessions 2013; Chicago, IL.

HONORS

2012 Vanderbilt University Diabetes Scholar- Graduate Student
2005-2008 Kappa Omicron Nu Honor Society
2004-2008 Varsity Football
Chi Alpha Sigma, National Collegiate Athlete Honor Society
Kenneth Brooks Holland Memorial Award
SCAC Academic Honor Roll

ACTIVITIES

Varsity Football, 2004-2007
Kappa Omicron Nu Honor Society, Student Congress Rep. 2007

REFERENCES

1. Ervin RB. Prevalence of metabolic syndrome among adults 20 years of age and over, by sex, age, race and ethnicity, and body mass index: United States, 2003-2006. Natl Health Stat Report. 2009;13:1-7.

2. Centers for Disease Control and Prevention. National diabetes fact sheet: national estimates and general information on diabetes and prediabetes in the United States, 2011. Atlanta, GA: U.S. Department of Health and Human Services, Centers for Disease Control and Prevention, 2011.

3. Gallagher EJ, Leroith D, Karnieli E. Insulin resistance in obesity as the underlying cause for the metabolic syndrome. Mt Sinai J Med. 2010;77(5):511-523.

4. DeFronzo RA. Pathogenesis of type 2 diabetes: metabolic and molecular implications for identifying diabetes genes. Diabetes Reviews. 1997;5(3):177-269.

5. DeFronzo RA. The triumvirate: beta-cell, muscle, liver. A collusion responsible for NIDDM. Diabetes. 1988;37(6):667-687.

6. DeFronzo RA. Pathogenesis of type 2 diabetes mellitus. Medical Clinics of North America. 2004;88(4):787-835.

7. DeFronzo RA. From the triumvirate to the ominous octet: a new paradigm for the treatment of type 2 diabetes mellitus. Diabetes. 2009;58(4):773-795.

8. DeFronzo RA, Gunnarsson R, Bjorkman O, Olsson M, Wahren J. Effects of insulin on peripheral and splanchnic glucose metabolism in noninsulin-dependent (type II) diabetes mellitus. J Clin Invest. 1985;76(1):149-155.

9. Ferrannini E, Buzzigoli G, Bonadonna R, Giorico MA, Oleggini M, Graziadei L, Pedrinelli R, Brandi L, Bevilacqua S. Insulin resistance in essential hypertension. N Engl J Med. 1987;317(6):350-357.

10. Bressler P, Bailey SR, Matsuda M, DeFronzo RA. Insulin resistance and coronary artery disease. Diabetologia. 1996;39(11):1345-1350.

11. Muniyappa R, Iantorno M, Quon MJ. An integrated view of insulin resistance and endothelial dysfunction. Endocrinol Metab Clin North Am. 2008;37(3):685-711.

12. Baron AD, Brechtel G, Wallace P, Edelman SV. Rates and tissue sites of noninsulin and insulin mediated glucose uptake in humans. Am J Physiol. 1988;255:E769-E74.

13. Wasserman DH, Kang L, Ayala JE, Fueger PT, Lee-Young RS. The physiological regulation of glucose flux into muscle in vivo. J Exp Biol. 2010;214:254-262.

14. Wasserman DH. Four grams of glucose. Am J Physiol Endocrinol Metab. 2009;296:E11-E21.

15. Ayala J, Bracy DP, McGuinness OP, Wasserman DH. Considerations in the design of hyperinsulinemic-euglycemic clamps in the conscious mouse. Diabetes. 2006;55:390-397.

16. Berglund ED, Li CY, Poffenberger G, Ayala JE, Fueger PT, Willis SE, Jewell MM, Powers AC, Wasserman DH. Glucose metabolism in vivo in four commonly used inbred mouse strains. Diabetes. 2008;57:1790-1799.

17. Feuger PT, Shearer J, Bracy DP, Posey KA, Pencek RR, McGuinness OP, Wasserman DH. Control of muscle glucose uptake: test of the rate-limiting step paradigm in conscious, unrestrained mice. J Physiol. 2005;562(3):925-935.

18. Halseth AE, Bracy DP, Wasserman DH. Limitations to basal and insulin-stimulated skeletal muscle glucose uptake in the high-fat-fed rat. Am J Physiol Endocrinol Metab. 2000;279:E1064-E1071.

19. Halseth AE, Bracy DP, Wasserman DH. Functional limitations to muscle glucose uptake in muscles comprised of different fiber types. J Appl Physiol Endocrinol Metab. 2001;280:E994-E999.

20. O'Doherty RM, Halseth AE, Granner DK, Bracy DP, Wasserman DH. Analysis of insulin-stimulated skeletal muscle glucose uptake in the conscious rat using isotopic glucose analogs. Am J Physiol Endocrinol Metab. 1998;274:E287-E96.

21. Kacser H, Burns JA. The control of flux. Symp Soc Exp Biol. 1973;27:65-104.

22. Sherwin RS, Kramer KJ, Tobin JD, Insel PA, Liljenquist JE, Berman M, Andres R. A model of kinetics of insulin in man. J Clin Invest. 1974;53:1481-1492.

23. Barrett EJ, Eggleston EM, Inyard AC, Wang H, Li G, Chai W, Liu Z. The vascular actions of insulin control its delivery to muscle and regulate the rate-limiting step in skeletal muscle insulin action. Diabetologia. 2009;52:752-764.

24. Freidenberg GR, Suter S, Henry RR, Nolan J, Reichart D, Olefsky JM. Delayed onset of insulin activation of the insulin receptor kinase in vivo in human skeletal muscle. Diabetes. 1994;43(1):118-126.

25. Nolan JJ, Ludvik B, Baloga J, Reichart D, Olefsky JM. Mechanisms of the kinetic defect in insulin action in obesity and NIDDM. Diabetes. 1997;46(6):994-1000.

26. Prager R, Wallace P, Olefsky JM. In vivo kinetics of insulin action on peripheral glucose disposal and hepatic glucose output in normal and obese subjects. J Clin Invest. 1986;78(2):472-481.

27. Barrett EJ, Wang H, Upchurch CT, Liu Z. Insulin regulates its own delivery to skeletal muscle by feed-forward actions on the vasculature. Am J Physiol Endocrinol Metab. 2011;301:E252-E63.

28. Yang YJ, Hope ID, Ader M, Bergman RN. Insulin transport across capillaries is rate limiting for insulin action in dogs. J Clin Invest. 1989;84(5):1620-1628.

29. Yang YJ, Hope ID, Ader M, Poulin RA, Bergman RN. Dose-response relationship between lymph insulin and glucose uptake reveals enhanced insulin sensitivity of peripheral tissues. Diabetes. 1992;41(2):241-253.

30. Yang YJ, Hope ID, Ader M, Bergman RN. Importance of transcapillary insulin transport to dynamics of insulin action after intravenous glucose. Am J Physiol. 1994;266:E17-E25.

31. Chiu JD, Richey JM, Harrison LN, Zuniga E, Kolka CM, Kirkman E, Ellmerer M, Bergman RN. Direct administration of insulin into skeletal muscle reveals that the transport of insulin across the capillary endothelium limits the time course of insulin to activate glucose disposal. Diabetes. 2008;57:828-835.

32. King GL, Johnson SM. Receptor-mediated transport of insulin across endothelial cells. Science. 1985;227(4694):1583-1586.

33. Wang H, Liu Z, Li G, Barrett EJ. The vascular endothelial cell mediates insulin transport into skeletal muscle. Am J Physiol Endocrinol Metab. 2006;291(2):E323-E332.

34. Wang H, Wang AX, Barrett EJ. Caveolin-1 is required for vascular endothelial insulin uptake. Am J Physiol Endocrinol Metab. 2011;300(1):E134-E144.

35. Clerk LH, Vincent MA, Jahn LA, Liu Z, Lindner JR, Barrett EJ. Obesity blunts insulin-mediated microvascular recruitment in human forearm muscle. Diabetes. 2006;55:1436-1442.

36. Baron AD, Laakso M, Ginger Brechtel, Steven V. Edelman. Mechanism of insulin resistance in insulin-dependent diabetes mellitus: a major role for reduced skeletal muscle blood flow. J Clin Endocrinol Metab. 1991;73:637-643.

37. Baron AD, Tarshoby M, Hook G, Lazaridis EN, Cronin J, Johnson A, Steinberg HO. Interaction between insulin sensitivity and muscle perfusion on glucose uptake in human skeletal muscle: evidence for capillary recruitment. Diabetes. 2000;49:768-774.

38. Steinberg HO, Chaker H, Leaming R, Johnson A, Brechtel G, Baron AD. Obesity/insulin resistance is associated with endothelial dysfunction. J Clin Invest. 1996;97(11):2601-2610.

39. Zierath JR, Houseknecht KL, Gnudi L, Kahn BB. High-fat feeding impairs insulin and glucagon in glucose homeostasis in exercise. Diabetes. 1997;46:215-223.

40. Han XX, Handberg A, Petersen LN, Ploug T, Galbo H. Stability of GLUT-1 and GLUT-4 expression in perfused rat muscle stimulated by insulin and exercise. J Appl Physiol. 1995;78:46-52.

41. Liu S, Baracos VE, Quinney H, Clandinin MT. Dietary fat modifies exercise-dependent glucose transport in skeletal muscle. J Appl Physiol. 1996;80:1219-1224.

42. Bonadonna RC, Del Prato S, Bonora E, Saccomani MP, Gulli G, Natali A, Frascerra S, Pecori N, Ferrannini E, Bier D, Cobelli C, DeFronzo RA. Roles of glucose transport and glucose phosphorylation in muslce insulin resistance of NIDDM. Diabetes. 1996;45:915-925.

43. Braithwaite SS, Palazuk B, Colca JR, Edwards CW, Hofmann C. Reduced expression of hexokinase II in insulin-resistant diabetes. Diabetes. 1995;44:43-48.

44. Clerk LH, Vincent MA, Barrett EJ, Lankford MF, Lindner JR. Skeletal muscle capillary responses to insulin are abnormal in late-stage diabetes and are restored by angiogensin-converting enzyme inhibition. Am J Physiol Endocrinol Metab. 2007;293:E1804-E1809.

45. Vincent MA, Clerk LH, Lindner JR, Klibanov AL, Clark MG, Rattigan S, Barrett EJ. Microvascular recruitment is an early insulin effect that regulates skeletal muscle glucose uptake in vivo. Diabetes. 2004;53:1418-1423.

46. De Boer MP, Meijer RI, Wijnstok NJ, Jonk AM, Houben AJ, Stehouwer CD, Smulders YM, Eringa EC, Serne EH. Microvascular dysfunction: a potential mechanism in the pathogenesis of obesity-associated insulin resistance and hypertension. Microcirculation. 2011;19:5-18.

47. Ellmerer M, Hamilton-Wessler M, Kim SP, Huecking K, Kirkman E, Chiu J, Richey J, Bergman RN. Reduced access to insulin-sensitive tissues in dogs with obesity secondary to increased fat intake. Diabetes. 2006;55:1769-1775.

48. Kubota T, Kubota N, Kumagai H, Yamaguchi S, Kozono H, Takahashi T, Inoue M, Itoh S, Takamoto I, Sasako T, Kumagai K, Kawai T, Hashimoto S, Kobayashi T, Sato M, Tokuyama K, Nishimura S, Tsunoda M, Ide T, Murakami K, Yamazaki T, Ezaki O, Kawamura K, Masuda H, Moroi M, Sugi K, Oike Y, Shimokawa H, Yanagihara N, Tsutsui M, Terauchi Y, Tobe K, Nagai R, Kamata K, Inoue K, Kodama T, Ueki K, Kadowaki T. Impaired insulin signaling in endothelial cells reduces insulin-induced glucose uptake by skeletal muscle. Cell Metab. 2011;13:294-307.

49. Benedict KF, Coffin GS, Barrett EJ, Skalak TC. Hemodynamic systems analysis of capillary network remodeling during the progression of type 2 diabetes. Microcirculation. 2010;18:63-73.

50. Kim F, Pham M, Maloney E, Rizzo NO, Morton GJ, Wisse BE, Kirk EA, Chait A, Schwartz MW. Vascular inflammation, insulin resistance, and reduced nitric oxide production precedes the onset of peripheral insulin resistance. Arterioscler Thromb Vasc Biol. 2008;28:1982-1988.

51. Gavin TP, Stallings HW 3rd, Zwetsloot KA, Westerkamp LM, Ryan NA, Moore RA, Pofahl WE, Hickner RC. Lower capillary density but no difference in VEGF expression in obese vs. lean young skeletal muscle in humans. J Appl Physiol. 2005;98:315-321.

52. Gudbjörnsdóttir S, Sjöstrand M, Strindberg L, Lönnroth P. Decreased muscle capillary permeability surface area in type 2 diabetic subjects. J Clin Endocrinol Metab. 2005;90:1078-1082.

53. Guo Q, Mori T, Jiang Y, Hu C, Ohsaki Y, Yoneki Y, Nakamichi T, Ogawa S, Sato H, Ito S. Losartan modulates muscular capillary density and reverses thiazide diuretic-exacerbated insulin resistance in fructose-fed rats. Hypertens Res. 2011:1-7.

54. Lillioja S, Young AA, Culter CL, Ivy JL, Abbott WGH, Zawadzki JK, Yki-Jarvinen H, Christin L, Secomb TW, Bogardus C. Skeletal muscle capillary density and fiber type are possible determinants of in vivo insulin resistance in man. J Clin Invest. 1987;80:415-424.

55. Marin P, Andersson B, Krotkiewski M, Bjorntorp P. Muscle fiber composition and capillary density in women and men with NIDDM. Diabetes Care. 1994;17:382-386.

56. Roberts CK, Barnard RJ, Sindhu RK, Jurczak M, Ehdaie A, and Vaziri ND. A high-fat, refined-carbohydrate diet induces endothelial dysfunction and oxidant/antioxidant imbalance and depresses NOS protein expression. J Appl Physiol. 2005;98:203-210.

57. Laasko M, Edelman SV, Bretchel G, Baron AD. Decreased effect of insulin to stimulate skeletal muscle blood flow in obese man. A novel mechanism of insulin resistance. J Clin Invest. 1990;85:1844-1852.

58. Vollus GC, Bradley EA, Roberts MK, Newman JMB, Richards SM, Rattigan S, Barrett EJ, Clark MG. Graded occlusion of perfused rat muscle vascular decreases insulin action. Clin Sci (Lond). 2007;112:457-466.

59. Vincent MA, Bradley EA, Lindner JR, Clark MG, Rattigan S. Inhibiting NOS blocks microvascular recruitment and blunts muscle glucose uptake in response to insulin. Am J Physiol Endocrinol Metab. 2003;285:E123-E129.

60. Clark MG. Impaired microvascular perfusion: A consequence of vascular dysfunction and a potential cause of insulin resistance in muscle. Am J Physiol Endocrinol Metab. 2008;295:E732-E750.

61. Pinkney JH, Stehouwer CD, Coppack SW, Yudkin JS. Endothelial dysfunction: cause of the insulin resistance syndrome. Diabetes. 1997;46:Suppl 2:S9-13.

62. Muris DM, Houben AJ, Schram MT, Stehouwer CD. Microvascular dysfunction is associated with a higher incidence of type 2 diabetes mellitus: a systemic review and meta-analysis. Arterioscler Thromb Vasc Biol. 2012;32:3082-3094.

63. Serne EH, Coen DA, Stehouwer CD, ter Maaten JC, ter Wee PM, Rauwerda JA, Donker AJ, Gans RO. Microvascular function relates to insulin sensitivity and blood pressure in normal subjects. Circulation. 1999;99:896-902.

64. Levy BI, Schiffrin EL, Mourad JJ, Agostini D, Vicaut E, Safar ME, Struijker-Boudier HA. Impaired tissue perfusion: a pathology common to hypertension, obesity, and diabetes mellitus. Circulation. 2008;118:986-976.

65. Serné EH, de Jongh RT, Eringa EC, IJzerman RG, Stehouwer CD. Microvascular dysfunction: a potential pathophysiological role in the metabolic syndrome. Hypertension. 2007;50:204-211.

66. Jiang ZY, Lin YW, Clemont A, Feener EP, Hein KD, Igarashi M, Yamauchi T, White MF, King GL. Characterization of selective insulin to insulin signaling in the vasculature of obese Zucker (fa/fa) rats. J Clin Invest. 1999;104:447-457.

67. Steinberg HO, Brechtel G, Johnson A, Fineberg F, Baron AD. Insulin-mediated skeletal muscle vasodilation is nitric oxide dependent: A novel action of insulin to increase nitric oxide release. J Clin Invest. 1994;94:1172-1179.

68. Shankar RR, Wu Y, Shen HQ, Zhu JS, Baron AD. Mice with gene disruption of both endothelial and neuronal nitric oxide synthase exhibit insulin resistance. Diabetes. 2000;49:684-687.

69. Chadderdon SM, Belcik JT, Smith E, Pranger L, Kievit P, Grove KL, Lindner JR. Activity restriction, impaired capillary function, and the development of insulin resistance in lean primates. Am J Physiol Endocrinol Metab. 2012;303:E607-E613.

70. Gerber HP, Hillan KJ, Ryan AM, Kowalski J, Keller GA, Rangell L, Wright BD, Radtke F, Aguet M, Ferrara N. VEGF is required for growth and survival in neonatal mice. Development. 1999;126:1149-1159.

71. Carmeliet P, Ferreira V, Breier G, Pollefeyt S, Kieckens L, Gertsenstein M, Fahrig M, Vandenhoeck A, Harpal K, Eberhardt C, Declercq C, Pawling J, Moons L, Collen D, Risau W, Nagy A. Abnormal blood vessel development and lethality in embryos lacking a single VEGF allele. Nature. 1996;380:435-439.

72. Ferrara N, Carver-Moore K, Chen H, Dowd M, Lu L, O'Shea KS, Powell-Braxton L, Hillan KJ, Moore MW. Heterozygous embryonic lethality induced by targeted inactivation of the VEGF gene. Nature. 1996;380:439-442.

73. Adams RH, Alitalo K. Molecular regulation of angiogenesis and lymphanogenesis. Nat Rev Mol Cell Biol. 2007;8:464-478.

74. Breen EC, Johnson EC, Wagner H, Tseng HM, Sung LA, Wagner PD. Angiogenic growth factor mRNA responses in muscle to a single bout of exercise. J Appl Physiol. 1996;81(1):355-361.

75. Tang K, Breen EC, Gerber HP, Ferrara NM, Wagner PD. Capillary regression in vascular endothelial growth factor-deficient skeletal muscle. Physiol Genomics. 2004;18:63-69.

76. Olfert IM, Howlett RA, Tang K, Dalton ND, Gu Y, Peterson KL, Wagner PD, Breen EC. Muscle-specific VEGF deficiency greatly reduces exercise endurance in mice. J Physiol. 2009;587(8):1755-1767.

77. Giordano FJ, Gerber HP, Williams SP, VanBruggen N, Bunting S, Ruiz-Lozano P, Gu Y, Nath AK, Huang Y, Hickey R, Dalton N, Peterson KL, Ross J Jr, Chien KR, Ferrara N. A cardiac myocyte vascular endothelial growth factor paracrine pathway is required to maintain cardiac function. Proc Natl Acad Sci U S A. 2001;98(10):5780-5785.

78. Lee S, Chen TT, Barber CL, Jordan MC, Murdock J, Desai S, Ferrara N, Nagy A, Roos KP, Iruela-Arispe ML. Autocrine VEGF signaling is required for vascular homeostasis. Cell. 2007;130:691-703.

79. Hazarika S, Dokun AO, Li Y, Popel AS, Kontos CD, Annex BH. Impaired angiogenesis after hindlimb ischemia in type 2 diabetes mellitus: differential regulation of vascular endothelial growth factor receptor 1 and soluble vascular endothelial growth factor 1. Circ Res. 2007;101:948-956.

80. Chung AW, Hsiang YN, Matzke LA, McManus BM, van Breemen C, Okon EB. Reduced expression of vascular endothelial growth factor paralleled with the increased angiostatin expression resulting from the upregulated activities of matrix metalloproteinase-2 and -9 in human type 2 diabetic arterial vasculature. Circ Res. 2006;99:140-148.

81. Yoon YS, Uchida S, Masuo O, Cejna M, Park JS, Gwon HC, Kirchmair R, Bahlman F, Walter D, Curry C, Hanley A, Isner JM, Losordo DW. Progressive attenuation in myocardial vascular endothelial growth factor expression is a seminal event in diabetic cardiomyopathy: Restoration of microvascular homeostasis and recovery of cardiac function in diabetic cardiomyopathy after replenishment of local vascular endothelial growth factor. Circulation. 2005;111:2073-2085.

82. Chou E, Suzuma I, Way KJ, Opland D, Clermont AC, Naruse K, Suzuma K, Bowling NL, Vlahos CJ, Aiello LP, King GL. Decreased cardiac expression of vascular endothelial growth factor and its receptors in insulin-resistant and diabetic states: a possible explanation of impaired collateral formation in cardiac tissue. Circulation. 2002;105:373-379.

83. Khazaei M, Fallahzadeh AR, Sharifi MR, Afsharmoghaddam N, Javanmard SH, Salehi E. Effects of diabetes on myocardial capillary density and serum angiogenesis biomarkers in male rats. Clinics. 2011;66(8):1419-1424.

84. Baron AD, Steinberg H, Brechtel G, Johnson A. Skeletal muscle blood flow independently modulates insulin-mediated glucose uptake. Am J Physiol 1994;266:E248-E253.

85. Murdolo G, Sjöstrand M, Strindberg L, Gudbjörnsdóttir S, Lind L, Lönnroth P, Jansson PA. Effects of intrabrachial metacholine infusion on muscle capillary recruitment and forearm glucose uptake during physiological hyperinsulinemia in obese, insulin-resistant individuals. J Clin Endocrinol Metab. 2008;93(7):2764-2773.

86. Ayala JE, Bracy DP, Julien BM, Rottman JN, Feuger PT, Wasserman DH. Chronic treatment with sildenafil improves energy balance and insulin action in high-fat fed conscious mice. Diabetes. 2007;56:1025-1033.

87. Kang L, Ayala JE, Lee-Young RS, Zhang Z, James FD, Neufer PD, Pozzi A, Zutter MM, Wasserman DH. Diet-induced muscle insulin resistance is associated with extracellular matrix remodeling and interaction with integrin a2 b1 in mice. Diabetes. 2011;60:416-426.

88. Hisaw FL. Exerperimental relaxation of the pubic ligament of the guinea pig. Proc Soc Exp Biol Med. 1926;23:661-663.

89. Jeyabalan A, Shroff SG, Novak J, Conrad KP. The vascular actions of relaxin. Adv Exp Med Biol. 2007;612:65-87.

90. Bani D. Relaxin as a natural agent for vascular health. Vasc Health Risk Manag. 2008;4(3):515-524.

91. Taylor MJ, Clark CL. Evidence for a novel source of relaxin: atrial cardiocytes. J Endocrinol. 1994;143(2):R5-R8.

92. Gunnersen JM, Crawford RJ, Tregear GW. Expression of the relaxin gene in rat tissues. Mol Cell Endocrinol. 1995;110:55-64.

93. Hsu SY, Nakabayashi K, Nishi S, Kumagai J, Kudo M, Sherwood OD, Hsueh AJ. Activation of orphan receptors by the hormone relaxin. Science. 2002;295:671-674.

94. Jeyabalan A, Novak J, Doty KD, Matthews J, Fisher MC, Kerchner LJ, Conrad KP. Vascular matrix metalloproteinase-9 mediates the inhibition of myogenic reactivity in small arteries isolated from rats after short-term administration of relaxin. Endocrinology. 2007;148(1):189-197.

95. McGuane JT, Danielson LA, Debrah JE, Rubin JP, Novak J, Conrad KP. Angiogenic growth factors are new and essential players in the sustained relaxin vasodilatory pathway in rodents and humans. Hypertension. 2011;57:1151-1160.

96. Unemori EN, Pickford LB, Salles AL, Peircy CE, Grove BH, Erikson ME, Amento EP. Relaxin induces an extracellular matrix-degrading phenotype in human lung fibroblasts in vitro and inhibits lung fibrosis in a murine model in vivo. J Clin Invest. 1996;98(12):2739-2745.

97. Yoshida T, Kumagai H, Suzuki A, Kobayashi N, Ohkawa S, Odamaki M, Kohsaka T, Yamamoto T, Ikegaya N. Relaxin ameliorates salt-sensitive hypertension and renal fibrosis. Nephrol Dial Transplant. 2012; 27(6):2190-2197.

98. Hewitson TD, Ho WY, Samuel CS. Antifibrotic properties of relaxin: in vivo mechanism of action in experimental renal tubulointerstitial fibrosis. Endocrinology. 2010;151(10):4938-4948.

99. Heeg MH, Koziolek MJ, Vasko R, Schaefer L, Sharma K, Müller GA, Strutz F. The antifibrotic effects of relaxin in human renal fibroblasts are mediated in part by inhibition of the Smad2 pathway. Kidney Int. 2005;68:96-109.

100. Williams EJ, Benyon RC, Trim N, Hadwin R, Grove BH, Arthur MJ, Unemori EN, Iredale JP. Relaxin inhibits effect collagen deposition by cultured hepatic stellate cells and decrease rat liver fibrosis in vivo. Gut. 2001;49:577-583.

101. Samuel CS, Hewitson TD, Zhang Y, Kelly DJ. Relaxin ameliorates fibrosis in experimental diabetic cardiomyopathy. Endocrinology. 2008;149(7):3286-3293.

102. Lekgabe ED, Kiriazis H, Zhao C, Xu Q, Moore XL, Su Y, Bathgate RA, Du XJ, Samuel CS. Relaxin reverses cardiac and renal fibrosis in spontaneously hypertensive rats. Hypertension. 2005;46:412-418.

103. Samuel CS, Unemori EN, Mookerjee I, Bathgate RA, Layfield SL, Mak J, Tregear GW, Du XJ. Relaxin modulates cardiac fibroblast proliferation, differentiation, and collagen production and reverses cardiac fibrosis in vivo. Endocrinology. 2004;145(9):4125-4133.

104. Segal MS, Sautina L, Li S, Diao Y, Agoulnik AI, Kielczewski J, McGuane JT, Grant MB, Conrad KP. Relaxin increases human endothelial progenitor cell NO and migration and vasculogenesis in mice. Blood. 2012. 119(2):629-636.

105. Unemori EN, Lewis M, Constant J, Arnold G, Grove BH, Normand J, Deshpande U, Salles A, Pickford LB, Erikson ME, Hunt TK, Huang X. Relaxin induces vascular endothelial growth factor expression and angiogenesis selectively at wound sites. Wound Repair Regen. 2000;8(5):361-370.

106. Hisaw FL, Hisaw FL Jr, Dawson AB. Effect of relaxin on the endothelium of endometrial blood vessels in monkey. Endocrinology. 1967;81:375-385.

107. Teichman SL, Unemori E, Teerlink JR, Cotter G, Metra M. Relaxin: review of biology and potential role in treating heart failure. Curr Heart Fail Rep. 2010;7(2):75-82.

108. Formigli L, Perna AM, Meacci E, Cinci L, Margheri M, Nistri S, Tani A, Silvertown J, Orlandini G, Porciani C, Zecchi-Orlandini S, Medin J, Bani D. Paracrine effects of transplanted myoblasts and relaxin on post-infarction heart remodeling. J Cell Mol Med. 2007;11(5):1087-1100.

109. van der Westhuizen ET, Halls ML, Samuel CS, Bathgate RA, Unemori EN, Sutton SW, Summers RJ. Relaxin family peptide receptors--from orphans to therapeutic targets. Drug Discov Today. 2008;13:640-651.

110. Metra M, Cotter G, Davison BA, Felker GM, Filippatos G, Greenberg BH, Ponikowski P, Unemori E, Voors AA, Adams KF Jr, Dorobantu MI, Grinfeld L, Jondeau G, Marmor A, Masip J, Pang PS, Werdan K, Prescott MF, Edwards C, Teichman SL, Trapani A, Bush CA, Saini R, Schumacher C, Severin T, Teerlink JR; RELAX-AHF Investigators. Effect of serelaxin on cardiac, renal, and hepatic biomarkers in the relaxin in acute heart failure (RELAX-AHF) development program: correlation with outcomes. J Am Coll Cardiol. 2013;61(2):196-206.

111. Berria R, Wang L, Richardson DK, Finlayson J, Belfort R, Pratipanawatr T, De Filippis EA, Kashyap S, Mandarino LJ. Increased collagen content in insulin-resistant skeletal muscle. Am J Physiol Endocrinol Metab. 2006;290:E560-E565.

112. Gerber HP, Hillan KJ, Ryan AM, Kowalski J, Keller GA, Rangell L, Wright BD, Radtke F, Aguet M, Ferrara N. VEGF is required for growth and survival in neonatal mice. Development. 1999;126:1149-1159.

113. Ayala JE, Bracy DP, Malabanan C, James FD, Ansari T, Fueger PT, McGuinness OP, Wasserman DH. Hyperinsulinemic-euglycemic clamps in conscious, unrestrained mice. J Vis Exp. 2011;57(pii: 3188).

114. Jornayvaz FR, Birkenfeld AL, Jurczak MJ, Kanda S, Guigni BA, Jiang DC, Zhang D, Lee HY, Samuel VT, Shulman GI. Hepatic insulin resistance in mice with hepatic overexpression of diacylglycerol acyltransferase 2. Proc Natl Acad Sci U S A. 2011;108(14):5748-5752.

115. Kim HJ, Higashimori T, Park SY, Choi H, Dong J, Kim YJ, Noh HL, Cho YR, Cline G, Kim YB, Kim JK. Differential effects of interleukin-6 and -10 on skeletal muscle and liver insulin action in vivo. Diabetes. 2004;53:1060-1067.

116. Jørgensen SB, Viollet B, Andreelli F, Frøsig C, Birk JB, Schjerling P, Vaulont S, Richter EA, Wojtaszewski JFP. Knockout of the α2 but not α1 5′-AMP-activated protein kinase isoform abolishes 5-aminoimidazole-4-carboxamide-1-β-4-ribofuranoside but not contraction-induced glucose uptake in skeletal muscle. J Biol Chem. 2004;279(2):1070-1079.

117. Hocking KM, Brophy C, Rizvi SZ, Komalavilas P, Eagle S, Leacche M, Balaguer JM, Cheung-Flynn J. Detrimental effects of mechanical stretch on smooth muscle function in saphenous veins. J Vasc Surg. 2011;53(2):454-460.

118. Li FD, Sexton KW, Hocking KM, Osgood MJ, Eagle S, Cheung-Flynn J, Brophy CM, Komalavilas P. Intimal thickness associated with endothelial dysfunction in human vein grafts. J Surg Res. Epub 2013;PMID: 22763213.

119. Chan TM, Exton JH. A rapid method for the determination of glycogen content and radioactivity in small quantities of tissue or isolated hepatocytes. Anal Biochem. 1976;71:96-105.

120. Golden S, Wals PA, Katz J. An improved procedure for the assay of glycogen synthase and phosphorylase in rat liver homogenates. Anal Biochem. 1977;77:436-445.

121. Weibel ER. Stereologic principles for morphometry in electron microscopic cytology. Int Rev Cytol. 1969;26:235-302.

122. Weibel ER. Stereological methods, volume 1. Practical methods for biological morphometry. NY, Academic Press. 1979.

123. Elias H, Hyde DM. A guide to practical stereology. Basel, S Karger AG. 1983.

124. Steele R, Wall JS, De Bodo RC, Altszuler N. Measurement of size and turnover rate of body glucose pool by isotope dilution method. Am J Physiol 1956;187:15-24.

125. Pfaffl MW. A new mathematical model for relative quantification in realtime RT-PCR. Nucleic Acids Res. 2001;29(9):2002-2007.

126. DeFronzo RA, Ferrannini E. Insulin resistance: a multifaceted syndrome responsible for NIDDM, obesity, hypertension, dyslipidemia, and atherosclerotic cardiovascular disease. Diabetes Care. 1991;14:173-194.

127. Frisbee JC. Hypertension-independent microvascular rarefaction in the obese zucker rat model of the metabolic syndrome. Microcirculation. 2005;12:383-392.

128. Solomon TP, Haus JM, Li Y, Kirwan JP. Progressive hyperglycemia across the glucose tolerance continuum in older obese adults is related to skeletal muscle capillarization and nitric oxide bioavailability. J Clin Endocrinol Metab. 2011;96:1377-1384.

129. Chai W, Wang W, Dong Z, Cao W, Liu Z. Angiotensin II receptors modulate muscle microvascular and metabolic responses to insulin in vivo. Diabetes. 2011;60:2939-2946.

130. Olsson AK, Dimberg A, Kreuger J, Claesson-Welsh L. VEGF receptor signalling - in control of vascular function. Nat Rev Mol Cell Biol. 2006;7:359-371.

131. Sasso FC, Torella D, Carbonara O, Ellison GM, Torella M, Scardone M, Marra C, Nasti R, Marfella R, Cozzolino D, Indolfi C, Cotrufo M, Torella R, Salvatore T. Increased vascular endothelial growth factor expression but impaired vascular endothelial growth factor receptor signaling in myocardium of type 2 diabetic patients with chronic coronary heart disease. J Am Coll Cardiol. 2005;46(5):827-834.

132. Arsic N, Zacchigna S, Zentilin L, Ramirez-Correa G, Pattarini L, Salvi A, Sinagra G, Giacca M. Vasclular endothelial growth factor stimulates skeletal muscle regeneration in vivo. Mol Ther. 2004;10(5):844-854.

133. Kim YB, Nikoulina SE, Ciaraldi TP, Henry RR, Kahn BB. Normal insulin-dependent activation of Akt/protein kinase B, with diminished activation of phosphoinositide 3-kinase, in muscle in type 2 diabetes. J Clin Invest. 1999;104:733-741.

134. Sjöstrand M, Gudbjörnsdottir S, Holmäng A, Lönn L, Strindberg L, Lönnroth P. Delayed transcapillary transport of insulin to muscle interstitial fluid in obese subjects. Diabetes. 2002;51:2742-2748.

135. Lindbom L. Microvascular blood flow distribution in skeletal muscle. An intravital microscopic study in the rabbit. Acta Physiol Scand Suppl. 1983;525:1-40.

136. Honig CR, Odoroff CL, Frierson JL. Active and passive capillary control in red muscle at rest and in exercise. Am J Physiol Heart Circ Physiol 1982;243:H196-H206.

137. de Jongh RT, Clark AD, IJzerman RG, Serné EH, de Vries G, Stehouwer CD. Physiological hyperinsulinaemia increases intramuscular microvascular reactive hyperaemia and vasomotion in healthy volunteers. Diabetologia. 2004; 47(6):978-986.

138. Trask RV, Billadello JJ. Tissue-specific distribution and developmental regulation of M and B creatine kinase mRNAs. Biochim Biophys Acta. 1990;1049:182-188.

139. Ruhrberg C, Gerhardt H, Golding M, Watson R, Ioannidou S, Fujisawa H, Betsholtz C, Shima DT. Spatially restricted patterning cues provided by heparin-binding VEGF-A control blood vessel branching and morphogenesis. Genes Dev. 2002;16(20):2684-2698.

140. Goldstein RE, Wasserman DH, McGuinness OP, Lacy DB, Cherrington AD, Abumrad NN. Effects of chronic elevation in plasma cortisol on hepatic carbohydrate metabolism. Am J Physiol. 1993;264:E119-E127.

141. Baron AD, Clark MG. Role of blood flow in the regulation of muscle glucose uptake. Annu Rev Nutr. 1997;17:487-499.

142. Baron AD. Hemodynamic actions of insulin. Am J Physiol. 1994;267:E187-E202.

143. Conrad KP. Emerging role of relaxin in maternal adaptations to normal pregnancy: implications for preeclampsia. Semin Nephrol. 2011;31:15-32.

144. McGuane JT, Debrah JE, Sautina L, Jarajapu YP, Novak J, Rubin JP, Grant MB, Segal M, Conrad KP. Relaxin induces rapid dilation of rodent small renal and human subcutaneous arteries via PI3 kinase and nitric oxide. Endocrinology. 2011;152(7):2786-2796.

145. Conrad KP. Unveiling the vasodilatory actions and mechanisms of relaxin. Hypertension. 2010;56:2-9.

146. Debrah DO, Conrad KP, Jeyabalan A, Danielson LA, Shroff SG. Relaxin increases cardiac output and reduces systemic arterial load in hypertensive rats. Hypertension. 2005;46:745-750.

147. Sasser JM, Molnar M, Baylis C. Relaxin ameliorates hypertension and increases nitric oxide metabolite excretion in angiotensin II but no N-nitro-L-arginine methyl ester hypertensive rats. Hypertension. 2011;58:197-204.

148. Molnar J, Yu S, Mzhavia N, Pau C, Chereshnev I, Dansky HM. Diabetes induces endothelial dysfunction but does not increase neointimal formation in high-fat diet fed C57BL/6J Mice. Circulation. 2005;96:1178-1184.

149. Ma L, Ma S, He H, Yang D, Chen X, Luo Z, Liu D, Zhu Z. Perivascular fat-mediated vascular dysfunction and remodeling through the AMPK/mTOR pathway in high-fat diet-induced obese rats. Hypertens Res. 2010;33:446-453.

150. Bonner JS, Lantier L, Hasenour CM, James FD, Bracy DP, Wasserman DH. Muscle-specific vascular endothelial growth factor deletion induces muscle capillary rarefaction creating muscle insulin resistance. Diabetes. 2013; 62(2):572-580.

151. Halls ML, van der Westhuizen ET, Bathgate RA, Summers RJ. Relaxin family peptide receptors--former orphans reunite with their parent ligands to activate multiple signaling pathways. Br J Pharmacol. 2007;150(6):977-691.

152. Bathgate RA, Halls ML, van der Westhuizen ET, Callander GE, Kocan M, Summers RJ. Relaxin family peptides and their receptors. Physiol Rev. 2013;93(1):405-480.

153. Paradis V, Perlemuter G, Bonvoust F, Dargere D, Parfait B, Vidaud M, Conti M, Huet S, Ba N, Buffet C, Bedossa P. High glucose and hyperinsulinemia stimulate connective tissue growth factor expression: a potential mechanism involved in progression to fibrosis in nonalcoholic steatohepatitis. Hepatology. 2001;34:738-744.

154. Zaman AK, Fujii S, Goto D, Furumoto T, Mishima T, Nakai Y, Dong J, Imagawa S, Sobel BE, Kitabatake A. Salutary effects of attenuation of angiotensin II on coronary perivascular fibrosis associated with insulin resistance and obesity. J Mol Cell Cardiol. 2004;37:525-535.

155. Shimizu M, Umeda K, Sugihara N, Yoshio H, Ino H, Takeda R, Okada Y, and Nakanishi I. Collagen remodeling in myocardia of patients with diabetes. J Clin Pathol. 1993;46:32-36.

156. Chiang DJ, Pritchard MT, Nagy LE. Obesity, diabetes mellitus, and liver fibrosis. Am J Physiol Gastrointest Liver Physiol. 2011;300:G697-G702.

157. MacDonald GA, Bridle KR, Ward PJ, Walker NI, Houglum K, George DK, Smith JL, Powell LW, Crawford DH, Ramm GA. Lipid peroxidation in hepatic steatosis in humans is associated with hepatic fibrosis and occurs predominantly in acinar zone 3. J Gastroenterol Hepatol. 2001;16:599-606.

158. Kurella M, Lo JC, Chertow GM. Metabolic syndrome and the risk for chronic kidney disease among nondiabetic adults. J Am Soc Nephrol. 2005;16:2134-2140.

159. Hedblad B, Nilsson P, Engström G, Berglund G, Janzon L. Insulin resistance in non-diabetic subjects is associated with increased incidence of myocardial infarction and death. Diabet Med. 2002;19:470-475.

160. Utsunomiya K. Treatment strategy for type 2 diabetes from the perspective of systemic vascular protection and insulin resistance. Vasc Health Risk Manag. 2012;8:429-436.

161. Tsugane S, Inoue M. Insulin resistance and cancer: epidemiological evidence. Endocr Relat Cancer. 2012;19(5):F1-8.

162. Feng S, Agoulnik IU, Bogatcheva NV, Kamat AA, Kwabi-Addo B, Li R, Ayala G, Ittmann MM, Agoulnik AI. Relaxin promotes prostate cancer progression. Clin Cancer Res. 2007;13(6):1695-1702.

163. Feng S, Agoulnik AI. Expression of LDL-A module of relaxin receptor in prostate cancer cells inhibits tumorigenesis. Int J Oncol. 2011;39(6):1559-1565.

164. Wang H, Wang AX, Liu Z, Barrett EJ. Insulin signaling stimulates insulin transport by bovine aortic endothelial cells. Diabetes. 2008;57(3):540-547.

165. Schubert W, Frank PG, Razani B, Park DS, Chow CW, Lisanti MP. Caveolae-deficient endothelial cells show defects in the uptake and transport of albumin in vivo. J Biol Chem. 2001;276(52):48619-48622.

166. Bar RS, Boes M, Sandra A. Vascular transport of insulin to rat cardiac muscle. Central role of the capillary endothelium. J Clin Invest. 1988;81(4):1225-1233.

167. Schutzer WE, Reed JF, Mader SL. Decline in caveolin-1 expression and scaffolding of G protein receptor kinase-2 with age in Fischer 344 aortic vascular smooth muscle. Am J Physiol Heart Circ Physiol. 2005;288(5):H2457-H2464.

168. Doehner W, Rauchhaus M, Godsland IF, Egerer K, Niebauer J, Sharma R, Cicoira M, Florea VG, Coats AJ, Anker SD. Insulin resistance in moderate chronic heart failure is related to hyperleptinaemia, but not to norepinephrine or TNF-alpha. Int J Cardiol. 2002;83(1):73-81.

169. McCarthy JJ, Srikuea R, Kirby TJ, Peterson CA, Esser KA. Inducible Cre transgenic mouse strain for skeletal muscle-specific gene targeting. Skelet Muscle. 2012;2(1):2-8.

170. Kraus RM, Stallings HW 3rd, Yeager RC, Gavin TP. Circulating plasma VEGF response to exercise in sedentary and endurance-trained men. J Appl Physiol. 2004;96(4):1445-1450.

171. Kang L, Lantier L, Kennedy A, Bonner JS, Mayes W, Bracy D, Bookbinder L, Hasty A, Thompson C, Wasserman D. Hyaluronan accumulates with high fat feeding and contributes to insulin resistance. Diabetes. Epub 2013;PMID: 23349492.

172. Eggleston EM, Jahn LA, Barrett EJ. Hyperinsulinemia rapidly increases human muscle microvascular perfusion buts fails to increases muscle insulin clearance: evidence that a saturable process mediates muscle insulin uptake. Diabetes. 2007;56:2958-2963.

173. Varma V, Yao-Borengasser A, Bodles AM, Rasouli N, Phanavanh B, Nolen GT, Kern EM, Nagarajan R, Spencer HJ 3rd, Lee MJ, Fried SK, McGehee RE Jr, Peterson CA, Kern PA. Thrombospondin-1 is an adipokine associated with obesity, adipose inflammation, and insulin resistance. Diabetes. 2008;57(2):432-439.

174. Kishlyansky M, Vojnovic J, Roudier E, Gineste C, Decary S, Forn P, Bergeron R, Desplanches D, Birot O. Striated muscle angio-adaptation requires changes in vasohibin-1 expression pattern. Biochem Biophys Res Commun. 2010;399(3):359-364.

175. Li YJ, Guan H, Hazarika S, Liu CW, Annex BH. Impaired angiogenesis following hind-limb ischemia in diabetes mellitus mice. Chin Med Sci J. 2007;22(4):232-237.

176. Karvinen H, Pasanen E, Rissanen TT, Korpisalo P, Vähäkangas E, Jazwa A, Giacca M, Ylä-Herttuala S. Long-term VEGF-A expression promotes aberrant angiogenesis and fibrosis in skeletal muscle. Gene Ther. 2011;18(12):1166-1172.

177. Shyu KG, Chang H, Isner JM. Synergistic effect of angiopoietin-1 and vascular endothelial growth factor on neoangiogenesis in hypercholesterolemic rabbit model with acute hindlimb ischemia. Life Sci. 2003;73(5):563-579.